ISSN No. 2231-3273

# INTERNATIONAL JOURNAL OF ENGINEERING SCIENCES AND MANAGEMENT

A Bi-annual Research Journal of

DRONACHARYA
GROUP OF INSTITUTIONS
GREATER NOIDA, U.P., INDIA

Volume II / Issue I / Jan-Jun 2012

ISSN No. 2231-3273

# INTERNATIONAL JOURNAL OF ENGINEERING SCIENCES AND MANAGEMENT

Volume II / Issue I / Jan-Jun 2012

ISSN No. 2231-3273

# INTERNATIONAL JOURNAL OF ENGINEERING SCIENCES AND MANAGEMENT

A Bi-annual Research Journal of
DRONACHARYA
GROUP OF INSTITUTIONS
GREATER NOIDA, U.P., INDIA

Volume II Issue I Jan-Jun 2012

# INTERNATIONAL JOURNAL OF ENGINEERING SCIENCES AND MANAGEMENT



**Editorial Information:**
For details please write to the Executive Editor, International Journal of Engineering Sciences and Management,
Dronacharya Group of Institutions, B-27 Knowledge Park-III, Gautam Budh Nagar,
Greater Noida (U.P)-201308

**Telephones:**
Landline: 0120-2323851, 2323852, 2323854, 2323855
Mobile : 09312247845, 09910380107

**Telefax:**
0120-2323853

**E-mail.:**
advisor.r&d@gnoida.dronacharya.info
principal@gnoida.dronacharya.info
info@dronacharya.info

**Website:**
www.dronacharya.info

# ADVISORY BOARD

# FROM THE DESK OF
# EXECUTIVE EDITOR

Dear Readers,

We are highly excited to present to you the first issue of the second volume of our biannual research journal. Authors from different parts of India, besides USA and Singapore, have joined us in this Issue. We sincerely hope that their papers will be appreciated and cited by a large section of the academia across the globe.

The earlier issues of this journal can be viewed at http://gnoida.dronacharya.info, the website our college (Go to: RESEARCH, and then "Research Journal"). One can also see the "Abstracts" of these papers by referring to http://isa.niscair.res.in/isasimple_search.jsp, the website of "National Institute of Science Communication and Information Resources (NISCAIR)".

We shall be failing in our duty if we do not thankfully acknowledge the laudatory messages about the quality of our journal received from a large number of eminent scientists from India and abroad. Further, we are indebted to the unflinching support and cooperation of our honourable Chairman, the Management Board, our Director, the members of "Advisory Board", "Editorial Board" and all the authors who sent their research papers for consideration of publication in our journal.

We invite all the readers and their professional colleagues to send their research papers for consideration of publication in the forthcoming issues of our journal as per the "Scope and Guidelines to Authors" given at the end of this Issue.

Wishing you a very happy new year 2012 and a highly stimulating reading,

Sincerely,

**Prof. (Dr.) Jai Paul Dudeja**
*Executive Editor*
*International Journal of Engineering Sciences and Management (IJESM)*
*A Bi-annual Research Journal of Dronacharya Group of Institutions, Greater Noida.*

January 2012

# CONTENTS

# ON THE INFLUENCE OF NATURE OF REINFORCEMENT ON QUASI-STATIC DEFORMATION AND FRACTURE BEHAVIOR OF A MAGNESIUM ALLOY

C. Godbole
Division of Materials Science and Engineering
Department of Mechanical Engineering
The University of Akron, Akron, Ohio 44325-3903, USA

T.S. Srivatsan
Division of Materials Science and Engineering
Department of Mechanical Engineering
The University of Akron, Akron, Ohio 44325-3903, USA
tss1@uakron.edu

T. Quick
Department of Geology
The University of Akron, Akron, Ohio 44325-3903, USA

M. Paramsothy
Department of Mechanical Engineering
National University of Singapore, Singapore

M. Gupta
Department of Mechanical Engineering
National University of Singapore, Singapore

## ABSTRACT

An alumina particulate reinforced (Al2O3p) and a carbon nanotube (CNT) reinforced magnesium alloy-based composites were fabricated using the technique of disintegrated melt deposition followed by hot extrusion. In this research endeavor the conjoint and interactive influences of reinforcement and processing on microstructural development, tensile properties and final fracture behavior of the magnesium alloy-based composites, denoted as AZ31/Al2O3 and AZ31/CNT, were studied and comparisons made with the unreinforced counterpart (alloy AZ31). The interactive influences of nature of the reinforcing phase and processing in governing engineering stress versus engineering strain response and resultant tensile properties is presented and discussed. The macroscopic fracture mode and intrinsic microscopic mechanisms governing quasi-static deformation and fracture behavior of both the reinforced and unreinforced magnesium alloy is rationalized in light of the specific role played by (i) presence of the reinforcing phase in the magnesium alloy metal matrix, (ii) intrinsic microstructural effects, and (iii) nature of loading.

***Keywords***: *Magnesium alloy; Metal matrix composite; Alumina particulates; Carbon nanotube; Tensile response; Fracture.*

## 1. INTRODUCTION

The continuing need for high-performance capability and lightweight materials for a range of weight-critical applications has provided the much needed impetus, incentive and interest to both material scientists and engineers to initiate and execute sustained and systematic research efforts towards (i) developing metal matrix-based composites, and (ii) engineering efficient, effective and economically viable techniques to process them. Magnesium and magnesium alloys due to their inherent low density (1.74 gm/cm3) are potentially viable candidates for the development of metal matrix composites (MMCs). In recent years, sustained research and development efforts have been undertaken with the primary objective of improving the mechanical properties of magnesium alloys by selective reinforcement with either ceramic or metallic phases and using novel and innovative processing techniques to obtain a material that offered high specific strength ($\sigma/\rho$), high specific stiffness ($E/\rho$), good damping capacity coupled with other required and desirable mechanical properties [1-5].

Magnesium with 99.8% purity is readily available but the primary factor that has placed constraints in the selection and use of magnesium-base alloys and magnesium-base composites for a wide spectrum of applications is that they suffer from a combination of low ductility, inferior fracture toughness, inadequate strength coupled with an innate difficulty in forming and shaping them into intricate shapes and patterns. This can be attributed to its hexagonal close-packed (HCP) crystal structure, which has limited slip systems when compared one-on-one with aluminum-base alloys and their composite counterparts that have a face-centered cubic (FCC) crystal structure [6, 7]. This therefore necessitates the need for selective alloying of pure magnesium for the purpose of achieving improved plasticity and reinforcing magnesium with a high modulus second-phase for the purpose of obtaining high strength.

Physical properties of the magnesium-based MMC are based on properties of the constituents, i.e., the matrix and the reinforcing phase. The volume fraction, size, shape and distribution of the particulate reinforcing phase does exert an observable influence on both the kinetics and intrinsic microscopic mechanisms governing the movement of dislocations through the composite microstructure and resultant tensile behavior of the composite. In more recent years, an extensive amount of research has been carried out with the primary objective of reinforcing few magnesium alloys with hard, brittle and elastically deforming particulates of either a ceramic or metallic phase with the purpose of improving the mechanical properties of the matrix alloy. Few of the reinforcements that have been tried, studied and results documented in the "open" literature are silicon carbide (SiC) [8, 9], particulates of copper [10] and titanium carbide (TiC) [11].

Alumina (Al2O3) particulates and sort fibers have engineered noticeable attention and interest among researchers who are in the pursuit of developing magnesium-based composites. Paramsothy and co-workers in their study synthesized a hybrid magnesium alloy (AZ31/AZ91) reinforced with nano-size particles of aluminum oxide or alumina (Al2O3) [12] and reported improved tensile strength and compressive strength of the composite when compared with the monolithic counterpart. Zuzanka and co-workers [13] manufactured the magnesium alloy (AZ91) composite reinforced with δ-Al2O3 (Saffil®) short fibers using the technique of squeeze casting. The resultant composite was investigated for its deformation response under conditions of compressive loading. In an independent study to quantify the effect of alumina (Al2O3) particulates on pure magnesium and AZ31 alloy-based composites, M. Habibnejad-Korayem and co workers [14] manufactured pure magnesium and magnesium alloy (AZ31) reinforced with 0.5 wt. pct., 1.0 wt. pct., and 2.0 wt. pct., of alumina nano-particles using stir-casting. Their microstructural observations revealed a near uniform distribution of the reinforcing Al2O3 nano-particles in the magnesium metal matrix and a refined grain structure. Also, they noted the presence of alumina nanoparticles to have a profound influence on decreasing the coefficient of thermal expansion of the composite. Q.B. Nguyen and M. Gupta in their exhaustive study investigated the effect of three different volume fractions of 50-nm size alumina particulates ( Al2O3)p on alloy AZ31B and manufactured using the technique of disintegrated melt deposition (DMD). They observed a noticeable increase in micro-hardness and failure strain but a reduction in both the offset (0.2%) yield strength and ultimate tensile strength (UTS) of the composite. An analysis of the fracture behavior revealed a transition from low-energy absorbing brittle fracture mode to high-energy absorbing ductile fracture for the composites.

Carbon nanotubes (CNT) offer extraordinary mechanical properties, which include high strength of upto 150 GPa, high elastic modulus of upto 1.2 TPa, and a high aspect ratio [16]. These specific attributes have made carbon nano-tubes (CNTs) to be both a desirable and preferred choice for reinforcing soft magnesium alloy metal matrices [17-20]. Habibi and co-workers in a recent research study reinforced magnesium with hybrid Al–CNT nano-particles. They observed fracture behavior of the composite to be predominantly ductile when compared one-on-one with the monolithic counterpart, which showed presence of cleavage steps, reminiscent of 'locally' brittle failure. Also, when compared to monolithic magnesium they reported a noticeable improvement in tensile strength and failure strain of the Mg/Al–CNT nano-composite. Paramsothy and co workers studied tensile behavior of wrought ZK60A magnesium alloy reinforced with carbon nano tubes (CNTs). They reported an increase in both tensile strength and failure strain of the composite (ZK60A/1.0 vol. % CNT) when compared to the monolithic alloy (ZK60A). The observed improvement in mechanical properties of the composite was attributed to the following factors pertaining to reinforcement: (a) presence and reasonably near uniform distribution of the reinforcing CNT nanoparticle, and (b) a possible reduction in size of the intermetallic phase(s). Park and co workers fabricated AZ91 reinforced with CNTs metal matrix composite using the squeeze infiltration method. The mechanical tests reported an 18% improvement in tensile strength and a 16.5% improvement in yield strength of the composite over the monolithic counterpart. The hardness test revealed an 87% increase in hardness of the composite over the monolithic counterpart. However, it is important to avoid an agglomeration of the reinforcing CNT in the magnesium alloy metal matrix during processing of the composite since this can be detrimental for the achievement of good to improved mechanical properties. The mechanical properties of carbon nanotubes- reinforced magnesium composite hybridized with nanoparticles of alumina was investigated by Thakur and co workers . They studied the specific role of distribution of the reinforcing CNT in an Mg + 1% CNT nanocomposite and reported inferior mechanical behavior. This was ascribed to be due to an uneven distribution of the CNT reinforcements in the magnesium alloy matrix. The tensile fracture surface of the deformed and failed composite specimen revealed macroscopically brittle failure and microscopically features reminiscent of 'locally' ductile and brittle failure mechanisms.

In this research paper, the intrinsic influence of nature of reinforcement and extrinsic influence of processing on microstructural development, mechanical properties enhancement, and final fracture behavior of two magnesium alloy-based metal-matrix composites, i.e., AZ31/1.5 vol. % Al203 and AZ31/1.0 vol. % CNT, is presented and compared with the unreinforced counterpart, i.e., monolithic alloy AZ31. The elastic modulus, yield strength, ultimate tensile strength of the reinforced magnesium alloy is compared with the unreinforced counterpart. The ductility quantified by elongation-to-failure over 12.7 mm (0.5 inches) gage length of the test specimen and reduction in cross-section area of the composite are compared with the monolithic alloy. A comprehensive examination of the tensile fracture behavior of the composites is compared with the monolithic counterpart to understand the specific role and influence of reinforcement and processing on microscopic mechanisms governing deformation and fracture.

## 2. MATERIALS

In the present study, the magnesium alloy AZ31 (refer Table 1 for nominal composition) was procured by National University of Singapore (Singapore) from Tokyo Magnesium Co. Ltd. (Yokohama, Japan). The as-provided AZ31 blocks were sectioned to smaller pieces for primary and secondary processing. The magnesium alloy blocks were 'precision' machined to remove oxide layers and other visible scales on the surface. All of the surfaces of the magnesium alloy were washed with ethanol subsequent to machining. Alumina particles ($Al_2O_3$) procured from Baikowski (Japan) having a size of 50 nm was used as the reinforcement to engineer the nanocomposite (AZ31/ 1.5 vol% $Al_2O_3$). The second AZ31 alloy-based nanocomposite was manufactured using Carbon Nano-Tubes (vapor grown, 94.7% purity, 40-70 nm outer diameters) as the reinforcing phase. The CNT was procured by National University of Singapore from Nanostructured & Amorphous Materials Inc (Texas, USA).

Table 1: Nominal chemical composition (in weight percentage) of the chosen magnesium alloy.

| Al | Zn | Mn | Si | Cu | Fe | Ni | Magnesium |
|---|---|---|---|---|---|---|---|
| 2.50 to 3.50 | 0.60 to 1.40 | 0.15 to 0.40 | 0.10 | 0.05 | 0.01 | 0.01 | Balance |

## 3. PROCESSING

**3.1 PRIMARY PROCESSING OF MONOLITHIC AZ31 ALLOY** Monolithic AZ31 was cast using the method of Disintegrated Melt Deposition (referred to henceforth as DMD) [21-25]. This technique involved heating of the as-provided blocks of the magnesium alloyAZ31, placed in a graphite crucible, to 750°C in an environment of inert argon gas using a resistance heating furnace. The purpose of an inert environment was to minimize metal-environment interactions. The crucible was equipped with an arrangement for pouring at the bottom. Upon reaching the superheat temperature, the molten slurry was well stirred for 2.5 min (150 seconds) at a speed of 460 rpm using a twin blade (pitch 45°) mild steel impeller. The purpose of stirring was to facilitate a uniform distribution of heat. The impeller was coated with Zirtex 25 [86%$ZrO_2$, 8.8%$Y_2O_3$, 3.6% $SiO_2$, 1.2%$K_2O$ and $Na_2O$, and 0.3% trace inorganic] with the purpose of avoiding contamination of the molten metal with iron. The melt was then released through an orifice having a diameter of 10-mm and located at the base of the crucible. The melt was carefully disintegrated by two jets of argon gas oriented normal to the melt stream and positioned 265 mm from the melt pouring point. The argon gas flow rate was maintained at 25 lpm (liters per minute). The disintegrated melt slurry was subsequently deposited on a metallic substrate that was positioned 500 mm from the disintegration point. An ingot having a diameter of 40-mm was obtained following the deposition stage.

**3.2 PRIMARY PROCESSING OF AZ31 /1.0 VOL. % AL2O3 COMPOSITE** To form the nanocomposite reinforced with 1.5 vol. % alumina (aluminum oxide ($Al_2O_3$)), fine powder of the reinforcing alumina was wrapped in an aluminum foil having minimal weight (< 0.50 wt. %) with respect to magnesium alloy (AZ31). All of the other parameters related to the technique of Disintegrated Melt Deposition (DMD) were essentially unchanged to that used for the monolithic alloy.

**3.3 PRIMARY PROCESSING OF AZ31 /1.0 VOL. % CNT COMPOSITE** To form the nanocomposite [AZ31 /1.0 vol. % CNT], powders of the carbon nanotube (CNT) were isolated by wrapping them in an aluminum foil having minimal contributions by way of weight (< 0.50 wt. % with respect to matrix weight of AZ31) and arranged on top of the blocks of alloy AZ31. All of the other parameters used for DMD were essentially unchanged.

**3.4 SECONDARY PROCESSING** The as-deposited billets of the monolithic alloy and the nanocomposites were machined to ingots having a diameter of 35 mm and subsequently hot extruded (350°C) on a 150-ton hydraulic press using an extrusion ratio of 20.25:1. The billets were held at 400°C in a furnace for full 60 minutes prior to extrusion. Colloidal graphite was used as the lubricant during extrusion. The rods obtained following extrusion measured 8-mm in diameter.

## 4. EXPERIMENTAL PROCEDURES

**4.1 SAMPLE PREPARATION** The as received extruded rods of the monolithic alloy and nanocomposites were precision machined to obtain cylindrical specimens with threaded ends. The machining was carried out in conformance with specifications outlined in Standard E-8 of American Society for Testing Materials Standard (ASTM) with the major stress axis taken to be along extrusion direction of the rod stock. The overall length of the specimen measured 2.3 inch (58 mm) with a diameter of 0.25 inch (6.3 mm) at the thread section and diameter of 0.125 inch (3-mm) at the gage section. The gage length measured 0.5 inch (12.5 mm).

**4.2 INITIAL MICRO STRUCTURAL CHARACTERIZATION** Standard metallographic techniques were employed to prepare magnesium alloy (AZ31) alloy and the magnesium-based nanocomposites (AZ31/$Al_2O_3$, AZ31/CNT) samples for purpose of microstructural characterization and examination. The samples were sectioned perpendicular to the direction of extrusion and mounted in bakelite for subsequent polishing. Coarse polishing of the mounted samples was performed using progressively finer grades (320 grit, 400-grit, and 600-grit) of silicon carbide (SiC) impregnated emery paper. Fine polishing was accomplished using 1-micron alumina powder suspended in distilled water as the lubricant. Etching of the polished surface was done using acetic-picral [a solution mixture of 5 ml acetic acid, 6 g picric acid, 10 ml water and 100 ml ethanol]. The fine polished surface of the test specimen was gently immersed in the etchant until a brown film was formed. This was followed by immediately rinsing in running water and drying using hot air. The etched surface of the monolithic alloy and the two composites were observed at low magnification in an optical microscope (Model: Mitutoyo FS70) and photographed using standard bright illumination technique.

**4.3 TENSILE TESTING** Uniaxial tension tests, up until failure, were performed in the room temperature (25oC) and laboratory air (Relative Humidity = 55 pct) environment. A closed-looped fully automated servo-hydraulic mechanical test machine (Model: INSTRON: 8500 Plus) was used to carry out the tests. The machine was equipped with a 22 kip (100 KN) load cell. The tests were performed at a constant strain rate of 0.0001 s-1. Measurement of strain was made using an axial 12.5-mm gage length clip-on extensometer attached to the test specimen at the gage section. The cylindrical test samples were precision machined in conformance with specifications outlined in Standard E-8 of the American Society for Testing Materials (ASTM). The overall length of the specimen measured 2.3 inch (58 mm) and 0.25 inch (6.3 mm) in diameter at the threaded end while at the gage section it measured 0.5 inch (12.5 mm) in length and 0.125 inch (3 mm) in diameter. The stress and strain measurements, parallel to the load line, were recorded on a PC-based data acquisition system (DAS).

**4.4 FAILURE-DAMAGE ANALYSIS** To establish the overall fracture surface morphology and the intrinsic features on the fracture surface, macroscopic and microscopic observations of the fracture surfaces of the deformed and failed tensile specimen were carried out in a scanning electron microscope (Model: FEI: Quanta 200). The macroscopic mode essentially refers to the overall nature of failure, while the microscopic observations include all of the failure processes occurring at the “local” level and spanning (a) microscopic void formation, (b) microscopic void growth and their eventual coalescence, or impingement, with each other to form one or more fine microscopic cracks, and (c) the nature, extent and severity of cracking spanning both macroscopic cracks and fine microscopic cracks.

## 5.RESULTS AND DISCUSSION

**5.1 MICRO STRUCTURE** The optical micro structure of monolithic AZ31 and the nanocomposite are shown in Figure 1. There is an observable reduction in grain size of the AZ31/Al2O3 and AZ31/CNT nano composites (Figure 1b and Figure 1c) when compared to the monolithic alloy (AZ31) (Figure 1a). The bright regions in the micrographs of both the monolithic alloy and the composites are the 'α' phase. The dark region, denoted for convenience as β phase, was identified in earlier studies using the technique of X-Ray diffraction to be the eutectic phase, i.e., the intermetallic Mg17Al12 [15, 26-28]. Compared to the monolithic alloy (Figure 1a) and the composite (AZ31/CNT) (Figure 1c), the Al2O3 (Figure 1b) reinforced magnesium alloy nanocomposite revealed higher amount of β to be located both at and along the grain boundaries of α phase.

The reduced grain size and near-uniform distribution of grain size observed in both the nano-composites when compared to the monolithic counterpart is ascribed to be due to the independent and/or synergistic influence of the following mechanisms:

(i) A uniform distribution of the second-phase particles made possible by minimal gravity associated segregation due to the appropriate selection of the stirring parameters [26].
(ii) An ability of the reinforcing phases (both CNT and Al2O3) to serve as potential sites for nucleation while concurrently being an obstacle to retarding grain growth during sodification.
(iii) A high extrusion temperature of 623 K (T~0.7 Tm) resulting in the occurrence of dynamic recrystallization (DRX) [29, 30].

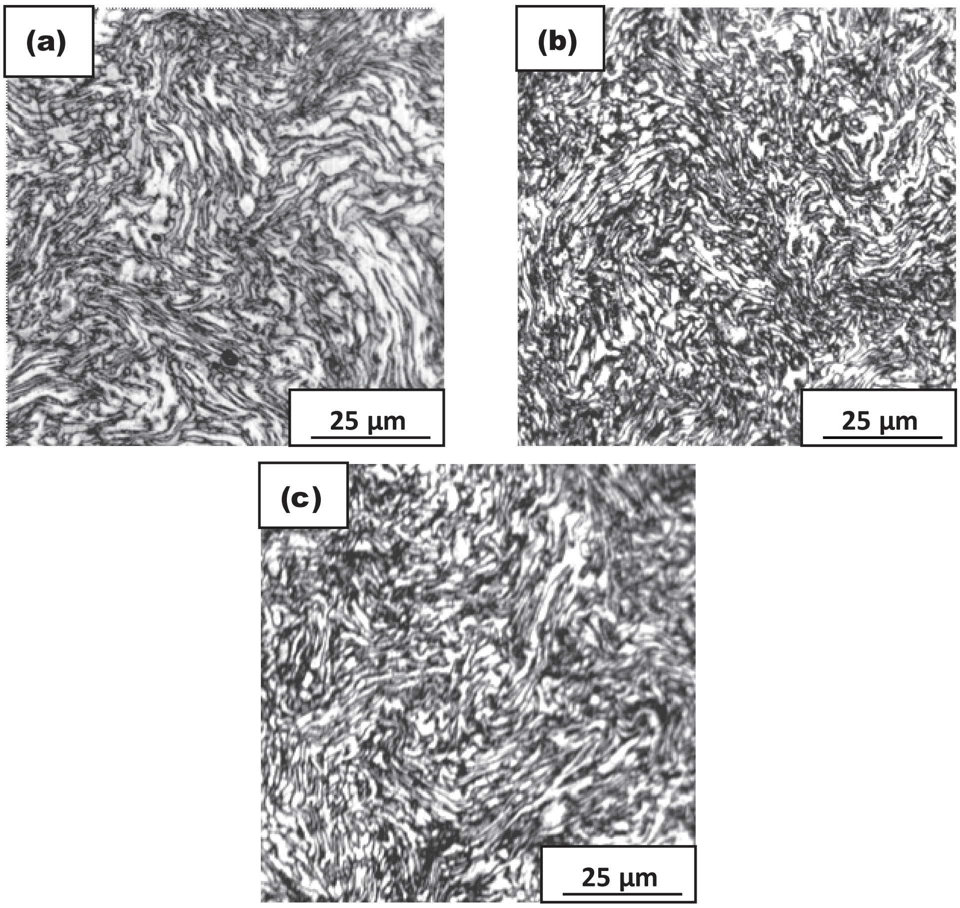


***Figure 1:*** Optical micrographs of Sample #1 of alloy steel 4140 (annealed) at the different magnifications showing the key micro structural constituents and grain size.

**5.2 TENSILE PROPERTIES** The tensile properties of the AZ31 alloy, AZ31/1.5 $Al_2O_3$ and AZ31/1.0 vol% CNT nanocomposite are summarized in Table 2. The results reported are the mean value based on duplicate tests.

***Table 2:*** Quasi-Static tensile properties of magnesium based alloy and composites recorded at room temperature (25oC).

| Specimen | Elastic Modulus | | Yield Strength | | Ultimate Tensile Strength | | Elongation GL=0.5" (%) | Reduction in Area (%) | Tensile Ductility ln (Ao/Ar)(%) |
|---|---|---|---|---|---|---|---|---|---|
| | ksi | GPa | ksi | Mpa | ksi | Mpa | | | |
| **Az31** | **6567.2** | **45.3** | **29.6** | **203.7** | **29.6** | **203.7** | **13.5** | **20.4** | **22.8** |
| **AZ31/1.5vol% Al2O3** | **7054.3** | **48.6** | **33.1** | **228.4** | **33.1** | **228.4** | **10.5** | **18.3** | **20.2** |
| **AZ31/1.0 vol% CNT** | **6307.6** | **43.5** | **34.4** | **237.4** | **34.4** | **237.4** | **16.8** | **25.0** | **28.8** |

1. Elastic modulus of the AZ31/$Al_2O_3$ composite revealed 7 pct increase (47 GPa) when compared to the elastic modulus of the monolithic alloy (AZ31), which is 45.3 GPa. The AZ31/CNT nanocomposite revealed a 4 percent decrease in elastic modulus (E = 43.5 GPa) when compared to the monolithic counterpart (AZ31).
2. A 12 pct increase in yield strength (228.4 MPa) of the AZ31/$Al_2O_3$ composite is observed when compared to the monolithic counterpart (203 MPa). The yield strength of AZ31/1.0 vol. % CNT nanocomposite is 237 MPa, which is higher than the monolithic alloy (AZ31) (203 MPa) by 16.5 %
3. The ductility of the three materials, i.e., monolithic alloy and the two composites, was quantified based on elongation over a 0.5 inch (12.7 mm) gage length. The carbon-nanotubes reinforced magnesium alloy showed a higher (17 pct) elongation when compared one-on-one with the monolithic counterpart AZ31 (13 pct) and the $Al_2O_3$ particulate-reinforced magnesium alloy composite (10 pct).

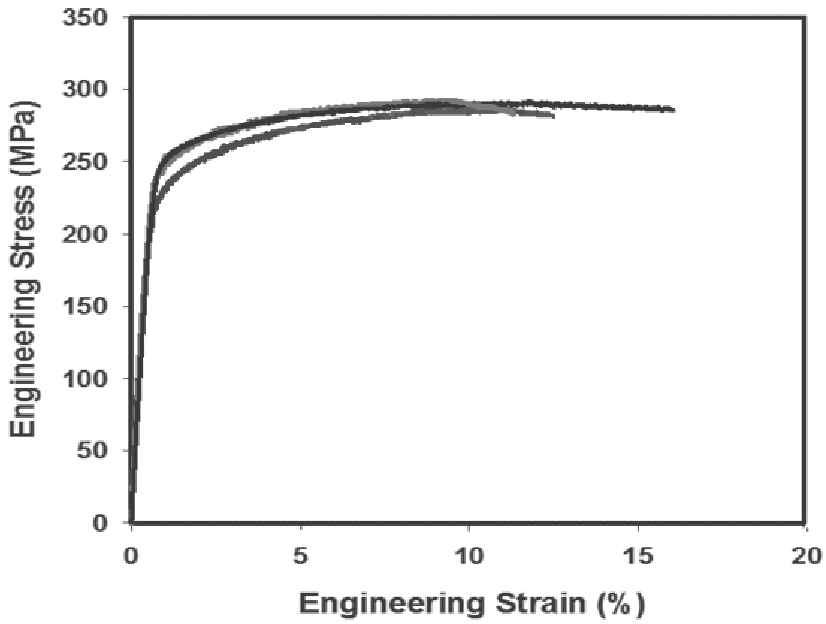


***Figure 2:*** Comparison of the engineering stress versus engineering strain curves for the AZ31 monolithic alloy and AZ31/$Al_2O_3$, AZ31/CNT nanocomposites.

The engineering stress versus strain curves for the extruded monolithic alloy (AZ31) and two nanocomposites are compared in Figure 2. Test samples of the monolithic alloy and the nanocomposites exhibited identical elastic behavior and near similar strain hardening characteristics from the onset of yield up until the maximum load, i.e., ultimate tensile strength, at which point occurs the onset of necking prior to catastrophic failure. Samples of the monolithic alloy and the two composites revealed sizeable plastic strain prior to failure. At any value of strain, from the onset of testing up until failure, the corresponding stress was marginally higher for the AZ31/CNT composite when compared to the monolithic alloy (AZ31) and the AZ31/$Al_2O_3$ nanocomposite.

Pure magnesium having hexagonal close-packed (HCP) crystal structure, favors slip only on its basal planes and has a limited, or restricted, number of slip systems at ambient temperature (25oC) thus placing a constraint on its ductility. The introduction of alloying elements (aluminum and zinc) and reinforcements (alumina ($Al_2O_3$) particulates and CNT) promotes the activation of non-basal slip systems while concurrently enabling an improvement in mechanical properties.

The observed improvement in mechanical properties of the $Al_2O_3$ particulate-reinforced magnesium alloy composite when compared to the monolithic alloy (AZ31) is ascribed to be due to following interactions,

(a) Matrix and alumina nano particle reinforcements [1, 31], and,
(b) Presence of the □ phase $Mg_{17}Al_{12}$) in the magnesium alloy metal matrix [32, 33].

These interactions result in a mismatch strain at the 'local' level thereby facilitating a higher density of dislocations and "localized" stress in the matrix immediately around the reinforcing phase. The increase in dislocations density contributes to strengthening of the material, i.e., it provides more resistance to deformation under uniaxial tension. The observed reduction in ductility of the AZ31/Al2O3 composite is partially attributed to the presence of a high volume of the eutectic β (Mg17Al12) both at and along the grain boundaries of the composite (Figure 1b). Due to strain incompatibility between the □-phase (body-centered cubic structure) and the matrix (hexagonal closed packed crystal structure) there is a tendency for fine microscopic cracks to nucleate at the interface under the influence of a far-field tensile load.

Similar improvements in mechanical properties were observed for the composite AZ31/CNT when compared to the monolithic alloy AZ31. A near uniform distribution of the CNT in the magnesium alloy metal matrix coupled with optimum processing (DMD) plays a key role in influencing properties of the composite. This in combination with high elastic modulus (up to 1 TPa) and good plastic deformation capability of the reinforcing CNTs contributed to improving the yield strength with a noticeable improvement in ductility of the nanocomposite (AZ31/1.0 vol. % CNT) when compared to monolithic counterpart (AZ31).

**5.3 TENSILE FRACTURE BEHAVIOR** The tensile fracture surface of monolithic alloy and the composites were examined in a scanning electron microscope (Model: FEI: Quanta 200) primarily to examine, interpret and rationalize the specific role and contribution of reinforcement and processing on microstructural features and resultant intrinsic microstructural effects on strength and ductility of the chosen composites. Representative scanning electron micrographs of the tensile fracture surface of the monolithic alloy and the composite are grouped and compared at a similar magnification in three different regions: (i) Overall morphology of failure (Figure 3), (ii) Region of predominantly transgranular failure (Figure 4), and (iii) The region of overload (Figure 5).

The overall morphology of the fracture surface of the three materials is shown in Figure 3. The fracture morphology of the monolithic alloy (AZ31) revealed a partial cup and cone type failure with the presence of an array of both macroscopic and fine microscopic cracks (Figure 3a). Compared to the monolithic alloy the fracture surface of the AZ31/Al2O3 (Figure 3b) was found to be essentially flat and normal to the far-field stress axis providing indication and/or evidence of little deformation by shear. For the AZ31/CNT composite (Figure 3c) the fracture surface revealed failure to be at an inclination to the far-field tensile stress axis suggesting the occurrence of shear prior to failure. Overall morphology of failure of the AZ31/CNT composite suggests deformation culminating in failure to be driven by shear stress.

The transgranular fracture surface observed at 500X is compared in Figure 4. High magnification observations of the transgranular regions of tensile fracture surface of the monolithic alloy (AZ31) revealed the profile, orientation and distribution of the macroscopic cracks indicative of the "locally" operating brittle failure mechanisms (Figure 4a). The transgranular regions of the alumina particle-reinforced composite (Figure 4b) was observed to be flat, near featureless inlaid with an observable population of fine microscopic voids and pockets of distinctly shallow dimples indicative of "localized" ductile and brittle deformation mechanisms. The transgranular fracture regions of the AZ31/CNT composite was observed to be covered with a noticeable population of dimples of varying size and shape (Figure 4c) intermingled with sparsely populated microscopic cracks indicative of the occurrence of intense plastic deformation around the reinforcing CNT nanoparticles and brittle deformation in the metal matrix at the 'local' level.

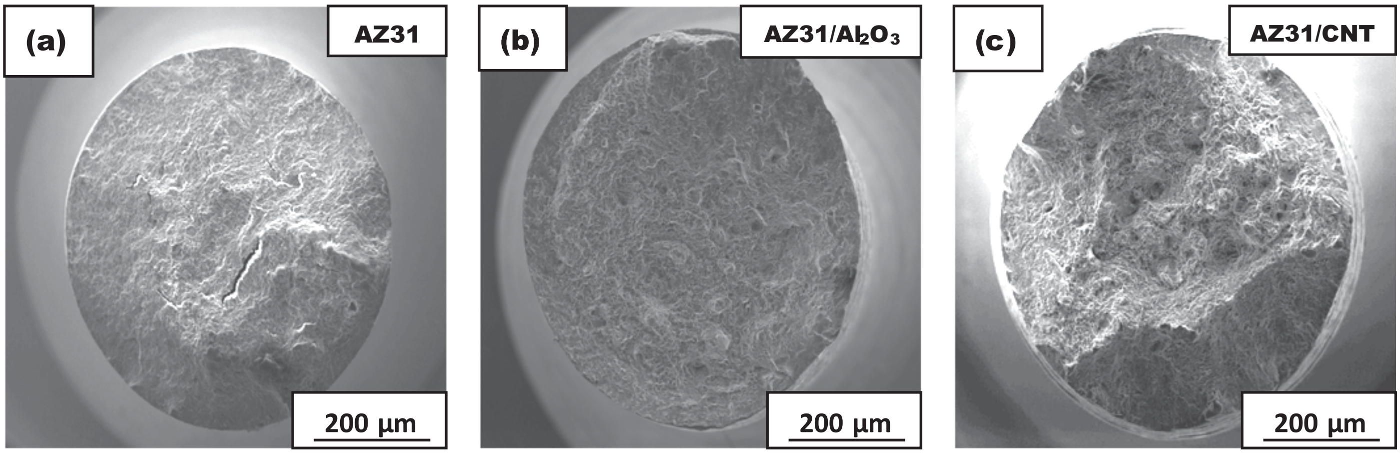


***Figure 3:*** Scanning electron micrographs showing overall morphology of failure:

(a) Magnesium alloy AZ31
(b) AZ31 reinforced with Al2O3p
(c) AZ31 reinforced with CNT

The overload region of the fracture surface of both the monolithic alloy and the composites is compared at a high magnification and shown in Figure 5. High magnification observation of the overload fracture surface of the monolithic alloy revealed a population of shallow voids and dimples intermingled with fine microscopic cracks (Figure 5a) suggesting the occurrence of both ductile and brittle failure mechanism at the 'local' level. Similar observations were made in the region of tensile overload (Figure 5b) of the Al2O3 particulate reinforced composite and revealed a noticeable distribution of fine microscopic cracks coupled with a random distribution of shallow dimples and fine microscopic voids. The region of tensile overload of the CNT-reinforced composite when viewed at progressively higher magnifications of the scanning electron microscope revealed a population of dimples (Figure 5c) indicative of the "locally" operating ductile failure mechanisms.

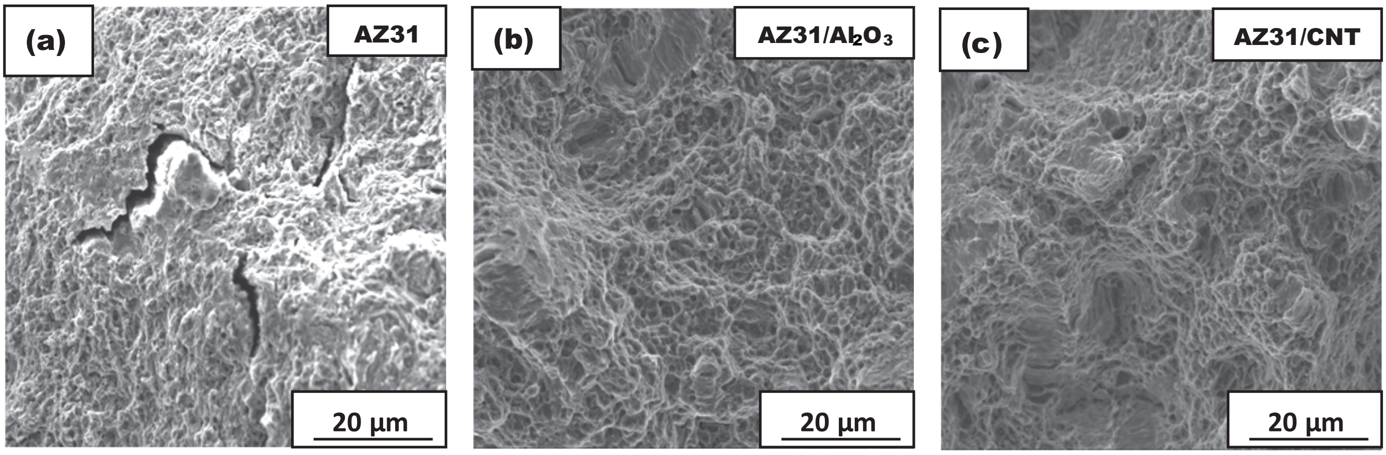


***Figure 4:*** High magnification observation showing intrinsic features on the tensile fracture surface.

(a) Macroscopic cracks of varying size and orientation on the tensile fracture surface (AZ31).
(b) Shallow dimples intermingled with microscopic cracks suggesting localized ductile and brittle deformation (AZ31/Al2O3).
(c) Higher population of dimples surrounded by microscopic cracks (AZ31/CNT).

These features observed on the fracture surface of the monolithic alloy (AZ31) are clearly indicative of the occurrence of "locally" operating brittle and ductile failure mechanisms at the microscopic level. Overall morphology of fracture of the monolithic alloy was macroscopically brittle, but features indicative of a blend of brittle and ductile mechanisms at the microscopic level. Compared to the monolithic alloy the alumina particulate-reinforced composite revealed a predominantly brittle type of failure evident from the presence of a healthy population of fine microscopic cracks and pockets of shallow dimples and voids on the fracture surface. The higher ductility (17 pct) of the CNT-reinforced composite is well reflected by the microscopic features observed on the tensile fracture surface, i.e., primarily dimples, voids and fewer microscopic cracks when compared to both the monolithic alloy and the AZ31/Al2O3 composite.

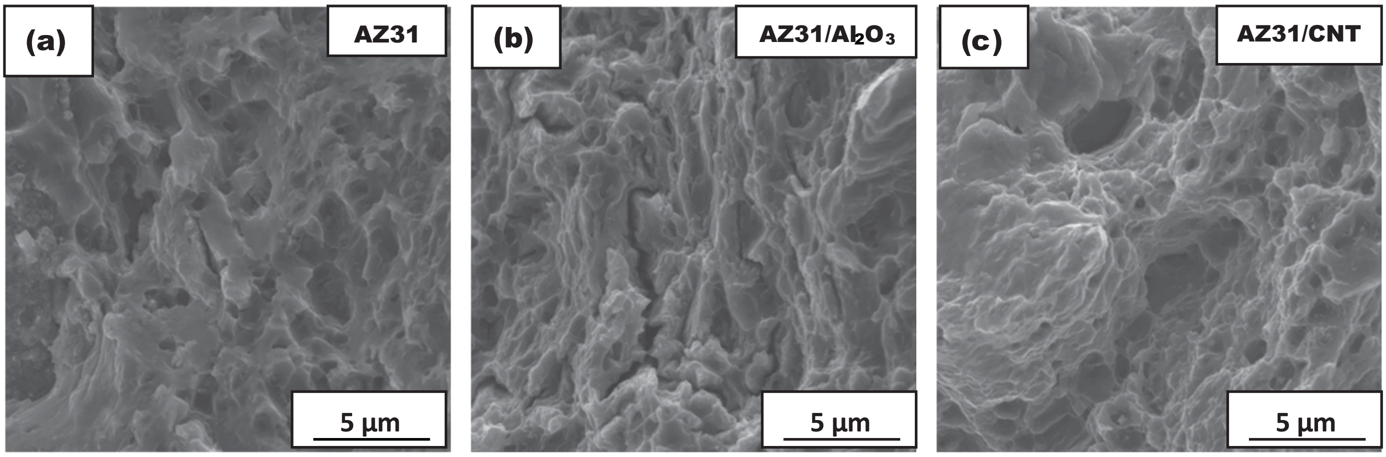


***Figure 5:*** High Magnification Scanning electron micrographs showing the region of overload.

(a) Microscopic cracks voids of varying size and shape and dimples (AZ31).
(b) Voids and dimples on the overload fracture surface reminiscent of locally ductile failure mechanisms (AZ31/Al2O3).
(c) The overload fracture surface showing the size, shape and distribution of dimples (AZ31/CNT).

# 6. CONCLUSIONS

Based on an investigation of the intrinsic influence of alumina nanoparticle and carbon nano-tube reinforcements on microstructural development, tensile response and tensile fracture behavior of a magnesium alloy (AZ31), following are the key findings:

1. The monolithic alloy (AZ31) and nano-composites AZ31/Al2O3 and AZ31/ CNT were successfully synthesized using the technique of disintegrated melt deposition technique followed by hot extrusion.

2. Microstructure of both the monolithic alloy (AZ31) and the composites consisted of α-Mg and the eutectic phase β-Mg17Al12. Presence of the carbon nanotubes assists in (i) refining the grain size, (ii) retaining a fine grain morphology, and (iii) morphology of the eutectic phase in the in AZ31/CNT nanocomposite. A refinement in grain size coupled with near uniform distribution of the fine grains was also observed in the alumina particle-reinforced composite (AZ31/Al2O3). However, unlike the CNT-reinforced composite, a higher volume of the eutectic Mg17Al12 (□) phase was observed along the grain boundaries of this composite.

3. Improvements in both yield strength and ultimate tensile strength was observed for the two composites when compared to the monolithic alloy (AZ31). This noticeable improvement is ascribed to be due the conjoint and mutually interactive influences of (i) a refined microstructure, (ii) high modulus of the reinforcing phases (Al2O3p and CNT), and (iii) compatibility between the reinforcing phase and the metal matrix resulting in proper load transfer between the two constituents of the composite.

4. Alumina particle-reinforced composite showed lower ductility when compared one-on-one with the monolithic alloy (AZ31) and the composite AZ31/CNT. This is ascribed to the presence of a higher volume of the eutectic Mg17Al12 (□) phase that was present along the grain boundaries of the composite and acted as preferential sites for crack initiation due to phase incompatibility. The CNT reinforced composite revealed superior ductility of the three materials studied. The observed improvement in ductility is attributed to the presence of well dispersed CNTs (achieved by processing) in the magnesium alloy metal matrix, presence of a stable intermetallic phase, coupled with properties of high elastic modulus and high strength of the reinforcing carbon nanotubes.

# REFERENCES


1. H. Zhi Ye, X Yang Liu, Journal of Materials Science, vol. 39 (2004), p. 6153 – 6171.

2. T.S. Srivatsan, T.S. Sudarshan, in: Rapid Solidification Technology: An Engineers Guide, Technomic Publishing Company, Lancaster (1993), pp. 603–720.

3. S. Nair, J. K. Tien and R. C. Bates: International Metals Reviews, Vol. 30, No. 6, 1985, p. 285-297.

4. K.K. Chawla: Composite Materials, Springer-Verlag New York, USA, 1987.

5. D.A. Koss and S.M. Copley: Metallurgical Transactions, Vol. 2A, 1971, p. 1557-1560.

6. M.M. Avedesian and H. Baker (editors) ASM Specialty Handbook: Magnesium and Magnesium Alloys, ASM International, Materials Park, Ohio, UA, 1999

7. Polmear, I.J., Light alloys: from traditional alloys to nanocrystals2006: Butterworth-Heinemann.

8. T.S. Srivatsan, Meslet Al-Hajri, P.C. Lam: Composites: Part B, Vol. 36 (2005), p. 209–222

9. S.Seshan, M.Jayamathy, S.V. Kailas, T.S. Srivatsan: Materials Science and Engineering A, Vol.363 (2003), pp. 345-351

10. K.F. Ho, M. Gupta, T.S. Srivatsan: Materials Science and Engineering A, Vol. 369 (2004), p. 302–308

11. Wang Ji-jie, Guo Jin-hua, Chen Li-qing: Trans. Nonferrous Met. Soc. China, Vol.16 (2006), p. 892-896

12. M. Paramsothy, J. Chan, R.Kwok, M. Gupta., Journal of Alloys and Compounds, 2011. 509(28), p. 7572-7578.

13. Z. Trojanova, V. Gartnerova, P. Lukac, Z. Drozd, Journal of Alloys and Compounds, vol. 378, Issues 1-2, (2004), p. 19-26

14. Habibnejad-Korayem, M., R. Mahmudi, and W.J. Poole, Materials Science and Engineering: A, 2009. 519(1-2),p. 198-203.

15. Q.B Nguyen and M. Gupta, Journal of Alloys and Compounds, 2008. 459(1-2),pp. 244-250.

16. T.S. Srivatsan and J. J. Lewandowski: Metal Matrix Composites: Types, Reinforcements, Processing, Properties and Applications, in Advanced Structural Materials (editors: W.O. Soboyejo and T. S. Srivatsan), Taylor & Francis, USA, 2005.

17. M.K Habibi, M Paramsothy, A.M.S. Hamouda , M Gupta . Composites Science and Technology, 2011. 71(5), p. 734-741.

18. M. Paramsothy, J. Chan, R. Kwok and M. Gupta, Composites Part A: Applied Science and Manufacturing, 2011. 42(2), p. 180-188.

19. Yongha Park, Kyungmox Cho, Ikmin Park, Yongho Park, Procedia Engineering, 2011. 10(10), p. 1446-1450.

20. Thakur, S.K., T.S. Srivatsan, and M. Gupta, Materials Science and Engineering: A, 2007. 466(1-2), p. 32-37.

21 L.M. Tham, M. Gupta, L. Cheng: Materials Science Technology, Vol. 15 (1999), p. 1139-1146.

22. M. Gupta, M.O. Lai, S.C. Lim, Journal of Alloys and Compounds. Vol. 260 (1997), p. 250-255.

23. M. Gupta and T. S. Srivatsan, Journal of Materials Engineering and Performance, Vol. 8, No. 4 (1999), p. 473-478.

24. P.S. Ling, M. Gupta, M.O. Lai and T.S. Srivatsan, Aluminum Transactions: An International Journal, Vol. 2, No. 2 (2000), p. 209-215,.

25. V. V. Ganesh, M. Gupta, and T. S. Srivatsan, Journal of Recent Research Developments in Materials Science and Engineering, ISBN: 81-7895-057-X, p. 119-136, 2002.

26. M. Marya, L. G. Hector, R. Verma, and W. Tong: Materials Science and Engineering A, Vol. 418 (2006), p. 341–356.

27. Z. Hong-liang, G. Shao-kang, Z. Fei-yan, L. Qing-kui, W. Li-guo, Transactions of Nonferrous Metals Society of China, vol 15 (2005), p. 144-148.

28. Magnesium Alloys - Design, Processing and Properties, Edited by : Frank Czerwinski, Katarzyna N. Braszczyńska-Malik, Published by InTech, 2011, p. 95-112

29. X. Fan, W. Tang, S. Zhang, D. LI and Y. Peng, Acta Metallurgica Sinica (English Letters), vol.23 No.5, (2010), p. 334-342.

30. Y. Radi; R. Mahmudi , Materials Science & Engineering: A, vol 527 (2010), p. 2764-2771

31. K.K. Deng, K. Wu, Y.W. Wu ,K.B. Nie, M.Y. Zheng , Journal of Alloys and Compounds, vol 504 (2010), p. 542-547

32. Gu Xin-fu, Zhang Wen-zheng , Zhang Min, YE Fei, Transactions of Nonferrous Metals Society of China , vol 17(2007), p. s1-s7.

33. J.F. Nie, Scripta Materialia, vol 48 (2003), p. 1009–1015.

# DETERMINATION OF FORMING LOADS OF Al-5Zn-1Mg USING ECAE AT VARIOUS TEMPERATURES

James Valder
Department of Metallurgical and Materials Engineering,
National Institute of Technology Karnataka Surathkal, Srinivasanagar,
D.K Dist., Mangalore, Karnataka
jamesvalder@gmail.com Tel: +91-824-2474000

Rijesh M
Department of Metallurgical and Materials Engineering,
National Institute of Technology Karnataka Surathkal, Srinivasanagar,
D.K Dist., Mangalore, Karnataka

A O Surendranathan
Department of Metallurgical and Materials Engineering,
National Institute of Technology Karnataka Surathkal, Srinivasanagar,
D.K Dist., Mangalore, Karnataka

## ABSTRACT

In the present study, an attempt has been made to study the flow stress of Al-5Zn-1Mg alloy in the temperature range of 303K to 673 K. Aluminium rods were melted and alloyed with Zinc and Magnesium to get an alloy of Al-5Zn-1Mg (5%Zn & 1% Mg). Cylindrical specimen of 20-mm diameter & 60-mm height were machined from Al-5Zn-1Mg alloy and annealed in a furnace at 573K for 2 hours. The equal channel angular extrusion experiments were carried out in a 250T hydraulic press at a cross head speed of 13 mm/sec. Lubricant based on molybdenum disulfide (MoS2) was used. The test was carried out at temperatures 303, 373, 473, 573 and 673 K. From the force stroke diagram, maximum load for equal channel angular extrusion was found out at various temperatures. The comparisons of maximum load at various temperatures were done. It shows maximum plasticity in the temperature range of 373-573 K and the stress required for deformation is more at 303 K. The plot of punch pressure vs temperature shows a maximum at 303 K and a minimum at 573 K. The working temperature range for this alloy is from 373-573 K from the aspect of lower flow stresses. Ring compression test conducted between 373-573 K gives the lowest friction factor at 373 K. Therefore Al-5Zn-1Mg alloy is best to work near 373 K. Lesser forces are sufficient implying lower capacity presses and less complicated design of tooling.

***Keywords:*** Al-5Zn-1Mg alloy, ECAE, Ring compression test, Force, Stroke, Stress

## 1. INTRODUCTION

Equal channel angular extrusion (ECAE) is a metal working process developed by Segal [1, 2] in the former Soviet Union. It comprises the deformation of a billet of material through two intersecting channels of equal cross-sectional area lying at an angle 2ø to each other (Fig.1).

The imposed strain per pass is a function of channel angle [1, 3]. Because the deformation is essentially simple shear in nature, the workpiece undergoes no change in cross-section, thus enabling the use of substantially smaller ingots / billets to obtain a semi-finished product of a given size. This feature is particularly advantageous for ingot metallurgy alloys prone to macro-segregation. Other advantages include the ability to impart large strains in multipass operations and the ability to vary crystallographic (and mechanical) texture through judicious selection of processing sequence during such multipass operations. The ability to impart large strains is specially attractive with regard to obtaining refined microstructures that may provide enhanced superplastic forming / isothermal forging / roll forming characteristics or ultrahigh strength for service. Submicron or even nanometer size will be gained, and strength and plastics will improve greatly with fine grains [4]. To the present, the majority of research and development on ECAE has been conducted on easy-to-work aluminum alloys and copper [5, 6]. Such materials are typically worked under nominally isothermal conditions (tooling and workpiece at the same initial temperature) and present few challenges with regard to workability. On the other hand, difficult-to-work materials such as those utilized in the aerospace industry have much lower workability. The present paper summarizes work on the ECAE behavior of a difficult-to-extrude alloy [7] Al-5Zn-1Mg. The material was cold-worked under isothermal conditions, warm worked and hot-worked via non-isothermal ECAE. The objectives of this research were to establish a working range of temperature where maximum plasticity is observed and further narrowing the range with the aspect of flow stress and frictional conditions.

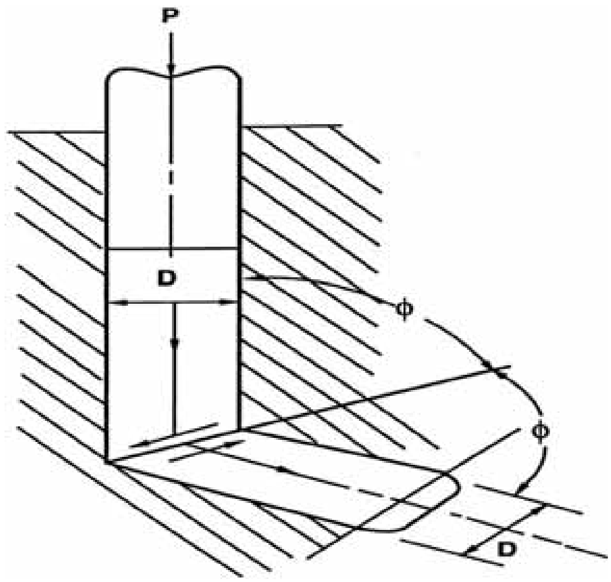


*Fig.1.* Schematic illustration of the equal channel angular extrusion process

## 2. MATERIALS AND METHODS

**2.1 MATERIALS** The materials used in this investigation comprised Al-5Zn-1Mg. The compositions of this alloy in weight percent is: 5 zinc, 1magnesium, balance aluminium. Its microstructure consisted of well developed dendrites which is typical for a cast structure. Prior to its use in the program, it was homogenized at temperature 573 K to promote uniformity of chemical composition and microstructure.

**2.2 EXTRUSION EXPERIMENTS** ECAE trials were conducted at temperatures between 303 K and 673 K to determine the flow characteristics of Al-5Zn-1Mg under cold, warm and hot working conditions. For this purpose, 60-mm long samples were cut and machined to cross-section dimensions of 19.8 mm diameter. The ECAE tooling for the present trials was of the design developed by Segal et al. The ECAE die was made of AISI M2 tool steel and was capable of being heated to a maximum temperature of 673 K. The tooling temperature was room temperature. The channel had an angle (2ø) equal to 150° and dimensions of 20 mm diameter; these die dimensions were conducive to easy insertion of the round billets but nonetheless ensured a snug fit and limited billet upsetting prior to extrusion.

The ECAE tooling was mounted into a 250T hydraulic press for the extrusion experiments. Prior to extrusion, the preform and the extrusion container were coated with a molybdenum disulfide (MoS2) base lubricant. During the actual experiments, the extrusion preform was heated in an electric resistance furnace, transferred to the tooling and extruded one pass through the tooling using a constant ram speed of 13 mm/sec.

**2.3 RING COMPRESSION TESTS** Rings of (6:3:2) outer diameter , 24 mm inner diameter, 12 mm and height, 8 mm were machined and annealed in a furnace at 573 K for 1 hr. Compression was carried out in 40 T Universal Testing Machine. Velocity of ram was fixed as 3.3 X 10 -4 m /s. Molybdenum disulfide (MoS2) was the lubricant used and testing was carried out at different temperatures between 303 K and 673 K. The reduction in height and decrease in internal diameter were measured and using the calibration chart (Male and Cockroft 1964-65). The friction factor was estimated for Al-5Zn-1Mg at various temperatures.

## 3. RESULTS AND DISCUSSION

**3.1 MICROSTRUCTURAL INVESTIGATION** Micrograph showing typical microstructures is obtained in Fig.2.

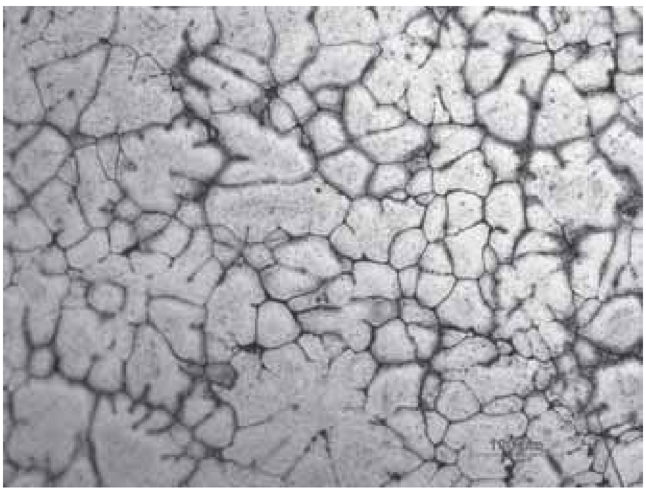

*Fig:2*. Typical microstrure of Al-5Zn-1Mg for as-cast material after homogenization

The as-cast material after homogenization and before extrusion shows partial breakdown of dendrites and uniformity in chemical structure. It is clear from the study conducted on as cast Al–0.63%Cu alloy by D. R. Fang et.al. that refining to submicron meter level by repeated shear deformation is possible for cast Al alloys. In addition, h phase in Al–3.9%Cu alloy disperses more uniformly than those of the as-received condition, and had almost been broken into many small disperse particles [8].Similar results are expected for Al-5Zn-1Mg alloys once the optimum processing temperature is determined.

**3.2 FORCE STROKE GRAPHS OF ECAE** During ECAE, the force –stroke graphs were recorded. Typical extrusion force versus stroke diagrams are shown in Fig.3. (Corresponding to first pass). The entry side of the specimens was tapered and this is indicated in the force stroke graph by a change in slope in the initial stage. The transition of slope indicates end of extrusion of the tapered length.

**3.3. ANALYSIS OF FORMING LOADS** One of the main aims of the study was to analyze the forming loads required and how they vary during the process temperatures. From the extrusion force versus stroke diagram (Fig. 3) it is observed that these curves show a maximum force between 10 – 20 mm stroke lengths. This value is taken to serve as a basis of comparison which is shown in Fig .4. This is in accordance with Djavanroodi and Ebrahimi[9] who observed an increase in the pressing pressure with the ram movement until shear strain imposed to the sample. From this point (maximum punch pressure), the pressing pressure decreases with a very slow rate which is continuous to the end of the process. The magnitude of punch pressure is a major factor to be considered for selecting the suitable hydraulic press in designing the ECAP die.

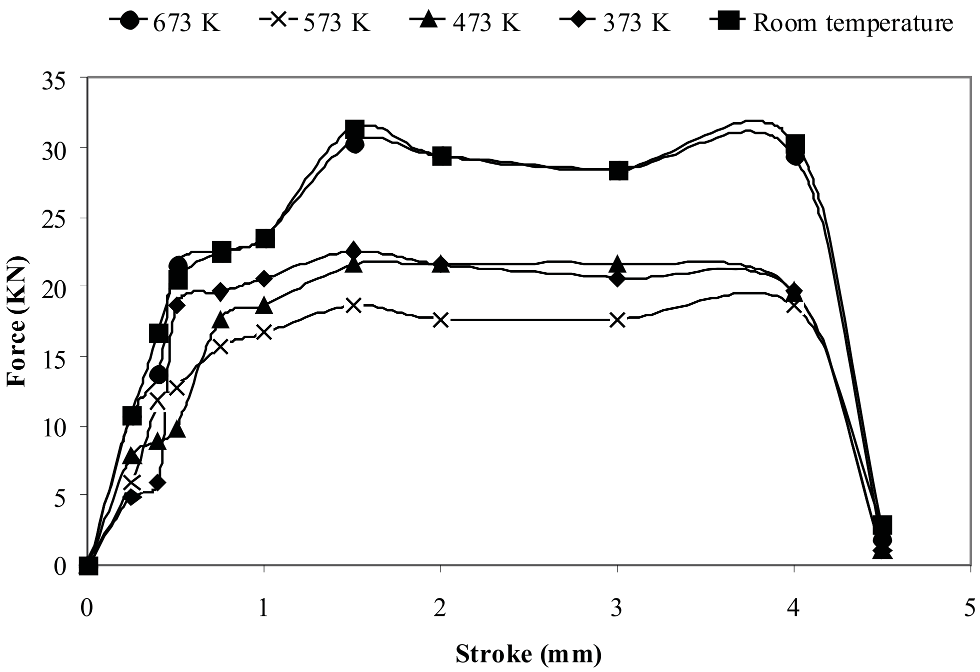


***Fig. 3.*** .Extrusion force – stroke curves obtained during pass1 at various temperatures of ECAE

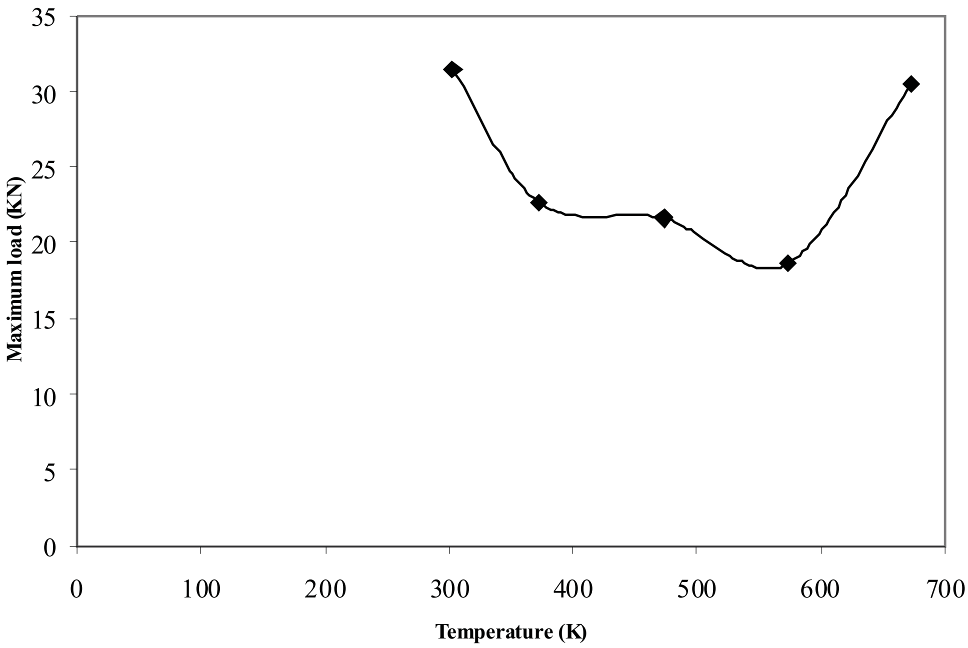


***Fig. 4.*** Forming load at various temperatures during pass1 of ECAE

The key results of this investigation are described below in Table.1. on ECAE behavior during isothermal cold-working and non-isothermal warm and hot working.

***Table.1.*** Deformation observation for ECAE of Al-5Zn-1Mg alloy

| Temperature (K) | Ram speed (mm/sec) | Maximum load (KN) |
|---|---|---|
| 303 | 13 | 31.4 |
| 373 | 13 | 22.6 |
| 473 | 13 | 21.6 |
| 573 | 13 | 18.6 |
| 673 | 13 | 30.4 |

**3.4. ISOTHERMAL ECAE OF AL-5ZN-1MG** Metal flow during isothermal ECAE of Al-5Zn-1Mg at room temperature was quantified using ECAE results. At room temperature, the Al-5Zn-1Mg (Fig. 3, Table 1.) took 31.4 KN to extrude completely.

**3.5. NON-ISOTHERMAL ECAE OF AL-5ZN-1MG** As the temperature was raised, a transition in flow was observed for same extrusion speed. Flow resistance of material was decreasing as the temperature was increasing. It shows maximum plasticity in the temperature range of 373-573 K and the stress required for deformation is more at 303 K.However at the highest extrusion temperature (673 K) flow stress increased because of dynamic strain ageing in this temperature range. Dynamic strain ageing increases the flow stress and decreases the ductility [10].DSA is totally undesirable during mechanical processing. Therefore this temperature range should be avoided while ECAE of Al-5Zn-1Mg

The plot of forming load Vs temperature (Fig.4) shows a maximum at 303K and a minimum at 573K. The working temperature range for this alloy is from 373-573 K from the aspect of lower flow stresses.

**3.6. ROLE OF FRICTION** Friction coefficient has a noticeable effect on the magnitude of the punch pressure requirement and this pressure increases with increasing the friction coefficient. For example, when friction coefficient decreases from 0.3 to 0.001 in the die channel angle of 110°, the magnitude of the punch pressure reduces by 60%.[9] For deformation to be uniform across the cross section of the billet, friction at the specimen-die interface has to be minimized. With moderate friction, a small dead end zone develops at the die corner. In the present study the friction factor m was found out at different temperatures between 303 K and 673 K (Fig.5). The key results of this investigation are described below in table.2.

***Table.2.*** Friction factor (m) at various temperatures using Molybdenum disulfide (MoS2) as lubricant

| Temperature (K) | Friction factor (m) |
|---|---|
| 303 | 0.42 |
| 373 | 0.44 |
| 473 | 0.62 |
| 573 | 0.75 |
| 673 | 0.9 |

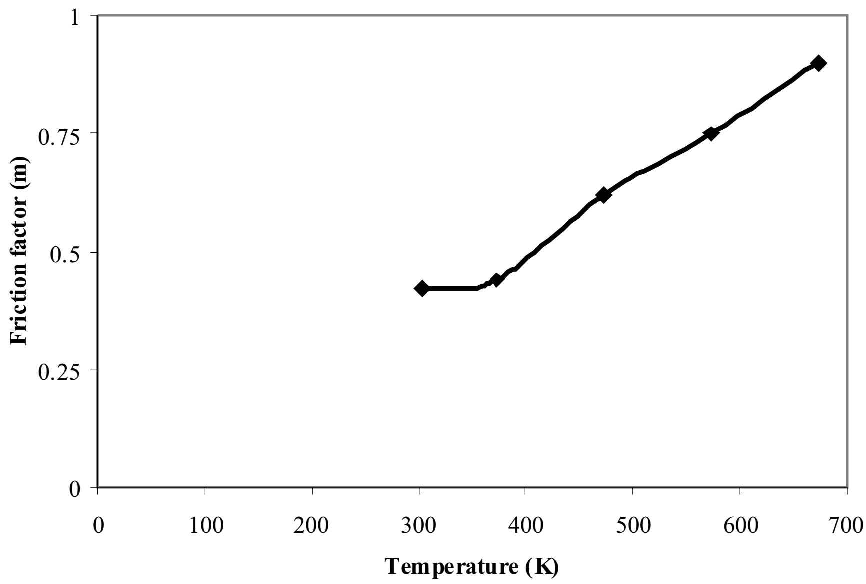


Fig.5. Friction factor (m) at various temperatures using Molybdenum disulfide (MoS2) as lubricant

## 4. CONCLUSIONS

An ECAE die was designed and specimens were subject to single pass at various temperatures 303 K and 673 K. It showed maximum plasticity in the temperature range of 373-573 K and the stress required for deformation is more at 303 K and a minimum at 573K. The ring compression results show least friction factor at 373 in the range of 373-573 K. Therefore below the recrystallisation temperature and above room temperature warm working is to be done to maximize the advantages of both hot and cold working (and minimize the disadvantages).

## ACKNOWLEDGMENT

The authors gratefully acknowledge the financial support by Board of Research in Nuclear Sciences India (Project Sanction No.:2006/37/35/T/BRNS).

## REFERENCES

[1] V. Segal, Equal channel angular Extrusion, ASM International Handbook, bulk metal forming, Vol 14A, 2006, p528-536.

[2] V.M. Segal, 'materials by simple shear' Mater. Sci.Eng. A 197, 1995, p157–164.

[3] Iwahashi Y, Wang J, Horita Z, Nemoto M, Langdon TG., Principle of equal channel angular pressing of ultrafine grained materials, Scr.Mater;35,1996, p143-147.

[4] Gang Yi Cai, Xiao Xia Liu “Finite Element Simulation of the Effects of Mould Angle on the Equal Channel Angular Pressing for Al-Zn-Mg-Cu Alloy” Advanced Materials Research, Volumes 97 - 101,2010

[5] R.Z. Valiev, T.G. Langdon, 'principles of equal channel angular pressing as a tool for grain refinement' Prog. Mater. Sci. 51, 2006, p881–981.

[6] Prangnell PB, Harris C, Roberts SM. 'Finite element modeling of equal channel angular extrusion', Scr Mater, 37, 1997, p983-989.

[7] M.Bauser, G.Saucer and K. Seigert, 'Extrusion second edition' ASM International Handbook, Materials Park, Ohio, 2006.

[8] D. R. Fang, Y. Z. Tian, Q. Q. Duan,S. D. Wu,Z. F. Zhang, N. Q. Zhao,J. J. Li “Effects of equal channel angular pressing on the strength and toughness of Al–Cu alloys” J Mater Sci (2011) 46:5002–5008.

[9] F. Djavanroodi , M. Ebrahimi 'Effect of die channel angle, friction and back pressure in the equal channel angular pressing using 3D finite element simulation', Materials Science and Engineering: A Volume 527, Issues 4-5, 15 February 2010, Pages 1230-1235.

[10] R.E.Reed Hill and Reza Abbaschean, Physical Metallurgy, Principles, PWS Publishing, Boston, 1994.

# INVESTIGATING AND UNDERSTANDING THE CYCLIC FATIGUE FRACTURE BEHAVIOR OF TWO HIGH STRENGTH SPECIALTY STEELS

T.S. Srivatsan
Division of Materials Science and Engineering
Department of Mechanical Engineering, The University of Akron
Akron, Ohio 44325-3903, USA, E-Mail: tsrivatsan@uakron.edu

K.Manigandan
Division of Materials Science and Engineering
Department of Mechanical Engineering, The University of Akron
Akron, Ohio 44325-3903, USA,

T.Quick
Department of Geology
The University of Akron, Akron, Ohio 44325-3903, USA

M.L. Schmidt
Alloy Development
Carpenter Technology Corporation, Reading, PA 19601, USA

## ABSTRACT

In this research paper, the cyclic fatigue fracture behavior of two high strength specialty steels, denoted as AerMet®100 and PremoMetTM 290, is presented and discussed. Both specialty steels have better properties to offer than most steels in this category and other high strength steels. This can be ascribed to be due to the synergistic and mutually interactive influences of chemical composition and secondary processing technique used for the two steels. The two high strength steels, designated by the manufacturer as AerMet® 100 and PremoMetTM 290, were produced using a combination of vacuum induction melting (VIM) and vacuum arc re-melting (VAR) and followed by casting as ingots. At the microscopic level, cyclic fatigue fracture of the two steels revealed features reminiscent of the occurrence of locally ductile and brittle failure mechanisms. Over a range of maximum stress and at the two different load ratios the steels were cyclically deformed it was observed that the cyclic fatigue resistance of the two steels was noticeably higher than companion high strength steels for which data is available in the published literature. The key mechanisms responsible for the observed fracture behavior of the two steels cyclically deformed over a range of maximum stress is presented and discussed.

***Key Words:*** Specialty steels, microstructure, cyclic fatigue, fracture behavior, mechanisms

## 1. INTRODUCTION

The burgeoning need created by the continuous demand for high performance materials for a spectrum of performance-critical applications culminated in the development and emergence of a variety of materials and metal alloys for a specific application and/or purpose. Attractive combinations of high specific strength ( ) and superior corrosion resistance coupled with noticeable innovations in vacuum processing techniques made possible the ease of manufacturing specialty steels, which provides a combination of good strength and acceptable ductility. The fatigue strength would increase with an increase in ultimate tensile strength of the low carbon and even the medium carbon steels having a lower strength. However, for the high strength steels whose ultimate tensile strength ($\sigma_{UTS}$) exceeds 1800 MPa; the fatigue strength would depend on both strength and toughness. The resultant microstructure of vacuum induction melted (VIM) / vacuum arc re-melted (VAR) steels is greatly refined when compared one-on-one with the conventionally processed counterpart, resulting in a noticeable improvement in both strength and toughness [1]. The high yield strength ($\sigma_{YS}$) provides the potential for an observable improvement in performance coupled with reduction in weight, attributes that are of both importance and need in a spectrum of structural applications and associated industries. For the low alloy high strength steels, the fatigue crack generally initiates at a larger non-metallic inclusions and the fracture surface often displays a fish-eye pattern [2–7]. In an independent study Kiedssling [8] proposed that the crack would not initiate at an inclusion when size of the non-metallic inclusion is less than 5 μm in "clean" steels from the point of view of fracture toughness. Similarly under conditions of cyclic fatigue there exists a critical size of the inclusion below which the origin of fatigue fracture will not occur by way of initiation at an inclusion.

***Table 1.*** Nominal chemical composition of the chosen materials

| Material | C | Mn | Si | P | S | Cr | Ni | Mo | Cu | Co | Al | Ti | Cb | V | N | O |
|---|---|---|---|---|---|---|---|---|---|---|---|---|---|---|---|---|
| **AerMet® 100** | 0.238 | <0.01 | 0.03 | 0.002 | 0.0007 | 2.99 | 11.2 | 1.18 | <0.01 | 13.4 | 0.003 | 0.011 | 0.003 | - | <0.001 | <0.001 |
| **PremoMet™ 290** | 0.404 | 0.79 | 1.50 | 0.003 | 0.0011 | 1.29 | 3.82 | 0.50 | 0.6 | 0.01 | 0.01 | 0.006 | <0.002 | 0.30 | 0.002 | <0.001 |

***Table 2.*** Primary and Secondary Processing History of the chosen High Strength Steels

| Material | Primary Processing | Secondary Processing plus finishing |
|---|---|---|
| **AerMet® 100** | (a) Melted by vacuum induction melting (VIM) and vacuum arc remelting (VAR) and cast to get ingots<br>(b) Ingot was then hot-worked to get 7.5 $inch^2$ block.<br>(c) Block was then hot rolled to get cylindrical bars having 0.75 inch diameter. | (i) The hot rolled bar (0.75 inch diameter) was annealed at 1250 F (677°C) for 6 hours and subsequently turned and ground to size.<br>(ii) The ground bar was tested and checked for defects using immersion sonic inspection.<br>(iii)The optimum annealed hardness was $40HR_C$<br>(iv)Exhibits minimal size change during heat treatment. |
| **PremoMet™ 290** | (a) Melted by vacuum induction melting (VIM) and vacuum arc remelting (VAR) and cast to get ingots<br>(b) Ingot was then hot-worked to get 7.5 $inch^2$ block.<br>(c) Block was then hot rolled to get cylindrical bars having 0.75 inch diameter. | (i) The hot rolled bar (0.75 inch diameter) was annealed and subsequently turned and ground to size.<br>(ii) The ground bar was tested and checked for defects using immersion sonic inspection. |

In this paper two steels which can be classified as being 'clean' in light of the processing techniques steels used were cyclically deformed over a range of maximum stress at two different load ratios (i.e.: ratio n of minimum stress to maximum stress). The observed difference in cyclic fatigue life and resultant failure behavior is discussed following scanning electron microscopy observation of the deformed and failed samples. At each load ratio two samples of the specialty steel that were cyclically deformed at high maximum stress and resultant short fatigue life and low maximum stress and resultant enhanced fatigue life were chosen for exhaustive examination in the microscope.

## 2. MATERIALS

The two high strength steels chosen for this study were AerMet ® 100 and PremoMetTM 290. The steels were provided by Carpenter Technology Inc., (based in Reading, PA, USA). The chemical composition of the two high strength specialty steels in provided in Table. 1. Presence of carbon provides solid solution strengthening coupled with hardenability through the formation and presence of alloy carbides. The presence of alloy carbides in the microstructure aids enhancing the high temperature resistance and overall creep strength of a predominantly ferrite matrix. Presence of the elements chromium [Cr], molybdenum [Mo], and cobalt [Co] aids in the formation and presence of second-phase carbide particles, which contribute to enhancing strength of the steel matrix. However, the presence and distribution of the alloy carbide particles in the microstructure is detrimental to fracture toughness, or impact resistance, arising as a result of an increase in the number of potential sites that are conducive for the early initiation of fine microscopic cracks. Presence of nickel [Ni] helps in lowering the transition temperature while concurrently enhancing toughness and stabilizing any austenite that is present in the high strength steel. The presence of molybdenum aids in refining the grain size, in addition to its role in forming molybdenum carbides and the resultant influence in enhancing toughness [9].

The high strength steels, designated by the manufacturer as AerMet® 100 (UNS K92580) and PremoMetTM 290, were produced using vacuum induction melting (VIM) immediately followed by vacuum arc re-melting (VAR) and then cast as ingots. AerMet® 100 is a high strength steel that possesses high hardness and high strength coupled with acceptable ductility and adequate toughness [10]. This steel has been used for designing components that require high strength, high fracture toughness coupled with exceptional resistance to stress-corrosion- cracking (SCC) and fatigue resistance [11]. The material has a nominal fracture toughness of 126 MPa$\sqrt{}$(m) and tensile yield strength of 1724 MPa [10]. The PremoMetTM 290 steel is free of cobalt. Further, this steel offers a combination of high strength and toughness in the quenched and tempered condition. This steel has an ultimate tensile strength ($\sigma$UTS) of 2040 MPa, a minimum fracture toughness of 77 MPa$\sqrt{}$(m) and excellent fatigue life [11]. A summary of the processing techniques used on the two specialty steels chosen for this research study is provided in Table 2.

# 3. EXPERIMENTAL PROCEDURES

**3.1 MICROSTRUCTURAL CHARACTERIZATION** Initial characterization of the as-provided specialty steels (AerMet 100 and PremoMet TM 290) was done using a low magnification optical microscope. Samples were cut to the desired size from the as-received stock of the specialty steel and then mounted in epoxy. The mounted samples were initially ground and rough polished using a series of silicon carbide impregnated emery paper [240-grit, 320-grit, 400-grit and 600-grit] with water being used both as a lubricant and coolant. Subsequently, the chosen two steel samples were fine polished using five-micron alumina suspended in distilled water and one-micron alumina suspended in distilled water. The polished samples were subsequently etched using Nital reagent [a solution mixture of 5-ml of nitric acid ($HNO_3$) and 90 ml of Ethanol]. The polished and etched surfaces of the two steel samples were observed in an optical microscope and photographed using standard bright field illumination technique.

**3.2 SAMPLE PREPARATION** Cylindrical test specimens, conforming to specifications outlined by American Society for Testing Materials, ASTM E8-06 [12], were precision machined for the four chosen high strength steels. The test specimens with threaded ends measured 120 mm in total length and 12.57 mm in diameter at the thread section. The gage section of the test specimen measured 25 mm in length and 6.25 mm in diameter. To minimize the effects of surface irregularities, the gage sections of the machined test specimens were initially mechanically ground using progressively finer grades of silicon carbide (SiC) impregnated emery paper and subsequently finish polished, to a mirror-like finish, using an alumina-based polishing compound. The purpose of polishing was to remove any and all of the circumferential scratches and surface machining marks [13].

**3.3 FAILURE-DAMAGE ANALYSIS.** A scanning electron microscope [Model: FEI Quanta 200] was used to examine the fracture surfaces of the deformed and failed fatigue samples. Observations were made over a range of magnifications to identify the macroscopic fracture mode and to concurrently establish the intrinsic microscopic mechanisms governing failure. Samples for observation in the microscope were obtained from the fully deformed and failed test specimens by sectioning parallel to the fracture surface.

# 4. RESULTS AND DISCUSSION

**4.1 INITIAL MICROSTRUCTURE** The microstructure of the chosen high strength steel is an important factor to be taken into account in evaluating its mechanical properties while concurrently establishing its performance when put to use in an application and its response in the event of failure or fracture while in use. Properties spanning tensile, fracture toughness, cyclic fatigue resistance and resultant fracture behavior must be analyzed or determined for it would help in providing an idea of how the material would perform while in service and potential applications for its use. The optical micrographs of AerMet® 100 and PremoMetTM 290 are shown in Figure 1 and Figure 2. The micrographs taken at a magnification of 100X essentially reveals the key ingredients in the microstructure of the two high strength steels to be a combination of martensite and ferrite. A higher carbon content in the steel resulted in a greater volume fraction of martensite. No attempt was made in this study to establish the volume fraction of martensite in the microstructure. The presence of martensite was noticeable in large numbers and has essentially'lath' morphology in both the AerMet® 100 and PremoMetTM 290 steels that were produced by vacuum induction melting (VIM) and vacuum arc re-melting (VAR). The presence of these key microstructural features is governed by a combination of chemical composition and the primary processing technique used and does exert an influence on fracture toughness, tensile properties, fatigue response and fracture behavior of the candidate steels.

**4.2 CYCLIC FATIGUE FRACTURE BEHAVIOR**

**4.2.1 Load Ratio [r] = 0.1**

**[A] AerMet® 100**

Scanning electron micrographs of the test specimen that was cyclically deformed at a maximum stress of 1672 MPa and a resultant fatigue life of 8126 cycles are shown in Figure 3. Overall morphology of the surface of the failed sample is as shown in Figure 3a and was essentially normal to the far-field stress axis. At gradually higher magnifications, a distinct demarcation is seen between the regions of fatigue and overload (Figure 3b). The region of crack initiation and early microscopic crack growth was predominantly transgranular and contained an array of fine microscopic cracks (Figure 3c). This is indicative of the occurrence of “locally” brittle failure mechanism. The region of stable crack growth when observed at a lower magnification failed to reveal any discernible or observable features, such as, striations (Figure 3d).

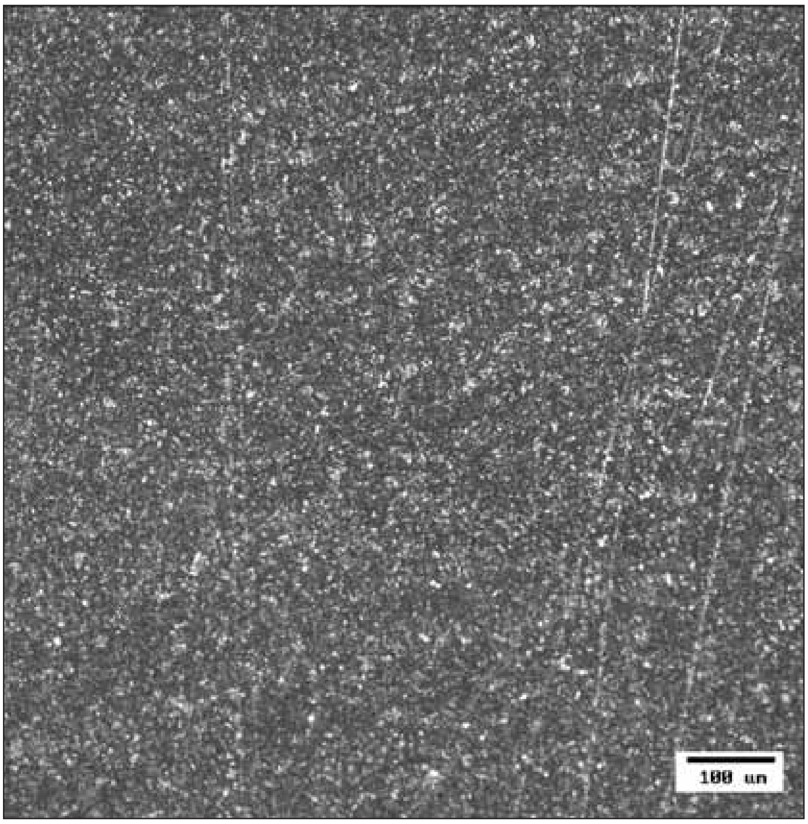


***Figure 1:*** Optical micrographs showing the key micro-constituents of AerMet® 100

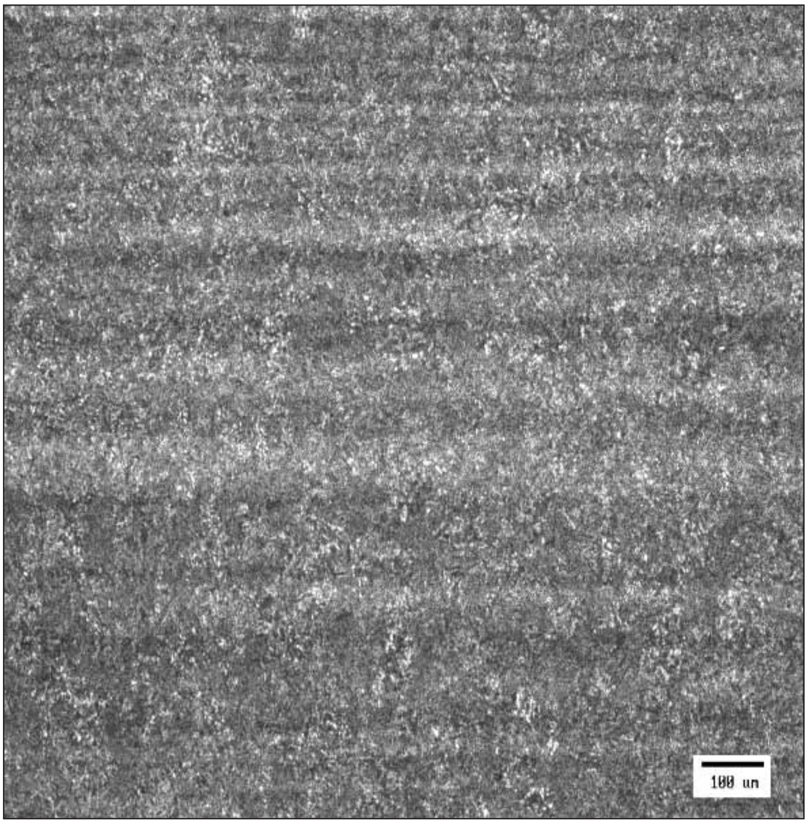


***Figure 2:*** Optical micrographs showing the key micro-constituents of PremoMetTM 290

At a lower maximum stress of 1232 MPa and resultant fatigue life of 38,051 cycles the key features of the deformed sample are shown in Figure 4. Overall morphology of the fatigue fracture surface was at an inclination to the far –field stress axis (Figure 4a). The region of stable crack growth revealed pockets of distinct striations randomly spaced and oriented, through the fracture region as shown in Figure 4b. Gradual high magnification observation of the region of stable crack growth revealed shallow nature of the striations intermingled with fine microscopic cracks, key features reminiscent of 'locally' ductile and brittle failure mechanisms (Figure 4c). The region of overload when observed at the higher allowable magnifications of the SEM revealed a noticeable population of microscopic voids and pockets of shallow dimples, features representative of the occurrence of 'locally' ductile failure at the fine microscopic level (Figure 4d).

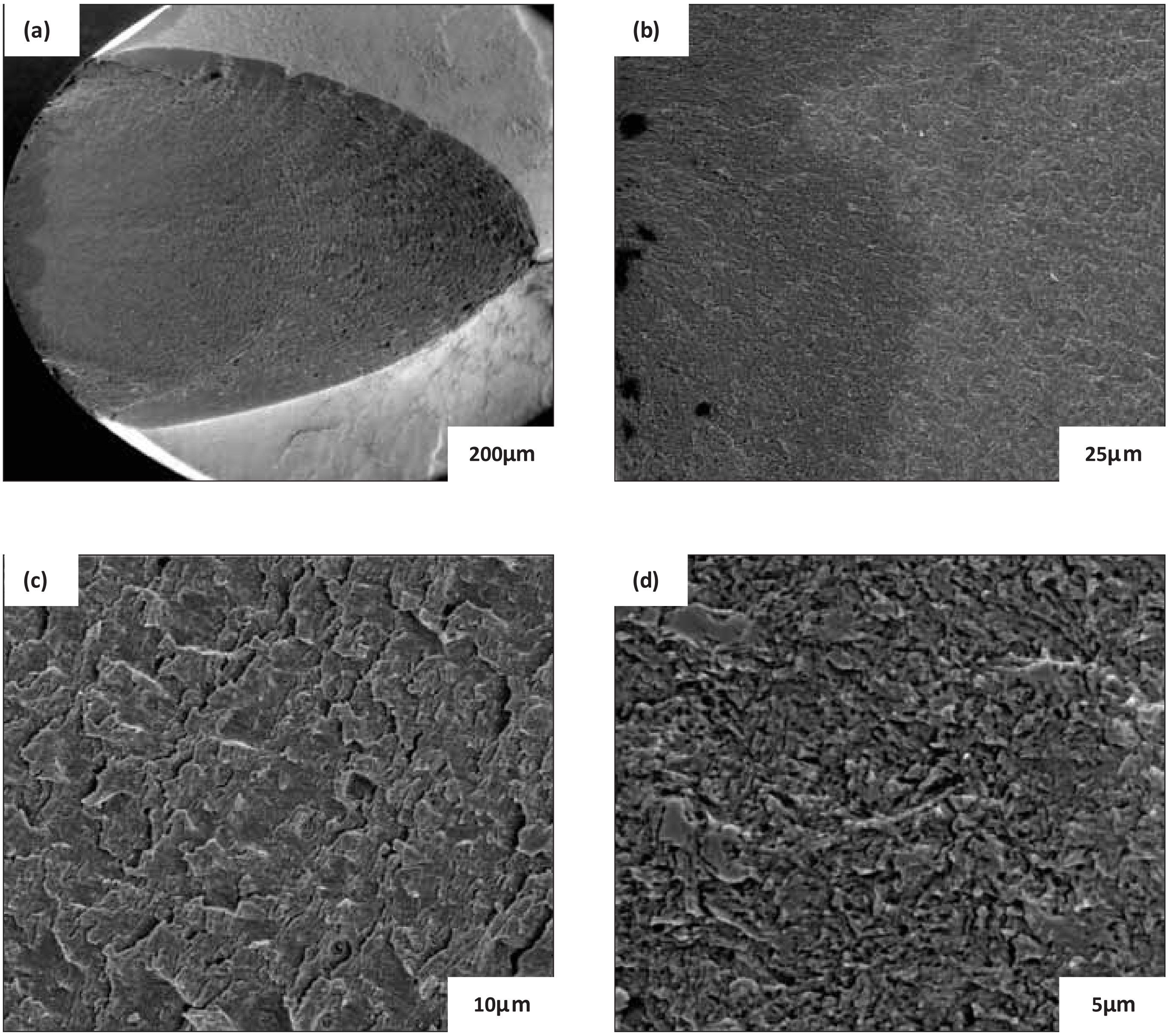


***Figure 3:*** Scanning electron micrographs of AerMet® 100 deformed in cyclic fatigue at maximum stress (σmax) of 1672Mpa, resultant fatigue life (Nf ) of 8126 cycles, showing:

(a) Overall morphology of failure.

(b) High magnification of (a) showing the distinct demarcation between the regions of fatigue and overload.

(c) The region of early microscopic crack growth predominantly transgranular with fine microscopic cracks.

(d) The region of stable crack growth at low magnification

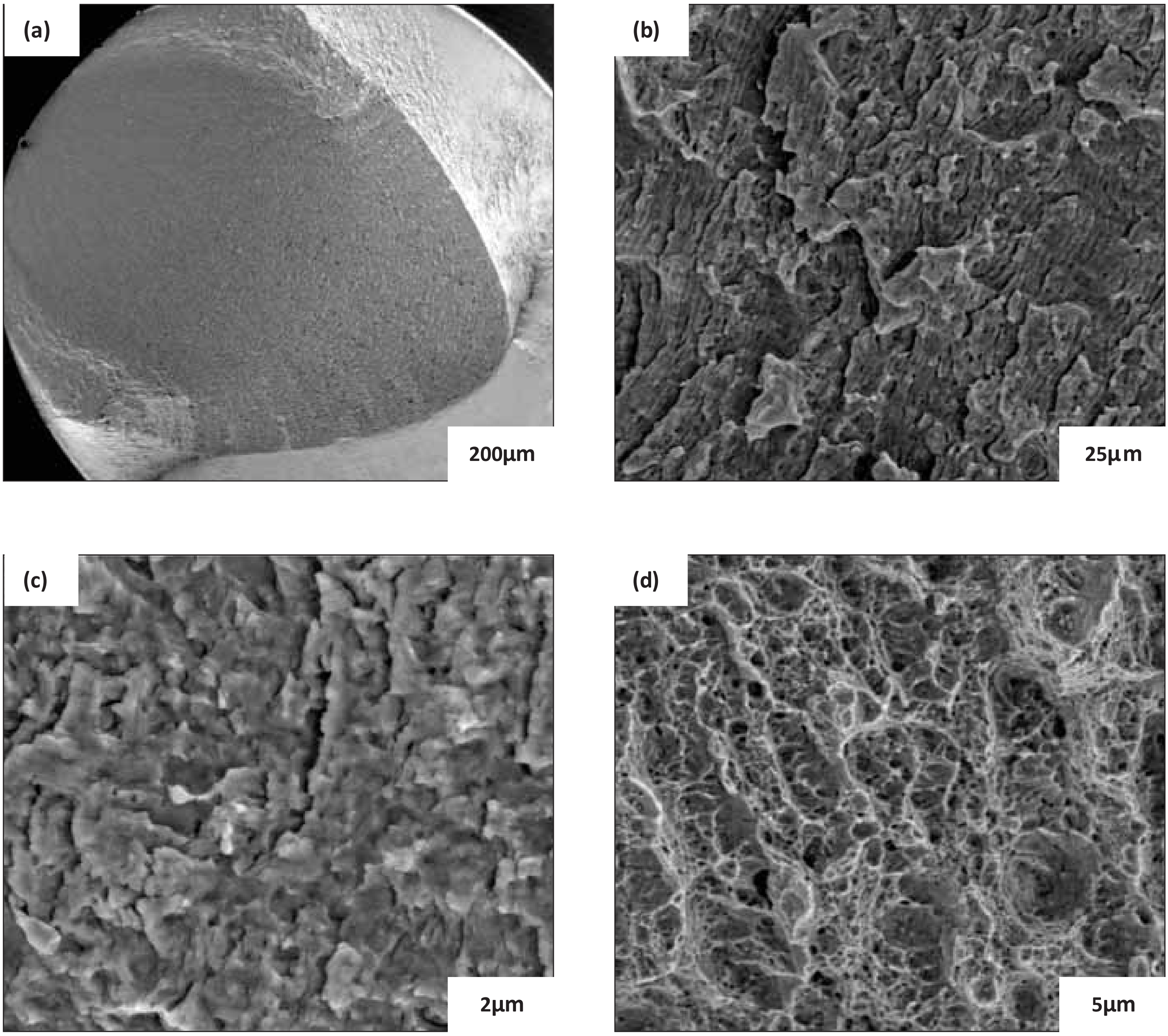


***Figure 4:*** Scanning electron micrographs of AerMet® 100 deformed in cyclic fatigue at maximum stress (σmax) of 1232Mpa, resultant fatigue life (Nf) of 38051 cycles, showing:

(a) Overall morphology of failure.

(b) High magnification of (a) showing distinct striations randomly spaced and oriented in the region of early crack growth.

(c) High magnification of the region of stable crack growth showing shallow nature of striations intermingled with fine microscopic cracks.

(d) The region of overload covered with fine microscopic voids and pockets of shallow dimples.

**[B] PremoMetTM 290**

Key features of the zero cobalt steel when deformed at a maximum stress of 1437 MPa and a resultant fatigue life of 31,885 cycles are shown in Figure 5. Overall morphology of the fracture surface revealed two distinct regions as seen in Figure 5a. Gradual high magnification observation of the region revealed early microscopic crack growth to occur radially from the point or onset of initiation. (Figure 5b). At gradually higher allowable magnifications of the SEM the region of early microscopic crack growth revealed the key features on the transgranular fracture surface coupled with an observable population of fine microscopic cracks. (Figure 5c). The region of overload revealed a noticeable population of macroscopic and fine microscopic voids intermingled with shallow dimples. These key microscopic features are reminiscent of the occurrence of locally ductile failure mechanisms at the fine microscopic level (Figure 5d)

### 4.2.2 Load Ratio [R] = - 1

**[A] AerMet® 100**

Key features of the high strength AerMet 100 steel sample that was cyclically deformed at a maximum stress of 1099.87 MPa, under fully-reversed loading, and a resultant fatigue life of 15,102 cycles are shown in Figure 6. Macroscopic observations of the fracture surface revealed the overall morphology to be at an inclination to the far-field stress axis. (Figure 4a). Progressive high magnification observation revealed the region of crack initiation or the onset of crack initiation (Figure 6b). The region of early microscopic crack growth (Figure 6c) was observed to be flat and lacking in discernible features, i.e., an absence of striations reminiscent of micro-plastic deformation at the 'local' level. Higher magnification observation of this region revealed it to be near featureless as shown in Figure 6d.

For test specimen of this high strength specialty steel that was cyclically deformed at a lower maximum stress of 791.9 MPa with a resultant fatigue life of 417,073 cycles the key features are shown in Figure 7. Overall morphology of failure revealed to be at a slight inclination to the far-field stress axis and comprised of a smooth region indicative of fatigue and a rough region indicative of overload (Figure 7a). Progressive high magnification observation of the region of microscopic crack initiation and early microscopic the crack growth revealed it to be radially outward from the onset of initiation (Figure 7b). The region of stable crack growth when observed at higher magnification revealed a dispersion of shallow striations indicative of the occurrence of micro-plastic deformation at the 'local' level (Figure 7c). The striations were intermingled with fine microscopic cracks. The region of overload revealed a noticeable population of microscopic voids and shallow dimples (Figure 7d). These fine microscopic features are clearly indicative of the occurrence of both brittle and ductile failure mechanisms at the fine microscopic level.

**[B] PremoMetTM 290**

Fracture of the zero cobalt low alloy PremoMet 290 steel sample that was cyclically deformed at a maximum stress of 1117.6 MPa and resultant fatigue life of 13566 cycles is shown in Figure 8. Overall morphology of the fracture surface was observed to be at an inclination to the far-field stress axis and revealed distinct regions of crack initiation, stable crack growth and overload (Figure 8a). The crack propagated radially from the onset of initiation (Figure 8b). The key features and nature of the fracture surface in the domain of stable crack growth is shown in Figure 8c. Going away from the region of stable crack growth and immediately prior to overload the region of unstable crack growth revealed fine array of co-planar microscopic cracks (Figure 8d).

The key features observed for the high strength steel that was cyclically deformed at a maximum stress of 798.31 MPa with a resultant fatigue life of 96,986 cycles is shown in Figure 9. Overall morphology was distinctly at an inclination to the far-field stress axis (Figure 9a). The region of early microscopic crack growth was observed to be essentially flat and near featureless (Figure 9b). The region of unstable crack growth revealed a population of macroscopic and fine microscopic cracks (Figure 9c). The fracture surface immediately prior to overload revealed an observable population of macroscopic voids intermingled with fine microscopic voids and shallow dimples. These features are reminiscent of the “locally” occurring ductile failure mechanisms (Figure 9d)

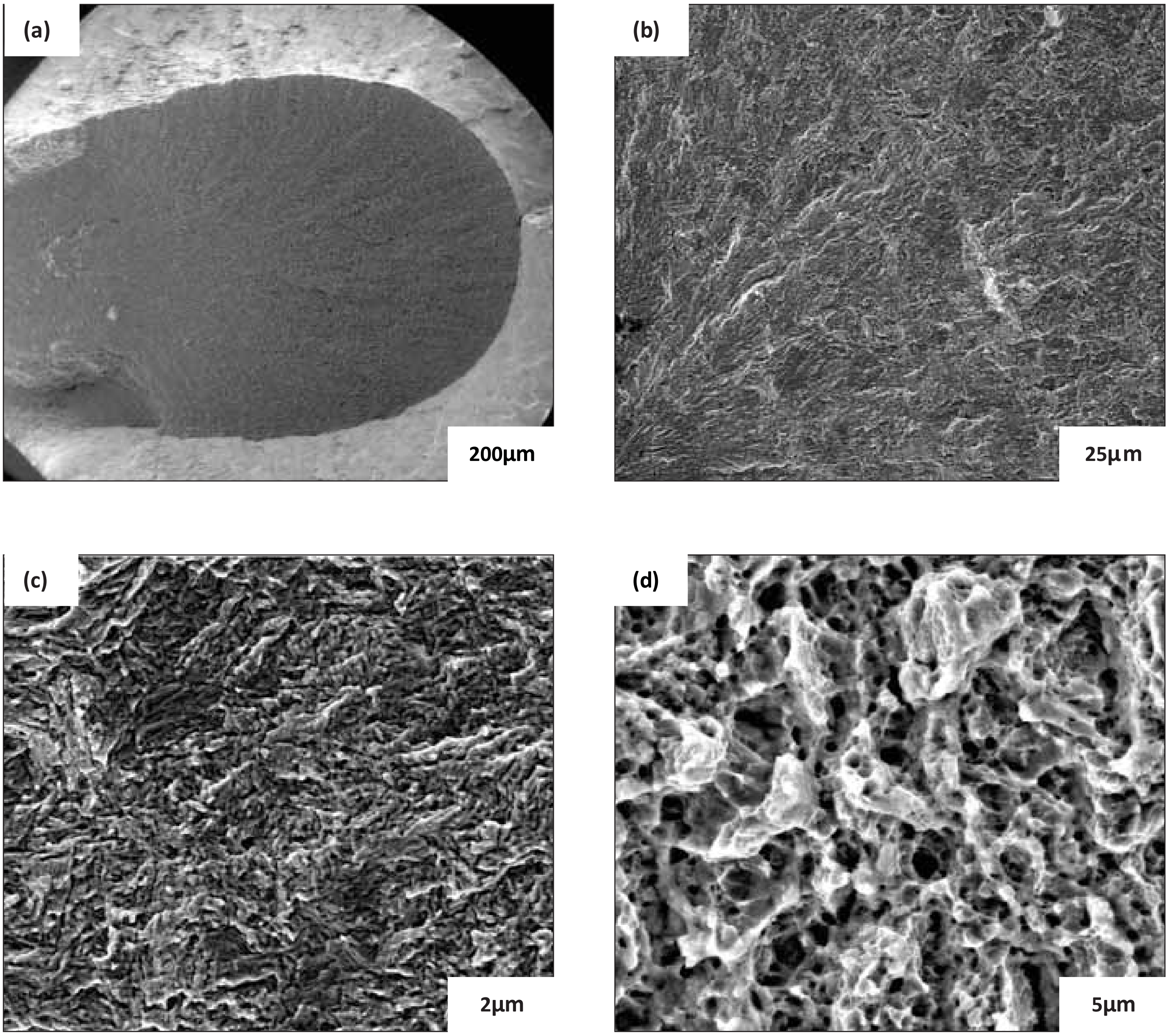


***Figure 5:*** Scanning electron micrographs of PremoMet™ 290 deformed deformed in cyclic fatigue at maximum stress (σmax) of 1437MPa, resultant fatigue life (Nf) of 31,885, showing:

(a) The overall morphology of fatigue fracture surface showing two distinct regions.

(b) High magnification observation in the region of early microscopic crack growth reveals radial propagation of damage from point of initiation.

(c) High magnification of (b) showing the intrinsic features on the transgranlar fracture surface, population of fine microscopic cracks.

(d) Macroscopic and fine microscopic voids intermingled with shallow dimples in the region of overload

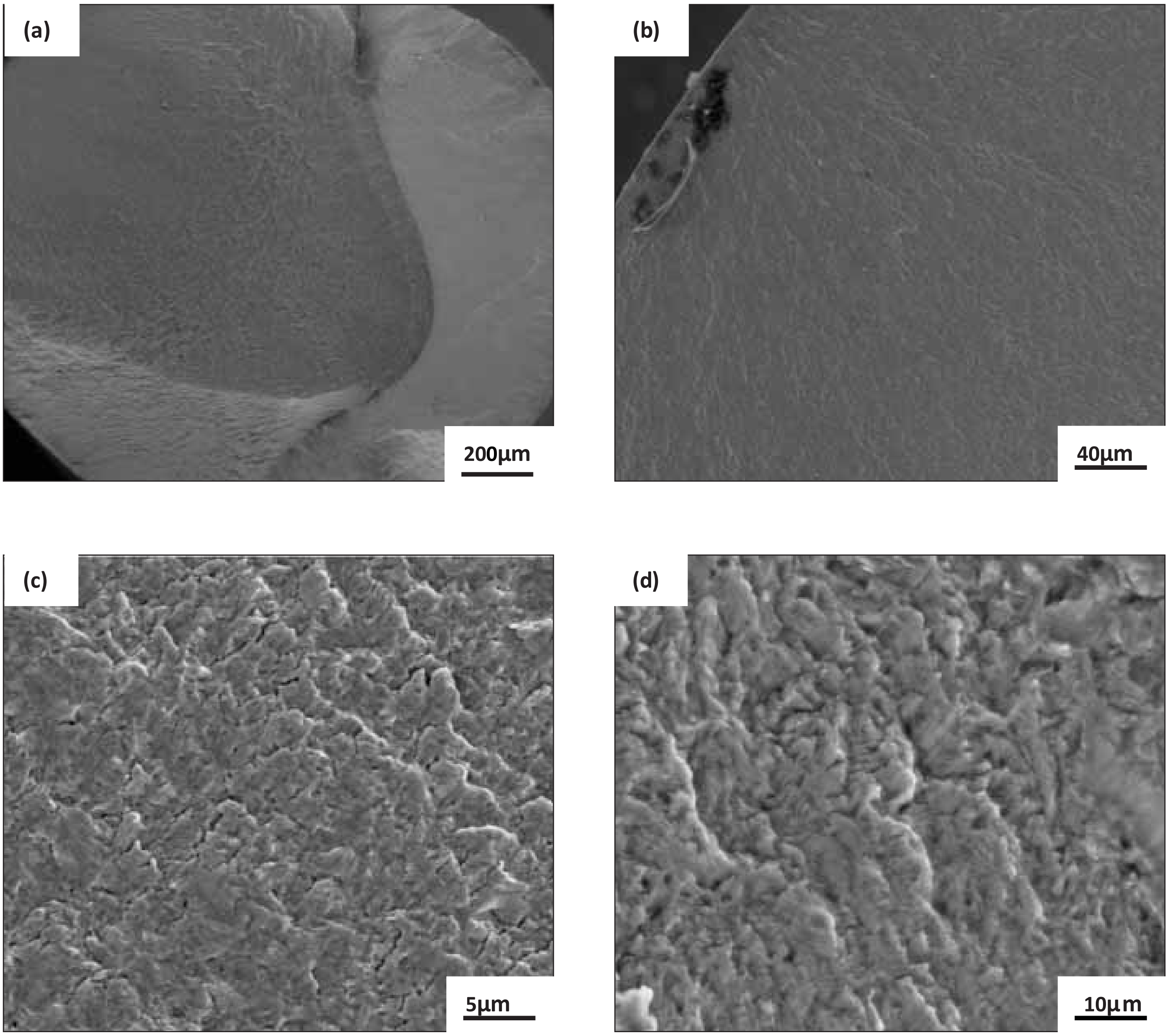


***Figure 6:*** Scanning electron micrographs of AerMet® 100 deformed in cyclic fatigue at load ratio [R] of -1.0, a maximum stress of 1099.87MPa, resultant fatigue life of 15,102 cycles, showing:

(a) Overall morphology of failure.

(b) High magnification of (a) showing the region and/or location of crack initiation or onset of crack initiation.

(c) The region of early crack growth observed to be near featureless

(d) High magnification observation of the region of early crack growth.

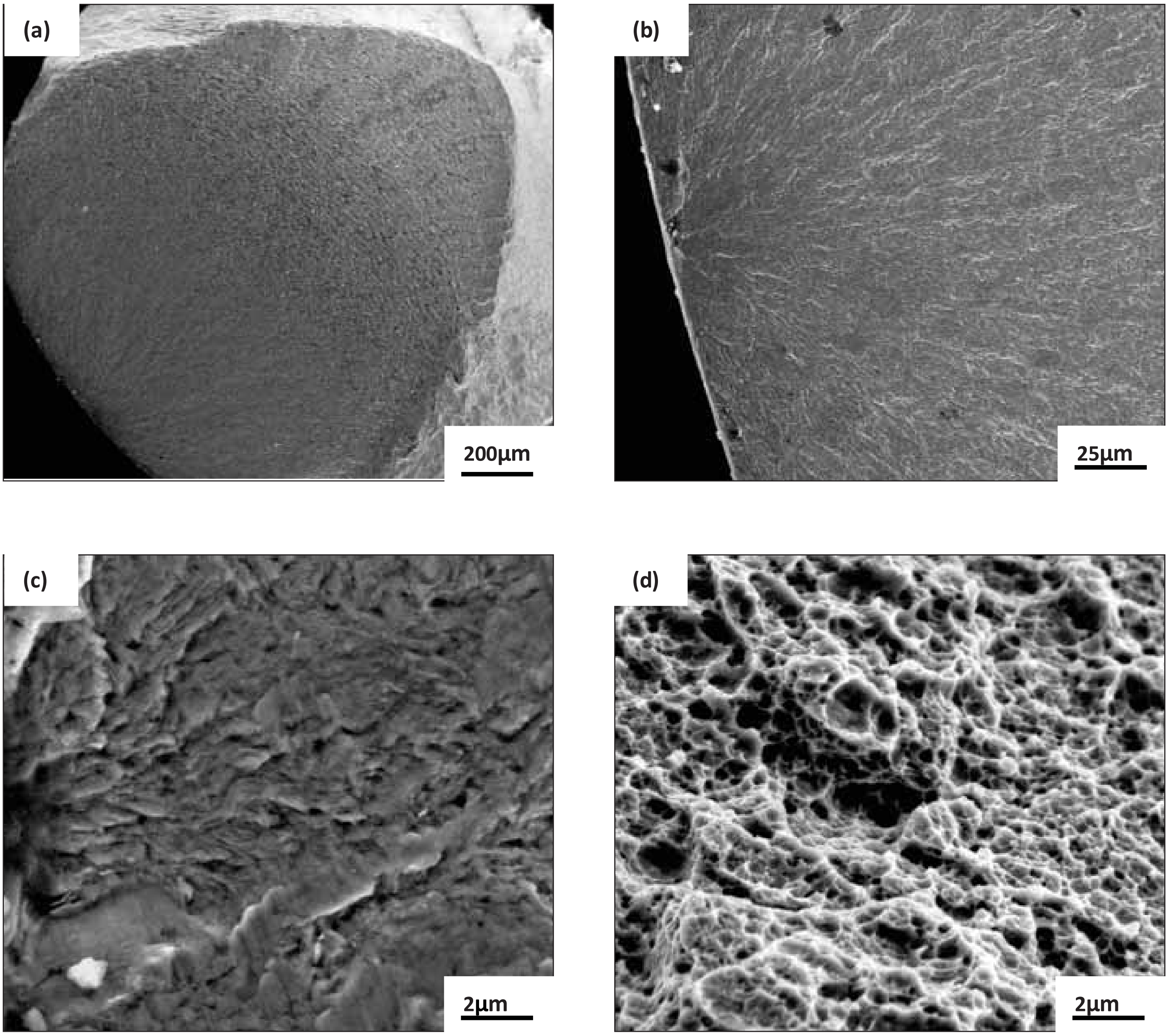


***Figure 7:*** Scanning electron micrographs of AerMet 100 deformed in cyclic fatigue at load ratio ( R) of -1, at a maximum stress of 791.9, resultant fatigue life of 417,073 cycles, showing:

(a) Overall morphology of the fatigue fracture surface.

(b) High magnification of (a) showing the region/location of crack initiation and nature of propagation: radially outward

(c) High magnification of the region of early microscopic crack growth showing shallow nature of striations intermingled with fine microscopic cracks.

(d) The region of overload covered with microscopic voids of varying size and pockets of shallow dimples.

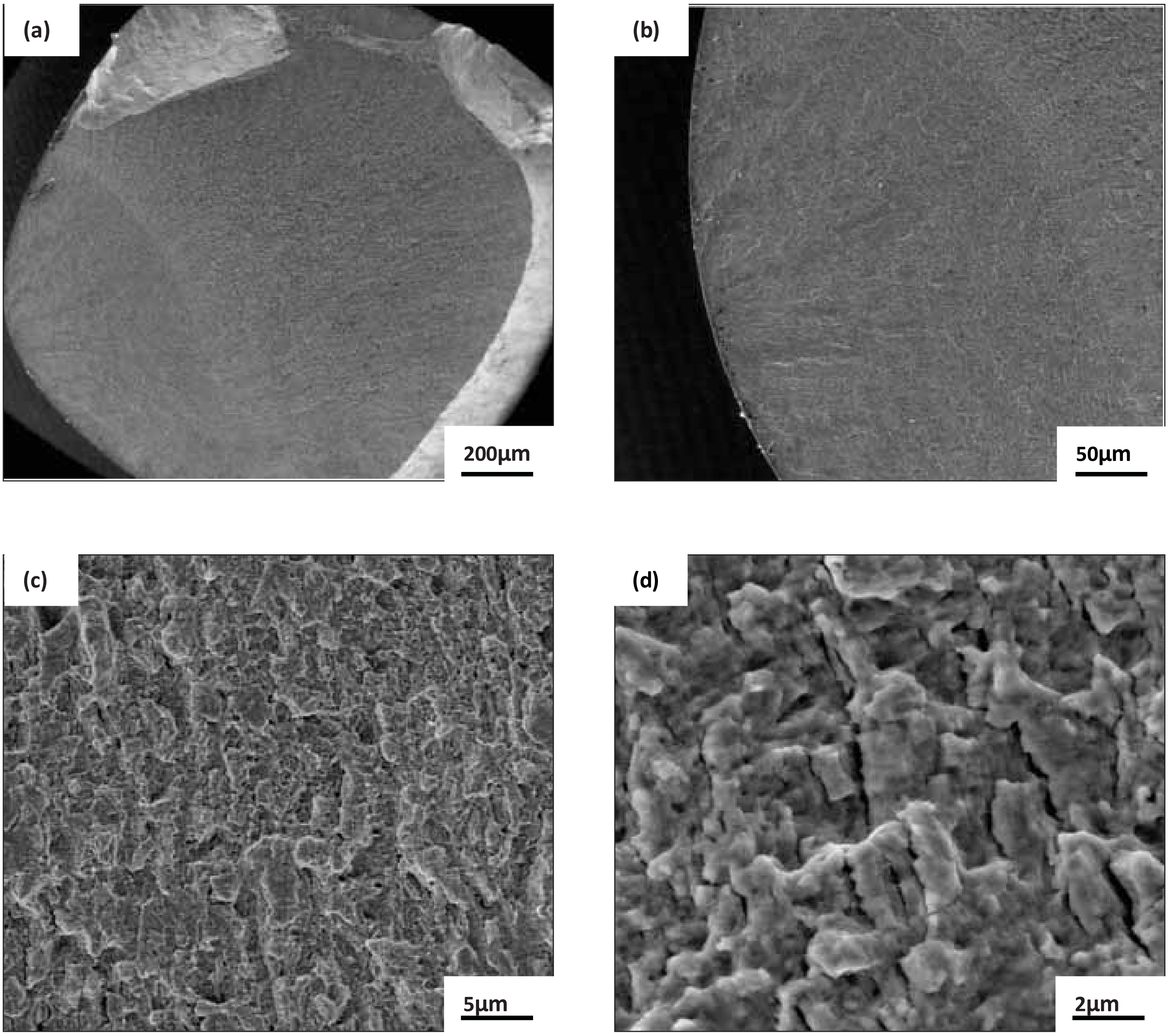


***Figure 8:*** Scanning electron micrographs of PremoMetTM 290 deformed in cyclic fatigue at load ratio of -1, at a maximum stress of 1117.6MPa, resultant fatigue life of 13,566 cycles, showing:

(a) The overall morphology of fatigue fracture surface showing the two distinct regions.

(b) High magnification observation of (a) showing the region of onset of microscopic crack initiation and nature of early crack propagation.

(c) High magnification observation of the region of early crack growth.

(d) Coplanar microscopic cracks in the region of unstable crack growth.

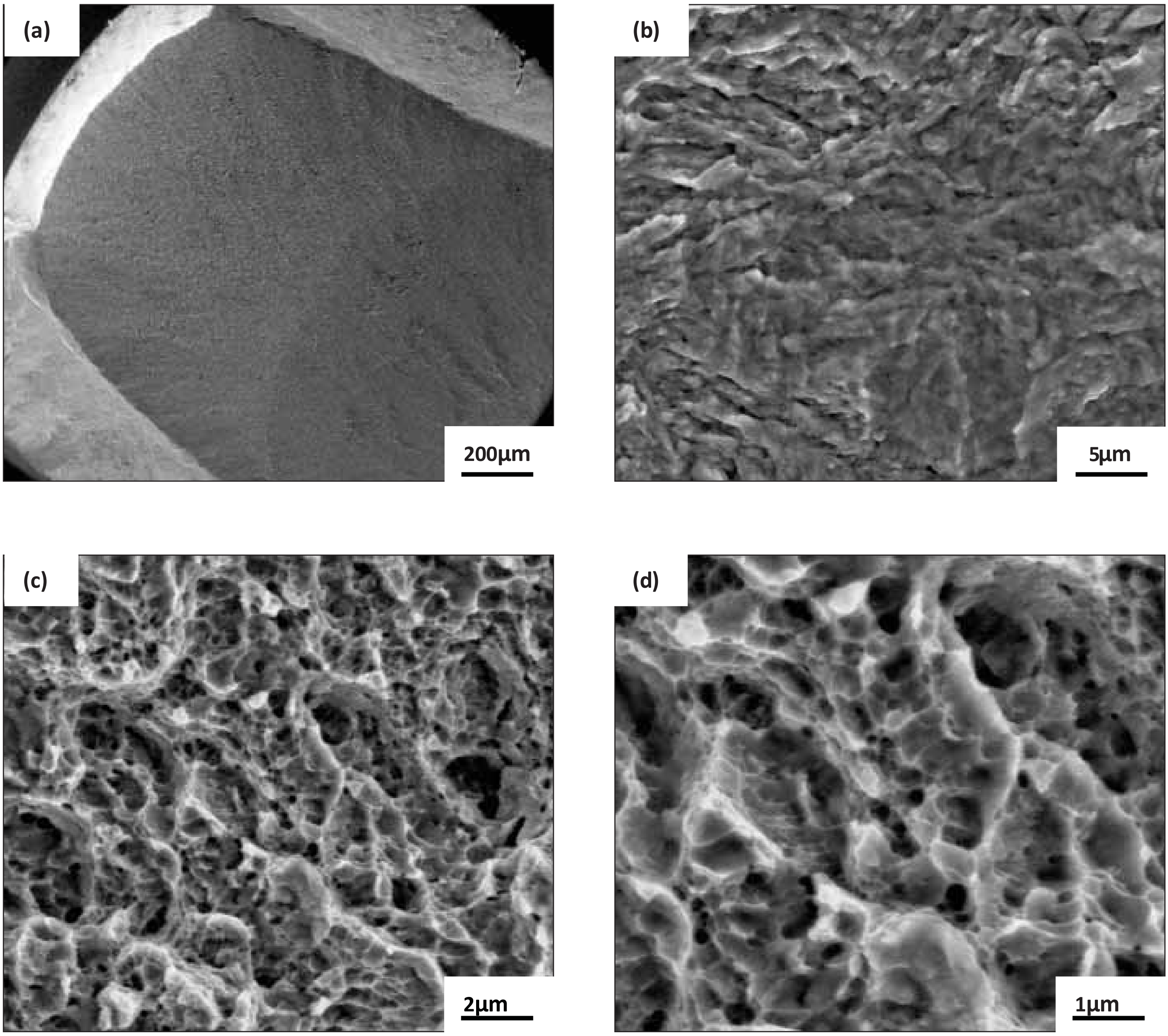


***Figure 9:*** Scanning electron micrographs of PremoMetTM 290 deformed in cyclic fatigue at load ratio of -1, at a maximum stress of 798.31MPa, resultant fatigue life of 96,986 cycles, showing:

(a) Overall morphology of the fatigue fracture surface.

(b) The region of early microscopic crack growth flat and essentially transgranular.

(c) A combination of macroscopic and fine microscopic cracks in the region of unstable crack growth.

(d) The macroscopic and fine microscopic voids and shallow dimples in the region of unstable crack growth prior to overload

# 5. CONCLUSIONS

Based on an exhaustive study of the fracture surfaces of two high strength specialty steels that were cyclically deformed at two different load ratios and over a range of maximum stress, following are the key findings.

1. Microstructure is typical of high strength steels and reveals a combination of carbon- rich region and a carbon-depleted region. A higher carbon and alloy content in the steel resulted in a noticeable volume fraction of martensite in the carbon-rich region. The presence and overall morphology of martensite was noticeable in large numbers in the form of "lath" in the two steels AerMet® 100 and PremoMetTM 290.

2. At the macroscopic level failure was essentially at an angle to the far-field tensile stress axis for samples that were deformed over a range of maximum stress resulting in different fatigue lives, spanning the very low life to very high life.

3. Cyclic fatigue fracture surfaces of samples of the candidate specialty steel revealed noticeable differences in both the nature and volume fraction of the microscopic features as a function of maximum stress at a given load ratio ( R).

4. The region of crack initiation and early microscopic crack growth was essentially flat, transgranular and lacking in easily discernible features. The region of stable crack growth did reveal an observable population of fine microscopic cracks intermingled with pockets of randomly distributed fine and shallow striations, reminiscent of the occurrence of micro-plastic deformation at the 'local' level. The region of tensile overload was covered with a noticeable population of dimples of varying size and shape, macroscopic voids and fine microscopic voids. These key features are reminiscent of the occurrence of "locally" operating failure mechanisms.

## ACKNOWLEDGMENTS

This research was made possible through material, test samples and funding provided by Carpenter Technology Corporation (Reading, PA, USA) [Program Manager: Mr. M. L. Schmidt]. Mr. Manigandan Kannan (Graduate student: Department of Mechanical Engineering, The University of Akron) extends thanks and appreciation to the University for providing support through tuition scholarship.

## REFERENCES

[1] Fukumoto,Y. New constructional steels and structural stability, Engineering Structures 786,1996, p. 18-21

[2] Bathias C, Drouillac L, Francois PL. How and why the fatigue S–N curve does not approach a horizontal asymptote. International Journal of Fatigue, 23,2001,p. s143–151.

[3] Mukami Y, Takada M, Toriyama T. Super-long life tensioncompression fatigue properties of quenched and tempered 0.46% carbon steel. International Journal of Fatigue, 20(9),1998,p. 661–669.

[4] Bathias C. There is no infinite fatigue life in metallic materials. Fatigue and Fracture of Engineering Materials and Structures, 22, 1999, p.559–565.

[5] Abe T, Furuya Y, Matsuoka S:. Gigacycle fatigue properties of 1800 MPa class spring steels. Fatigue Fracture of Engineering Materials and Structures, 2004; 27:159–67.

[6] Wang QY, Berara JY, Rathery S, Bathias C. High-cycle fatigue crack initiation and propagation behavior of high-strength spring steel wires. Fatigue and Fracture of Engineering Materials and Structures, 22,1999,p.673–677.

[7] Yang ZG, Li SX, Zhang JM, Zhang JF, Li GY, Li ZB, et al. The fatigue behaviors of zero-inclusion and commercial 42CrMo steels in the super-long fatigue life regime. Acta Materialia, 52,2004, 52: p.5235–5241.

[8] Kiedssling R. Non-metallic inclusions in steel. London: Met Soc; 1978. p. 155–165

[9] R. Hertzberg; Deformation and Fracture Mechanics of Engineering Materials, Second Edition, John Wiley and Sons, 1983

[10] K. Manigandan,T.S.Srivatsan, T Quick,M Petraroli and M.L Schmidt; Influence of Alloy Chemistry and Processing on Impact Toughness and Fracture Behavior of High Strength Steels; Processing and Fabrication of Advanced Materials XIX Auckland, New Zealand 2011, Section 1 p. 2-18.

[11] K. Manigandan,T.S.Srivatsan, T Quick,M Petraroli and M.L Schmidt; Influence of Alloy Chemistry and Processing on Tensile Deformation and Fracture Behavior of Four High Strength Steels; Processing and Fabrication of Advanced Materials XIX Auckland, New Zealand 2011 Section 1 pp. 19-32.

[12] ASTM Standards E-8-06:,53:,Standards method of Uniaxial tensile testing of Materials: ASTM, Philadelphia, PA,USA, 2006.

[13] Manigandan K- "The Microstructure, Hardness, Impact Toughness, Tensile Deformation and Final Fracture Behavior of four Specialty High Strength Steels", Master of Science Thesis-The University of Akron, Akron, Ohio USA, 2011

# AN ANALYSIS OF LASER MACHINING PROCESS OF ALUMINIUM-10WEIGHT% ALUMINA COMPOSITE MATERIAL

Arindam Ghosal
Research scholar (PhD), Punjab Engineering College, Chandigarh (India), Associate Professor,
Department of Mechanical Engineering, Dronacharya Group of Institutions, Greater Noida
Mobile: +919013619515 and +918826356956 Email: er_ghosal@yahoo.co.in

Alokesh Manna
Associate Professor, Department of Mechanical Engineering, Punjab Engineering College, Chandigarh

Arun K Lall
Professor, Department of Mechanical Engineering, Punjab Engineering College, Chandigarh.

## ABSTRACT

Non conventional machining processes have become popular today as compared to conventional machining processes. In the conventional machining process many problems may arise like high pressure on work piece, tool failure, accuracy, surface finish etc. In nonconventional machining processes like EDM, ECM, ECDM, LBM the above difficulties may be overcome. Some holes are drilled in Al-Al2O3 composites by 2 kW Ytterbium Fiber Laser. This paper presents the outcome of the study of the characteristic of drilled hole for different parameters.

***Key words:*** Laser Beam Machining, Conventional Machining, Non Conventional Machining

## 1. INTRODUCTION

In Fiber Laser Machining, material removal is possible from a selected area; good surface finish is also obtained. The principles of Laser Machining process are :

- LM process removes material in the form of vaporization.
- Pumping energy is utilized.

The process through which a material can be machined or drilled by Laser beam directly is called Laser Beam Machining (LBM).

## 2. EXPERIMENTAL SETUP

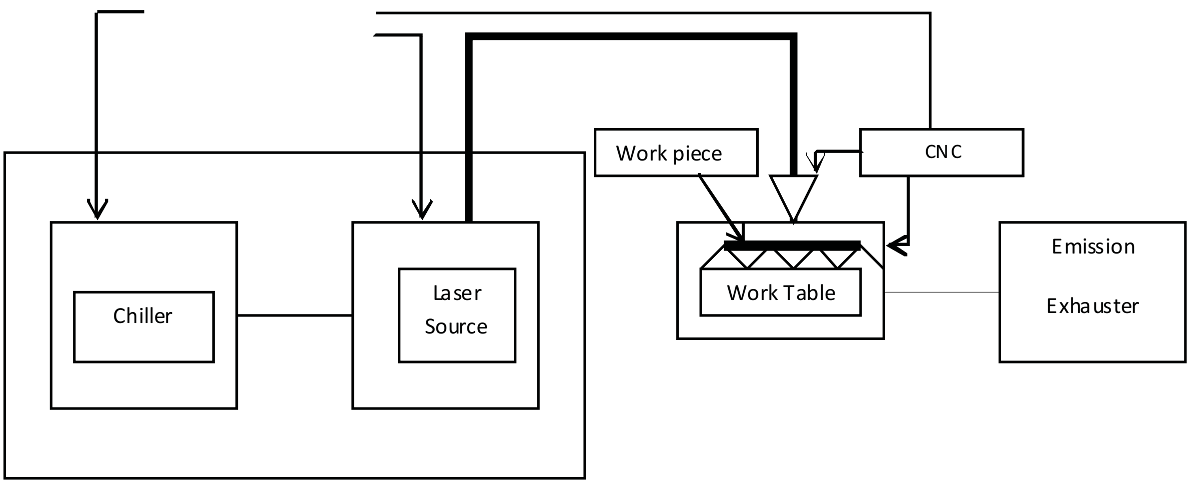


***Fig 1:*** Block diagram of fiber laser

***Fig 2:*** Fiber Laser machine YLR 2000 used to cut, Al-10 volume %Al2O3

***Table 1:*** Specifications of fiber laser machine

| | |
|---|---|
| Operation mode | CW |
| Nominal output power | 2kw |
| Emission wave length | 1070-1080 nm |
| Output fiber core dia. | 150µm |
| Fiber length | 10m |
| Polarization | Random |
| Operating voltage | 400-460 VAC |
| Power frequency | 50/60Hz |
| Power consumption | 8 kW |
| Operating ambient air temp. | 10-50 0 C |
| Laser cooling water temp. range | 22-24 0 C |
| Laser cooling water flow rate | 5 lit/min |
| Working area x ,y, z axis | 1500 mm,3000 mm 150mm, |
| Maximum work piece weight. | 750 kg |

***Fig 3:*** Al-10 weight% Alumina Casted work piece

***Fig 4:*** Al-10 weight% Alumina sample cut from casted work piece and drilled by fiber laser of 2 kW

## 3. DISCUSSION

Drilled holes as shown in fig-4 are done by 2KW ytterbium fiber laser machine setting different laser parameters. SEM analysis is done of these holes (fig-5).

In the following tables (2 & 3) combinations of parameters are given which are used to drill holes in Aluminium-10% weight Alumina composite material.

From fig-5, it is clear that at each run some molten material is deposited on the surface of the work piece. In each SEM photograph, it is clear that hole drilled by laser is taper, in each case there is a maximum hole diameter at upper surface and minimum hole diameter at lower surface. In fig-5 holes are round in shape and obtained by run 3 and run 7 respectively. So the combination of parameters of run 3 and run 7 are accepted for drill hole of Al- 10 weight % Al2O3 composite material.

***Table 2:*** Cutting parameters and their levels

| Symbols | Machining parameters | Levels | | | Units |
|---|---|---|---|---|---|
| | | 1 | 2 | 3 | |
| A | Laser Power | 1200 | 1500 | 2000 | watt |
| B | Modulation frequency | 800 | 900 | 1000 | Hz |
| C | Assist gas pressure (N2) | 15 | 17 | 20 | Bar |
| D | Wait time | 0.1 | 0.2 | 0.3 | Second |
| E | Distance between nozzle and work piece | 0.5 | 0.8 | 1 | mm |
| F | Pulse width | 80% | 90% | 100% | % |

**Table 3:** Drilling time and temperature during runs

| Run | A | B | C | D | E | F | Temp. (0C) | Drilling time (sec) |
|---|---|---|---|---|---|---|---|---|
| 1 | 1 | 1 | 1 | 1 | 1 | 1 | 782 | 3.9 |
| 2 | 1 | 1 | 1 | 1 | 2 | 2 | 785 | 3.19 |
| 3 | 1 | 1 | 1 | 1 | 3 | 3 | 790 | 3.55 |
| 4 | 1 | 2 | 2 | 2 | 1 | 1 | 791 | 3.91 |
| 5 | 1 | 2 | 2 | 2 | 2 | 2 | 789 | 4.02 |
| 6 | 1 | 2 | 2 | 2 | 3 | 3 | 788 | 3.03 |
| 7 | 1 | 3 | 3 | 3 | 1 | 1 | 782 | 4.34 |
| 8 | 1 | 3 | 3 | 3 | 2 | 2 | 785 | 3.38 |
| 9 | 1 | 3 | 3 | 3 | 3 | 3 | 789 | 3.82 |
| 10 | 2 | 1 | 2 | 3 | 1 | 2 | 796 | 4.20 |
| 11 | 2 | 1 | 2 | 3 | 2 | 3 | 787 | 4.10 |
| 12 | 2 | 1 | 2 | 3 | 3 | 1 | 781 | 3.92 |
| 13 | 2 | 2 | 3 | 1 | 1 | 2 | 785 | 3.95 |
| 14 | 2 | 2 | 3 | 1 | 2 | 3 | 789 | 3.79 |
| 15 | 2 | 2 | 3 | 1 | 3 | 1 | 788 | 4.00 |
| 16 | 2 | 3 | 1 | 2 | 1 | 2 | 780 | 4.01 |
| 17 | 2 | 3 | 1 | 2 | 2 | 3 | 798 | 4.02 |
| 18 | 2 | 3 | 1 | 2 | 3 | 1 | 786 | 3.96 |
| 19 | 3 | 1 | 3 | 2 | 1 | 3 | 791 | 3.97 |
| 20 | 3 | 1 | 3 | 2 | 2 | 1 | 790 | 3.96 |
| 21 | 3 | 1 | 3 | 2 | 3 | 2 | 789 | 4.01 |
| 22 | 3 | 2 | 1 | 3 | 1 | 3 | 788 | 4.02 |
| 23 | 3 | 2 | 1 | 3 | 2 | 1 | 785 | 3.05 |
| 24 | 3 | 2 | 1 | 3 | 3 | 2 | 784 | 3.07 |
| 25 | 3 | 3 | 2 | 1 | 1 | 3 | 798 | 3.77 |
| 26 | 3 | 3 | 2 | 1 | 2 | 1 | 780 | 3.90 |
| 27 | 3 | 3 | 2 | 1 | 3 | 2 | 785 | 3.88 |

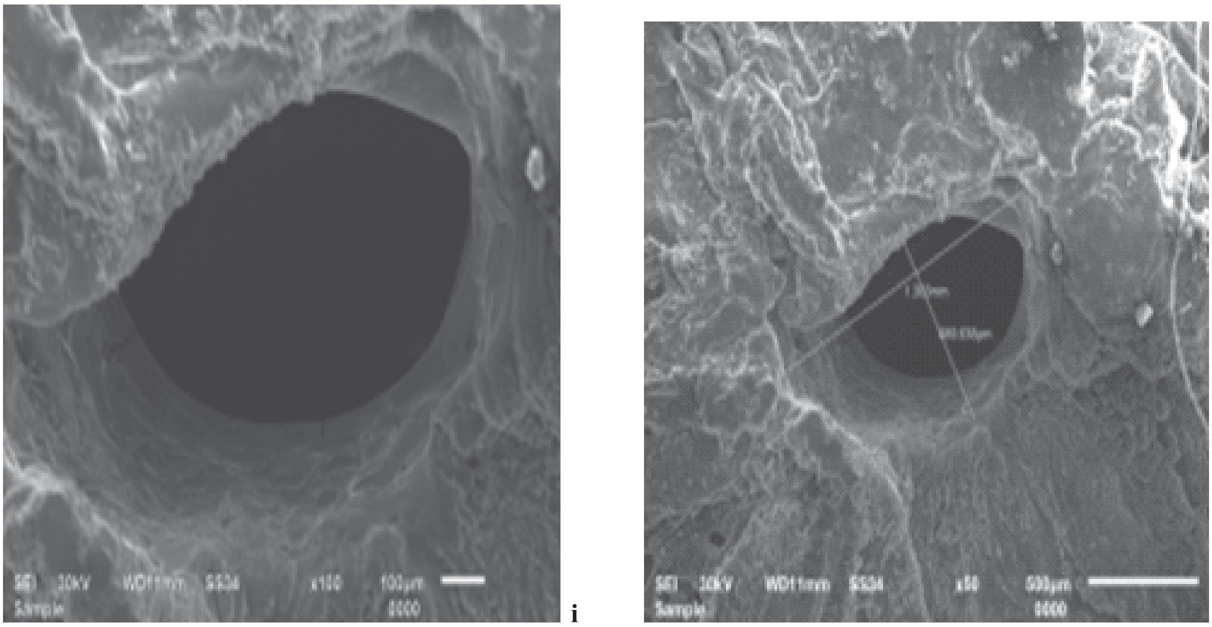


*Fig 5:* SEM photograph of drilled hole

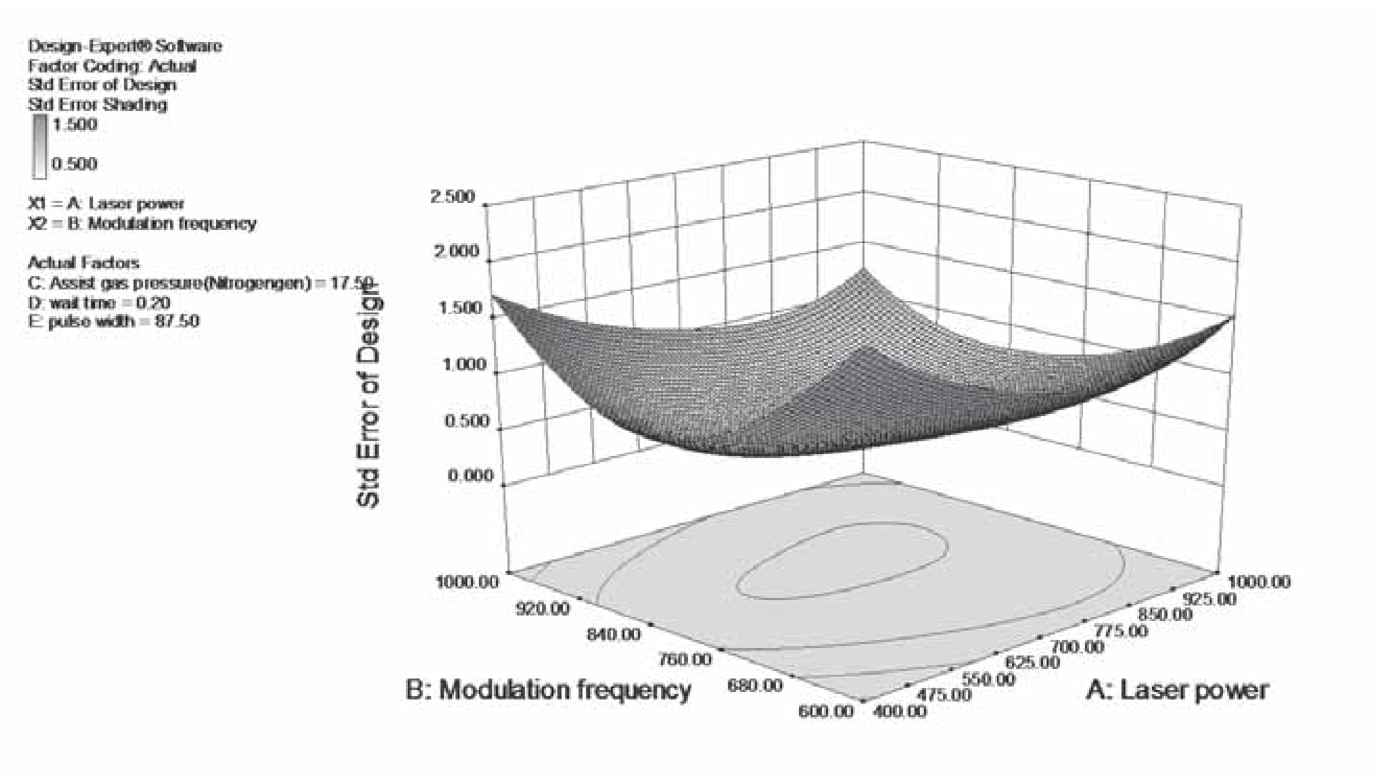


*Fig 6:* 3-D graph, standard error, modulation frequency and laser power

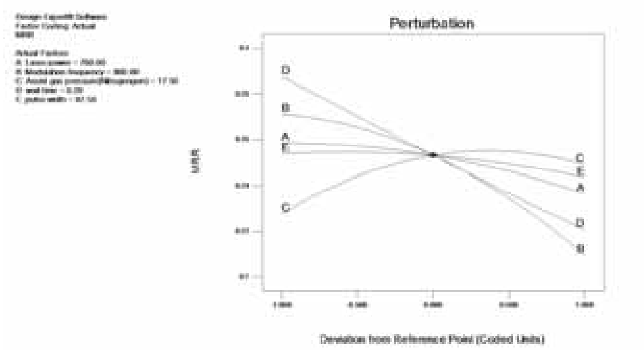


*Fig-7:* deviation from reference point vs MRR

# 4. CONCLUSION

From the above discussion, it is concluded that Laser Machining is a flexible, accurate and high level surface finishing process. Heat conducted and absorbed by the material is important to raise the surface temperature high for material vaporization. Laser Machining is time consuming and costly but high accuracy process. The hole made by laser drilling is not uniform from top surface to bottom surface, all holes are tapered and roundness of the hole may be controlled by properly adjusting the laser parameters. From fig-6 it is clear that with increasing in laser power standard error is also increasing and at 1000-W laser power the standard error is maximum. It is also clear that with increasing in modulation frequency, std error is also increasing and when modulation frequency is 1000 %, std error is the maximum. Fig-7 shows the deviation from reference point vs MRR graph.

# REFERENCES


1. E. Kacer, "Journal of material processing technology", vol-209, issue-4, pp 2008-2014:characterization of drilling Alumina ceramic using Nd:YAG pulsed laser.
2. K. Itoh and W. Watanabe, Toward nano and microprocessing in glass with femtosecond Laser pulses, RIKEN Review, 50, (2003), pp.90-94.
3. K. Zimmer and R. Böhme, Precise etching of fused silica for micro-optical applications, Applied Surface Science, Vol.243 (2005), pp.415-420.
4. A.F.M Arif, "Optics and laser technology", Vol. 41, issue 3, pp 224-232, Laser cutting of thick sheet metals: Residual stress analysis.
5. K.Li, "International journal of machine tool manufacturing", Vol. 35, No. 11, pp 1493-1506,1995, Plane stress model for fracture of ceramics during laser cutting.
6. Chwan Huei Tsai, "Journal of material processing technology", 2009, pp 2838-2846, Investigation of underwater laser drilling for brittle substrate.
7. Lee Mein Wee, "Applied surface science", vol-247, 2005,pp 277-284, An analytical model for striation formation in laser cutting.
8. K.C.P. LUM, "Optics and laser technology", vol-32, 2000, pp 67-76, CO2 laser cutting of MDF: Determination of process parameter settings.
9. R M Miranda, "Materials characterization", Vol. 53, 2004, pp 411-417, Structural analysis of heat affected zone of marble and lime stone tiles cut by CO2 laser.
10. Shbhranshu Roy, "International journal of Heat Mass transfer", vol-36, No. 14, pp 3515-3528, 1993, CW Laser machining of hard ceramics: Effects of three dimensional conduction properties and various laser parameters.

# INLINE MONITORING OF BOTTLE FILLING PROCESS USING IMAGE PROCESSING

Santhosh K V
kv.santhu@gmail.com
Research Scholar, Dept of Electrical Engineering, NIT Silchar, Assam

B K Roy
Associate Professor, Dept of Electrical Engineering, NIT Silchar, Assam

Pankaj Kumar Bhowmik
Scholar, Dept of Electrical Engineering, NIT Silchar, Assam

## ABSTRACT

This paper aims at designing an automated system to monitor the bottle filling process in a beverage industry. The objectives of this work are to (i) check whether the reused bottle is clean or not before beverage is filled, (ii) check whether the bottle is completely filled with beverage and (iii) check whether the bottle is properly labelled. The whole system is carried on with the help of image processing technique utilising the LabVIEW platform without disturbing the high speed production line. The images of bottle are captured using a high frame rate smart camera, then acquired on to the PC through RS232 port and processed with the help of LABVIEW software. After processing a trigger is generated and sent to circuitry to initiate a signal to divert that particular bottle which doesn't match the standards.

***Key words:*** Beverage Industry, Industrial automation, Image processing, Lab VIEW

## 1. INTRODUCTION

The Indian food industry is projected to grow by US$ 100 billion to US$ 300 billion by 2015. The food industry in India widely comprises of food production and food processing industry. Soft drinks industry is one of the most important food production industries. Soft drinks rank as favorite beverage segment, representing 25% of the total beverage market. In the early 1990s per capita consumption of soft drinks in the U.S. alone was 49 gallons. The $27 billion dollar soft drink industry generated about 110 billion containers each year in the early 1990s. About half of soft drink containers were aluminum cans and the other half, were reusable bottles.

Detection of foreign particles in reusable bottles in beverage industries is the main objective/ concern to an industry. In industries, bottles are reused to fill their products at the fast rate, manual check is not possible, the method of cleaning may be very accurate but practically it is not possible to assure that the bottle is free from micro-macro impurities. News of a pen cap found in the soft drink bottle, an insect found in soft drink bottle is heard many time, this is because of the above mentioned problem, so it's very important to check the bottle for detection of any impurity before the bottle is filled with soft drink. This paper aims at presenting a method which provides the solution to the above problem without causing any delay to the production process in an industry.

The solution is achieved by having a high frame rate camera to capture the image of the bottle before filling it with soft drink, process the data and check for impurities using the techniques of digital image processing and alert the system if any mismatch is detected, divert the bottle from the production line to cleaning process again. The similar technique is also incorporated here to check whether the bottle is completely filled with beverage after the bottle filling process and also check whether it is properly labeled, so as to achieve the complete monitoring and automation of the production line.

The paper is organised as follows: After introduction in Section 1, a brief description on Experimental setup is given in Section 2. A brief discussion on sensing elements i.e. smart camera is discussed in Section 3. Section 4 deals with the problem statement followed by proposed solution in Section 5. Finally, results and conclusion is given in Section 6.

## 2. EXPERIMENTAL SETUP

To demonstrate the working of the above proposed objective a laboratory model is setup which would mimic the industrial production line. The Fig. 1 Shows the model of the experimental setup which is used by us to carry out the project. The bottle is placed on the conveyor belt which is rolled at high speeds of the order of 60bottles per minute with the help of the stepper motor arrangement. The high frame rate smart camera is placed on the housing to capture the image before the bottle is filled. The solenoid is provided after the housing which will be actuated if the bottle does not meet the standard and is diverted. The same setup is also used to check the complete filling and proper labelling of bottle.

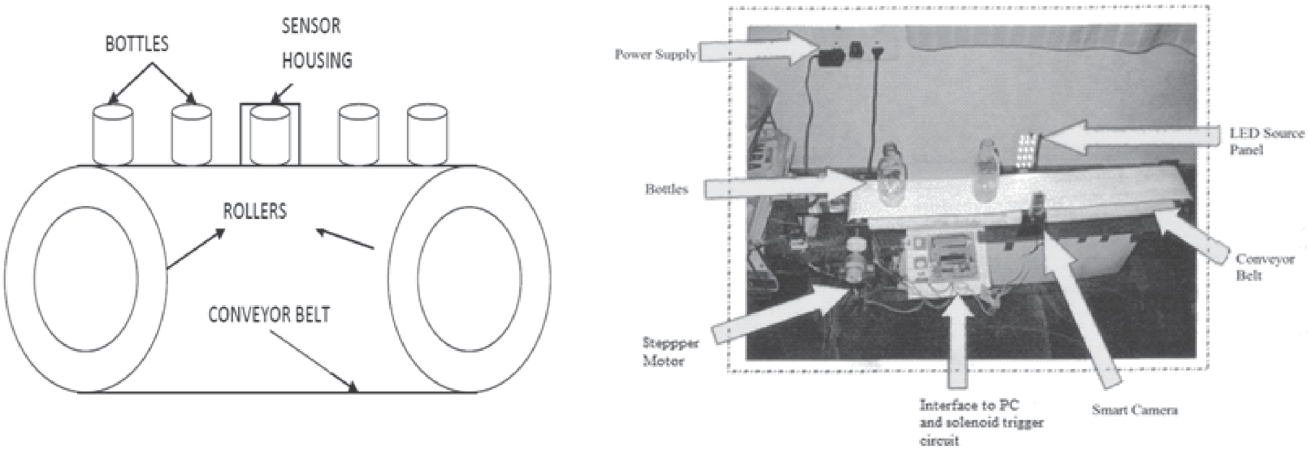


***Figure 1.*** Model and actual experimental setup

## 3. SENSING ELEMENT

The block diagram representation of the proposed instrument is given in Fig 2

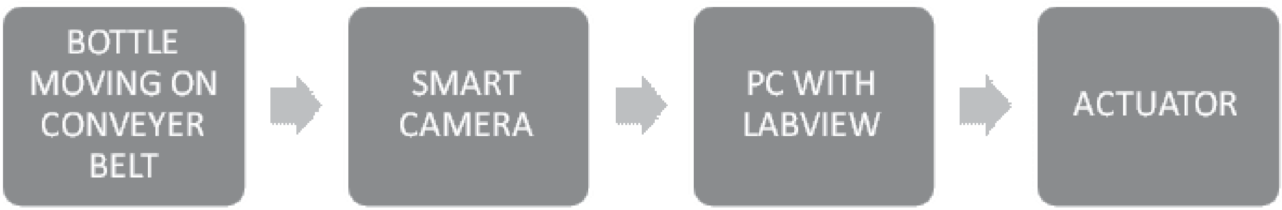


***Figure 2.*** Block diagram of the proposed instrument

**3.1 SMART CAMERA** The NI 1744 Smart Camera, powered by a 533 MHz PowerPC processor, is a real-time target for machine vision. The high-quality Sony CCD image sensor acquires monochrome SXGA (1280 x 1024) resolution images. This camera has four times the resolution of the NI 1722 and 1742 Smart Cameras. Camera I/O includes two opto-isolated digital inputs, two opto-isolated digital outputs, one RS232 serial port, and two Gigabit Ethernet ports. The NI 1744 also features quadrature encoder support and a direct drive lighting controller that can drive current controlled lights up to 500 mA continuous or 1 A strobed. It has a maximum frame rate of 13 fps at maximum resolution, with a sensor size of 1.25cm, pixel depth of 8 bit, minimum exposure time of 76.7 μs and exposure time increment 71.6 μs [9-10].

***Figure 3.*** 1744 Smart sensor

**3.2 LabVIEW** LabVIEW is a fully featured programming language produced by National Instruments. It is a graphical language quite unique in the method by which code is constructed and saved. There is no text based code as such, but a diagrammatic view of how the data flows through the program. Thus LabVIEW is a much loved tool of the scientist and engineer who can often visualize data flow rather than how a text based conventional programming language must be built to achieve a task. LabVIEW programs are called virtual instruments, or VIs, because their appearance and operation imitate physical instruments, such as oscilloscopes and multimeters. LabVIEW contains a comprehensive set of tools for acquiring analyzing, displaying, and storing data, as well as tools to help you troubleshoot your code.

LabVIEW VI's contains three components-the front panel, the block diagram, and the icon and connector pane. In LabVIEW, you build a user interface, or front panel, with controls and indicators. Controls are knobs, push buttons, dials, and other input devices. Indicators are graphs, LEDs, and other displays. After you build the user interface, you add code using VIs and structures to control the front panel objects. The block diagram contains this code. In some ways, the block diagram resembles a flowchart.

You can use LabVIEW to communicate with hardware such as data acquisition, vision, and motion control devices, and GPIB, PXI, VXI, RS-232, and RS-484 devices. LabVIEW also has built-in features for connecting your application to the Web using the LabVIEW Web Server and software standards such as TCP/IP networking and ActiveX. Using LabVIEW, you can create test and measurement, data acquisitions, instrument control, data logging, measurement analysis, and report generation applications. You also can create stand-alone executables and shared libraries, like DLLs, because LabVIEW is a true 32-bit compiler. [11-12]

## 4. PROBLEM STATEMENT

After the image is captured with the help of NI 1744 smart camera, now the image should be processed and compared with standard images to attain the following objectives:

(i) Check for impurity in the reused bottle before beverage is filled,
(ii) Check whether the bottle is completely filled with beverage after the bottle filling process is completed,
(iii) Check whether the bottle is properly labelled.

## 5. PROBLEM SOLUTION

From the discussions earlier the objective of the work to be carried is very clear. We have chosen LabVIEW platform to carry out the project. To attain the desired objectives, for the purpose of working in laboratory the model is constructed as shown in the Fig 1 and Fig 2. The stepper motor is calibrated in the way to move the bottle at the speed of 60 bottles per minute keeping in mind of the laboratory scenario. The original sample image has been acquired from the smart camera. The smart camera is initiated such that it acquires the image after every second since the bottle is moving at a rate of 60 bottles per minute. The image acquired by the smart camera is sent to the PC for processing under LabVIEW platform using the RS232 port. After the acquisition of the image by the LabVIEW program, the sample image is ready for being processed. In processing, we start off by extracting two color planes from the rgb plane (32-bit) image and converting it to a one color plane image, say red plane (8-bit) image. We convert it to a grayscale (8-bit) image because it reduces the matrix size of the image and computational time is immensely reduced as well as memory requirement is very less. Also it is very easy to analyze a grayscale image than a rgb plane image.

Now, the whole sample image is not required to be processed. We select our region of interest and mask all the pixels that are out of our region of interest. We extract out our masked region and we are left with only our region of interest. Now, we select the range of pixels in our region of interest which are bright by the operation of cluster thresholding. After thresholding, the whole image is highlighted with red colour but in case of a defective image, the defects are easily distinguishable as those portions are not highlighted with red colour in our region of interest. The thresholding operation further reduces the image from an 8-bit one to a binary image. Now, we remove those defective portions which were not highlighted in our thresholding operation using a filter. The filtered image is then analyzed by particle analysis process. This process displays measurement results for selected particle measurements performed on the filtered image. We analyze the centre of mass for this filtered image. If there is a defective sample, its center of mass will be different as compared to the good sample's center of mass. In this way, we can compare the sample's image and find out which sample is a defective one. Now, our program will compute the center of mass of a sample and compare it with the original good sample's center of mass and if it does not match, it will switch on an alarm signal which will alert the system to divert the defective sample from the conveyor belt. The whole processing is carried out within a second so that the next bottle is processed without affecting the speed of the production line [4-8].

The same process is repeated to achieve the three objectives like check for impurities, proper filling of bottles and proper labeling.

Fig 4 shows the picture of the front panel designed for the project. Fig 5 shows the block diagram.

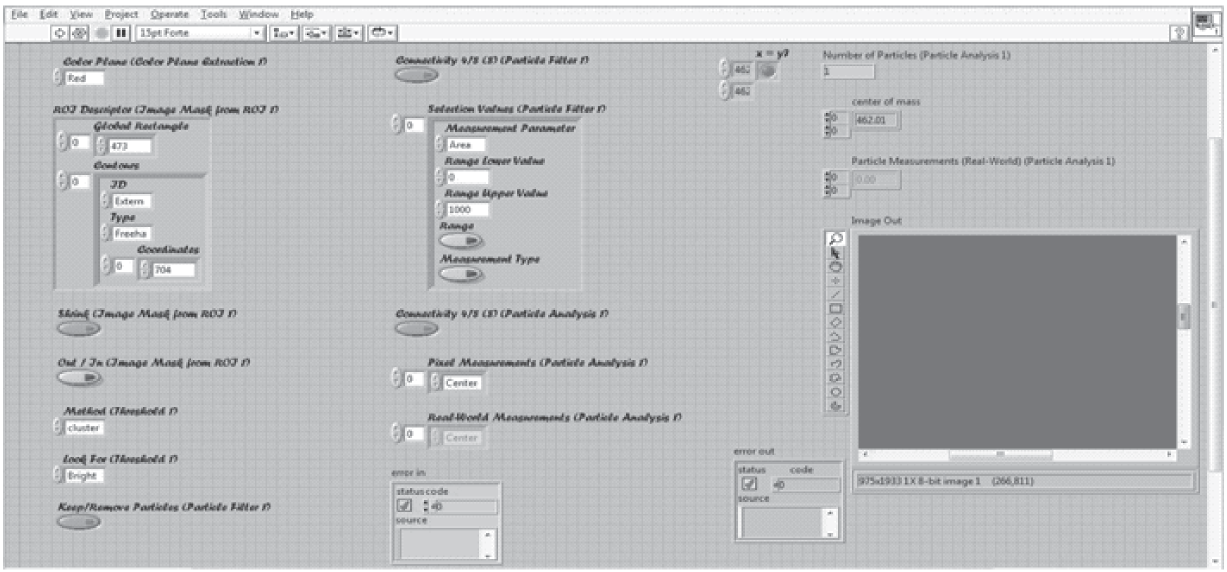

***Figure 4.*** Front panel vi

Font panel consists of many controls and indicators. Colour plane extraction is a control which extracts the image to a red plane one. ROI Descriptor Change Mask is used to define the region of interest. There are on/off button options for masking process which defines which region to be masked, namely. the region within or outside of ROI. There are Threshold controls to control the method of thresholding as well as what to look for dark or bright objects during thresholding. There are particle filter controls to remove the defective portions which were not highlighted during the thresholding process. At last, we have the particle analysis controls and indicators. The image out is the processed and filtered image upon which particle analysis is conducted. The connectivity, pixel measurements, and real world measurements are the controls required for particle analysis. The results of particle analysis are shown in indicators, viz. Number of particles, Centre of mass. The two unknowns x and y are our comparison variables. X is denoted by the good sample's centre of mass and Y is denoted by the present sample's centre of mass. If they match accurately, the alarm light glows and the conveyor belt system is left unhindered and if it does not glow, the bottle is thrown away from the conveyor belt.

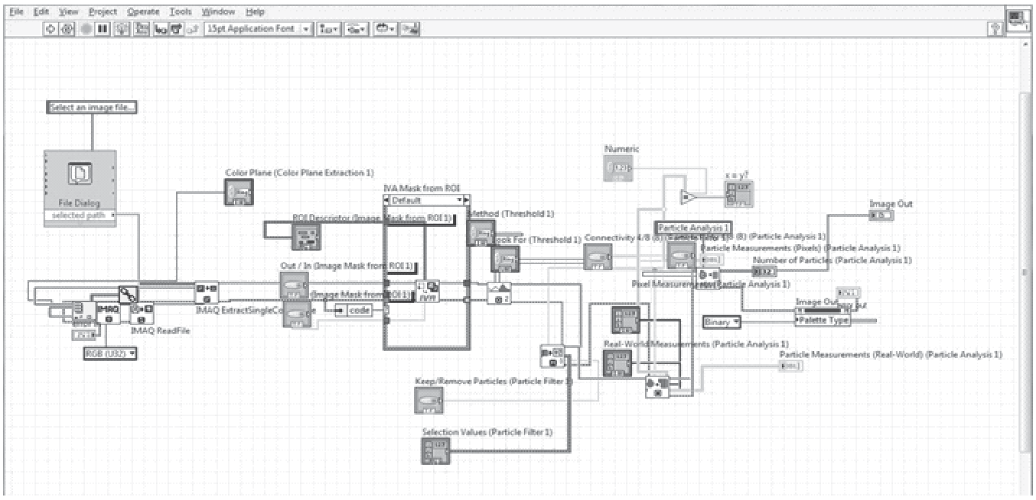


***Figure 5.*** Block diagram vi

Block diagram vi consist of many controls and indicators. We have an image acquisition control which acquires the image from the smart camera. The acquired image is stored in an IMAQ read file in RGB (32-bit) format. There is a colour plane extraction control which extracts out the red plane (in our case red, maybe blue or green). Now, the ROI controls are used to choose our region of interest and the range of pixels outside our region of interest are masked off. Now, the image mask from ROI is sent for thresholding process where we do cluster thresholding and select the bright objects. Now after thresholding, we send it to the particle filter from where the defective portions of image, if there is any is sent to particle analysis process. In particle analysis, the number of particles in the image and also the centre of mass of our processed image is found out and displayed in indicator. Now, the acquired centre of mass value of the present sample is compared with the original good sample's centre of mass value and if they are found equal, then present sample is good and light glows. On the contrary, if they are unequal, then present sample is defective and light does not glow and signal is sent to remove that bottle from the conveyor belt.

## 5. RESULT AND CONCLUSION

The proposed system was tested with different test cases and keeping the time constraint into consideration. The system produced satisfactory results. The proposed technique was able to detect the impure bottle and initiate action within the specified time interval. For testing the clean bottles, little dirty and very dirty bottles were allowed to pass through conveyer, the system was able to divert the little and very dirty bottles living the clean ones Fig 6 and Fig 7 shows the front panel for the clean and dirty bottle respectively. Similarly the completely filled and incompletely filled bottles were also tested, the system was able to initiate proper action Fig 8 and Fig 9 shows the front panel for completely and incompletely filled bottles respectively. Further it was also tested for the checking the proper labelling process on the bottle the system accurately performed the task with proper actions. Fig 10 and Fig 11 shows the front panel for proper and improper labelling respectively.

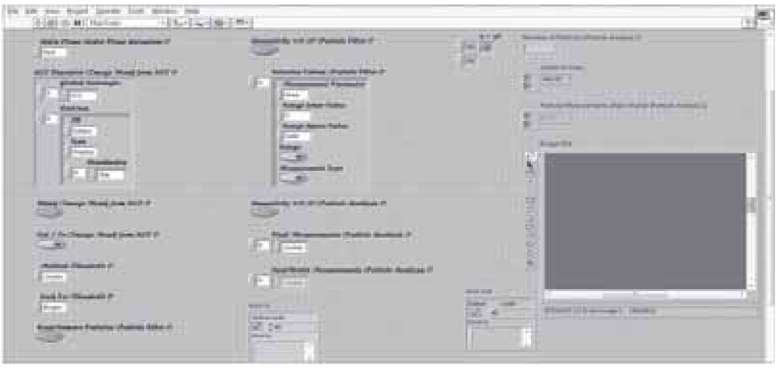

***Figure 6.*** Front panel view of clean bottle

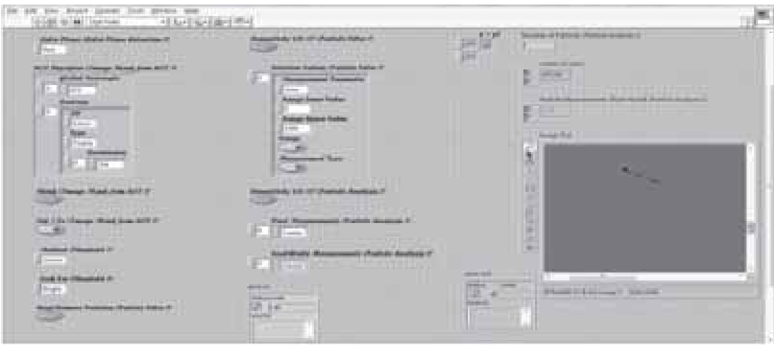

***Figure 7.*** Front panel view of dirty bottle

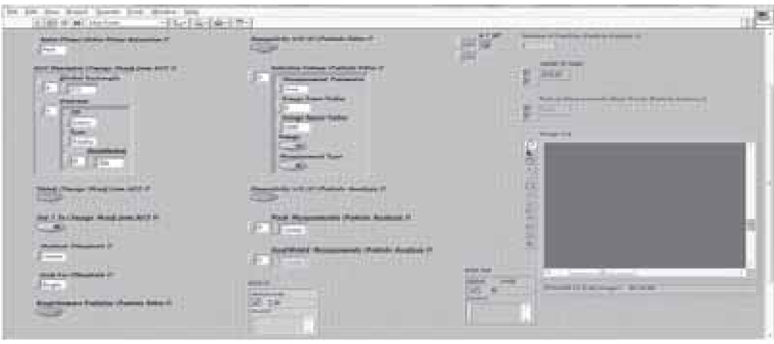

***Figure 8.*** Front panel view of filled bottle

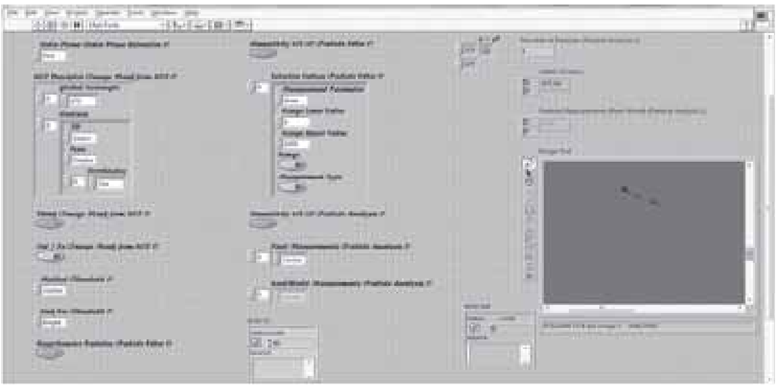

***Figure 9.*** Front panel view of incompletely filled bottle

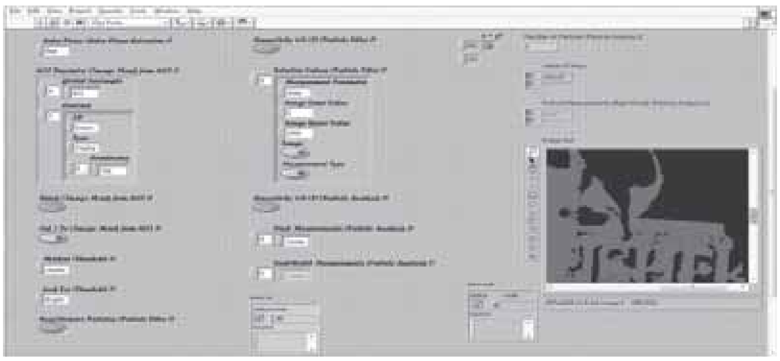

***Figure 10.*** Front panel view of properly labeled bottle

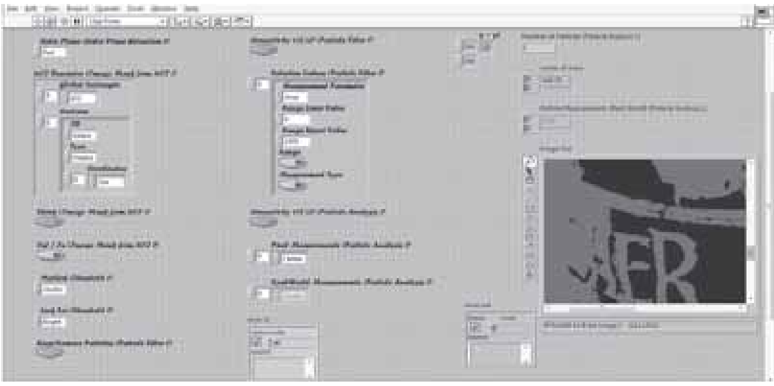

***Figure 11.*** Front panel view of improperly labeled bottle

The above figure clearly indicated the results obtained and these were able to meet the objective of the paper discussed without causing any deviation in the production line timing.

## REFERENCES


[1] Report on Indian beverage industry – Economics group India, 2000.

[2] Food Industry Overview, Plunkett Research. Retrieved 17 February 2006.

[3] Phosphates, in Smith, Andrew. The Oxford companion to American food and drink. Oxford University Press US, 2007.

[4] Ishizu K, Takemura H, Kawabata K, Asama, H, Mishizma T, Mizoguchi H, "Image processing of particle detection for asbestos qualitative analysis support method – particle counting by using color variance of background", proceedings of SICE Annual Conference ,20-22 august 2008.

[5] Wengcheng Wang, Xiaojun Cui, "A background correction method for particle image under non-uniform illumination conditions", proceedings of 2nd International Conference on Signal Processing Systems ( ICSPS ), 2010, 5-7 July 2010.

[6] Ishizu K, Takemura H, Kawabata K, Asama, H, Mishizma T, Mizoguchi H, "Image processing of particle detection for asbestos qualitative analysis support method – particle counting system based on classification of background area", proceedings of 10th International Conference Control, Automation, Robotics and Vision,2008, ICARCV 2008, 17-20 December 2008.

[7] Lu Jun, Li Pingping, "A Data Acquisition and 2-D Flow Measuring Technology in Agricultural Spray Field Based on High Speed Image Processing", proceedings of International Conference on Measuring Technology and Mechatronics Automation, 2009, ICMTMA '09, 11-12 April 2009.

[8] Haiyang Sun, Xuejin Sun, Zhidong Jiang, "Research on the method of precipitation particle image recognition", proceedings of International Conference on Remote Sensing, Environment and Transportation Engineering (RSETE), 2011, 24-26 June 2011.

[9] NI 1744 Smart Camera User Datasheet -June 2008

[10] Getting Started with the NI 1744 Smart Camera Datasheet-October 2010

[11] LabVIEW Data Acquisition Basics Datasheet

[12] LabVIEW User Datasheet - National Instruments

# MEASUREMENT OF RING GAUGE DIMENSION BY OPTICAL METHOD AND IMAGE PROCESSING

Shashi K. Singh
Dronacharya Group of Institutions, 27 Knowledge Park-III, Greater Noida 201308, U.P.
kumar.shashi651@gmail.com

Datta Raya Bhise
Dronacharya Group of Institutions, 27 Knowledge Park-III, Greater Noida 201308, U.P.
dvbhise@rediffmail.com

Vinod Kumar
Dronacharya Group of Institutions, 27 Knowledge Park-III, Greater Noida 201308, U.P
kumarvinod2007@gmail.com
.
G. Tangkeshwari
Dronacharya Group of Institutions, 27 Knowledge Park-III, Greater Noida 201308, U.P.
tangkeshwari.ec@gmail.com

Ravi
Dronacharya Group of Institutions, 27 Knowledge Park-III, Greater Noida 201308, U.P.
er.ravi28@gmail.com

## ABSTRACT

The dimensions of Ring gauge are measured using vernier caliper inside micrometer, precision coordinate measuring machine and length measuring machine (horizontal metroscope). These devises are used in order of accuracy required and quality of the ring gauge. The accuracy obtained with these devise between 0.020 mm and 0.0005 mm. However, all these instruments/ devices are traceable to the length standards through gauge blocks. The necessity for this development of image based procedures I mainly due to modern production technology that demands accurate dimensional measurement various mechanical components. An attempt has been made to measure the precision ring, gauges directly by image proceeding technique with conic kernels and their orientation which gives a more ;accurate noncontact apparatus. This paper presents a general framework for analyzing structure asymmetry of ring gauge.

***Keywords:*** Conic Kernel, steerable filters, spatio-temporal orientation, multi-scale algorithm

## 1. INTRODUCTION

In the Industry, there is a need for accurate measuring of 3D shapes of various objects to speed up the development new products and also to ensure manufacturing quality. Ring gauge are used for checking external diameter of a cylindrical object for; celibately or setting gauges or other standards. They are made to variety of tolerance grades for master application. Accurate dimension measurement of ring gauges is of great importance as ring gauge are used as standards.

We propose a new 3D kernel of 3D orientation for dimension measurement of ring gauges. In the Cartesian coordinates, the kernel has a shape of a truncated cone with its axis in the radial direction with very small angular support. In the local spherical coordinates, the angular part of the kernel is a 2D Gaussian function. A set of such kernels is obtained by uniformly sampling the 2D space of azimuth and elevation angles [1-2]. The projection of local neighborhood on such a kernel set produces a local 3D orientation. The kernel's local support enables the resulting spatio-temporal analysis to possess higher orientation resolution than 3D steerable filters. Consequently, maxima and minima can be detected and localized accurately. We describe the experiments, the superiority of the proposed kernels compared to Hough transformation or expectation-maximization detection. Radiometric differences are taken into account through an additive intensity field. We present an efficient multi-scale algorithm for the joint estimation of structural and radiometric asymmetry of ring gauges of different sizes. The initial results are quite satisfactory. More comparable calibration of this method against standard method is in progress. The motivation of our approach is the local detection and estimation of multiple planes in spatio-temporal imagery. In this paper, we focus on the estimation of multiple planes from the patio-temporal orientation aspect. It is pointed out that dimensions of 3D objects can be measured from spatial-temporal orientation.

## 2. CONIC KERNEL

There are several equivalent coordinates to represent 3D orientation. They differ in the number and form of orientation variables. For example, a 2D polar angle and an implicit elevations angle (between the polar radius and z-coordinate) are used together to describe 3D orientation in the cylindrical coordinates, while three directional angles, (i.e. three angles between three Cartesian coordinate [3-4] ). For orientation analysis, we believe that the orientation variables should be as small as possible to alleviate the complexity of indexing and visualization. Thus, we choose the spherical coordinates in which only two angles (azimuth and elevation) are needed to represent 3d representation.

The input data for plane analysis and measurement can be either the local image derivatives space (i.e. a space coordinated by partial derivatives of images with respect to different axes). They are the same for filtering purpose. For simplicity, we use the same representation $I\,(\mathrm{x, y, z})$ for both kinds of input data. Here we assume that $I\,(\mathrm{x, y, z})$ is correctly obtained for every (x, y, z). Thus, the error in obtaining image derivatives or spectrum is not considered. We start orientation analysis by computing a local spherical mapping on the input data $I\,(\mathrm{x, y, z}) \rightarrow \mathrm{I}\,(\mathrm{r}, \theta, \phi)$

We start by Cartesian coordinate to polar coordinate by following steps

In order to have fine orientation resolution we use conic kernels with small angular support to sample the orientation space locally these kernels are radial-angular separable. A conic kernel centered at $(\theta_i, \phi_j)$ reads.

$$k(\theta,\phi)\,(\mathrm{r},\theta,\phi) = \frac{\mathrm{G}_{\mathrm{o}}^{\theta i,\phi j}(\theta,\phi)}{\mathrm{N}_{R_{\min} R_{\max}}^{(\theta_{\mathrm{i}},\phi_{\mathrm{j}})}(r)} \tag{1}$$

where $N_{R\max,R\min}^{\theta i,\phi j}\,(r)$ is a compensation function along the radial direction, which will described in next sec. First we focus on the angular part of the kernel, which is a 2D Gaussian function [4-5] in $(\theta,\phi)-$ space.

$$G^{(\theta_i,\phi_j)}(\theta,\phi) = \frac{1}{2\pi\sigma^2}\exp\left(\frac{-(\mu(\theta,\theta_{\mathrm{i}}))^2 + (\phi-\phi_j)^2}{2\sigma^2}\right. \tag{2}$$

As the azimuth angle $\theta$ is periodic, we define a $a\mu(.)$ to represent the minimal circular difference between

$$\theta \text{ and } \theta_i \;(\theta, \theta_{\mathrm{i}} \in [0^{\circ}, 360^{\circ}])$$

$$\mu\,(\theta,\theta_{\mathrm{i}}) = \min\left(|\theta - \theta_{\mathrm{i}}|, |\theta - \theta_{\mathrm{i}} - 360^{\mathrm{o}}|, |\theta - \theta_{\mathrm{i}} + 360^{o}|\right) \tag{3}$$

Conic Kernel response to 3D planes: In the 3D coordinate systems, a plane passing through the origin (0, 0, 0) with a unit normal vector

$\mathrm{N} = (\mathrm{n1, n2, n3})\mathrm{T}$ reads

$\mathrm{xn1 + yn2 + zn3 = 0}$

In order to represents a plane with $(\theta and \phi)$ , we convert the Cartesian coordinates into spherical coordinates

$$(x, y, z) \rightarrow (\mathrm{r}, \theta, \phi) \text{ and } (\mathrm{n}_1, n_2, n_3) \rightarrow (1, \theta_n, \phi_n).$$

After dropping out r we obtain an equation with variable $(\theta and \phi)$

$$\cos(\phi)\cos(\phi_{\mathrm{n}})\cos(\theta - \theta_{\mathrm{n}}) + \sin(\phi)\sin(\phi_{\mathrm{n}}) = 0$$

After horizontal and vertical planes with normal parallel to the co-ordinate axes, their corresponding representations in the $(\theta,\phi)$ - space are straight lines. In 3d analysis, we usually encounter titled planes which turn into harmonic curves with different amplitudes and phases in the $(\theta,\phi)$- space (fig.) The normal vector of each plane i.e. $\theta_n, \phi_n$ is related to the extreme point $\theta_m, \phi_m$ on corresponding curve as follows

$$\theta_n = \theta_{\mathrm{m}} + 180^0$$

$$\phi_n = 90^0 - \phi_m$$

The titled phases parameters (u, v) can then be estimated using $\theta_n$ and $\phi$

$$u = \cos(\theta_n)\cot(\phi_n)$$
$$v = \sin(\theta_n)\cot(\phi_n)$$

Further, each harmonic curve has two zero- crossing points on the $\theta$ axis with a distance of 180° and $\theta_m$ lies exactly in the middle of two zero-crossing points[5-8].

The extra geometry constraint is very useful in determining the number of points. Further, each harmonic curve has two zero-crossing points on the $\theta$ axis with a distance of 180° and $\theta_m$ lies exactly in the middle of these two zero-crossing points. This extra geometry constraint is very useful in determining the number of planes automatically as well as in obtaining reasonable initial values of plane parameters. In practice, we obtain a set of points in the $(\theta, \phi)-$ space. Extracting the parameters $\theta_n, \phi_n$ form these points is then a standard fitting problem. For a simple curve, least square estimation is applicable [9-13].

## 3. EXPERIMENT AND RESULT

The experimental set up consists of CCD camera and image grabbing card installed on Pentium Computer. Front and back illumination is provided to obtain proper illumination through the 3d object. The experiment is done on two standard ring gauges as shown in fig.1 and fig.2. It is analysed and measurement is done by the program developed in Labview6

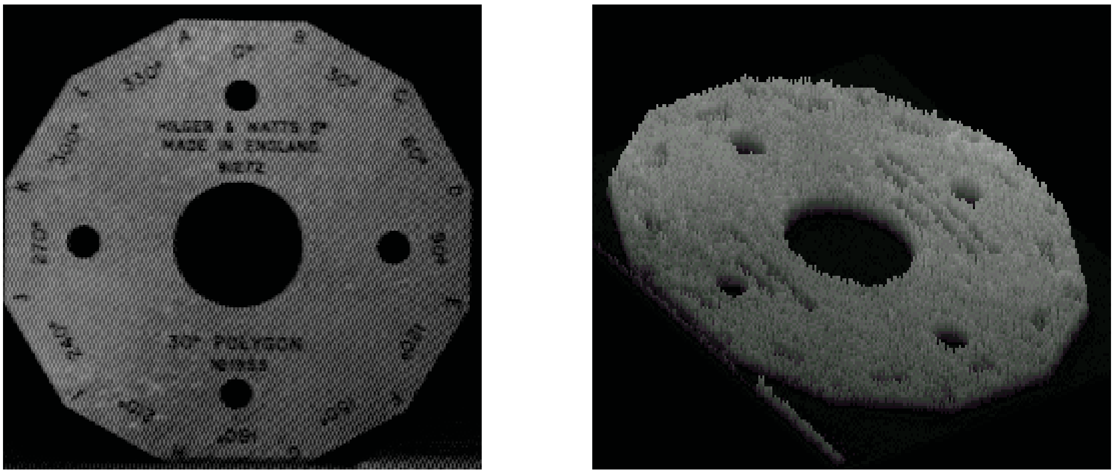

***Fig1.*** a. Original image of Ring Gauge 1 b. Analyzed image

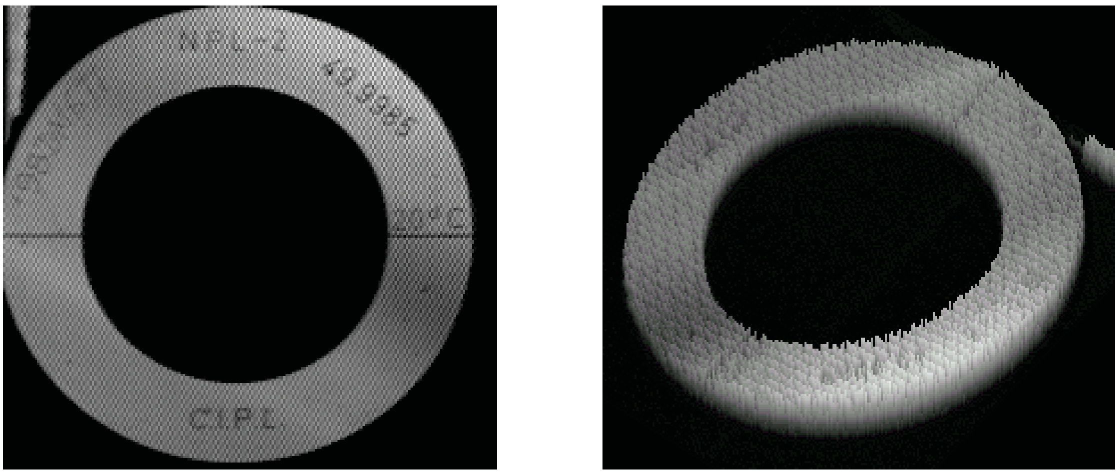


***Fig.2*** a. Original image of Ring Gauge2 b. Analyzed image

## 4. CONCLUSION

The results obtained by image processing system are compared with the results obtained using optical profile projector. It is seen that repeatability in our scheme is better than the standard method (using optical profile projector). In our case standard deviation comes to be 0.0006mm and as compared to 0.001mm in the case of profile projector. Uncertainty of measurement in our case is + 0.0001mm.

## REFERENCES


1. ReimerK. Lenz and Roger Y. Tsai ,Techniques for Calibration of scale factor and Image center for high Accuracy 3-D Machine Vision Metrology, IEEE Transactions on pattern analysis and Machine Intelligence 10, Sept. 1988.No.5

2. P.MA. Van Ooijen, R. Witkamp, Multi-detector CT and 3D imaging in a Multi-vendor PACS environment, International Congress Series ,1256 ,2003, p.860-865.

3. Michael Hunerbein, Michael Rasche,, Three-dimensional Ultrasonography of bone and soft tissue lesions, European Journal of Ultrasound, 13,2001,p.17-23.

4. R.T. Rodrigues, J. Rubio, New basis for measuring the size distribution of bubbles, Minerals Engineering, 16 2003, p.757-765.

5. Hang Cao, Xiaomei Chen, K.Tu. Grattan, Yujiu sun, Automatic micro dimension measurement using image processing methods, Measurement , 31 , 2002, p.71-76.

6. Douglas Fortune, Bradley A. Wilson, Constant time 0(1) pixel averaging with applicability to kernel filtering, Computers and Geosciences 29 ,2003, p. 605-611

7. Bauer, F., Schöner, H., Dorrington, A. A., Heise, B., Wieser, V., Payne, A. D., Cree, M. J., and Moser, B., . Image Processing for 3D-Scans Generated by TOF Range Cameras, IEEE/OSA Journal of Display Technology, 2009

8. Büttgen, B., Oggier, T., Lehmann, M., Kaufmann, R., and Lustenberger, F., CCD/CMOS Lock-In Pixel for Range Imaging: Challenges, Limitations and State-of-the-Art. In: 1st Range Imaging Research Day, Zurich, Switzerland, 2005. pp. 21-32.

9. Büttgen, B., and Seitz, P., Robust Optical Time-of-Flight Range Imaging Based on Smart Pixel Structures. In: IEEE Transactions on Circuits and Systems I: Regular Papers, 55(6), 2008, pp. 1512-1525.

10. Dorrington, A. A., Cree, M. J., Payne, A. D., Conroy, R. M. and Carnegie, D. A., Achieving sub-millimetre precision with a solid-state full-field heterodyning range imaging camera, Meas. Sci. Technol. 18, 2007pp. 2809–2816.

11. Dorrington, A. A., Cree, M. J., Carnegie, D. A., Payne, A. D., Conroy, R. M., Godbaz, J. P., and Jongenelen, A. P. P.,. Video-rate or high-precision: a flexible range imaging camera. In: SPIE 6813 - Image Processing: Machine Vision Applications, San Jose, CA, USA, 2008 pp 681307.

12. Balaban, M.O., Chombeau, M., Cırban, D. and Gümüş, Prediction of the weight of Alaskan pollock using Image analysis. Journal of Food Science, 75 (8): 2010, 552-556.

13. Balaban, M.O., Chombeau, M., Gümüş, B. and Cırban, D... Determination of volume of Alaska Pollock (Theragra chalcogramma) by image analysis. Journal of Aquatic Food Product Technology, 20: 2011, 45-52.

# DESIGN OF 4x4 ARRAY MICROSTRIP PATCH ANTENNAS at 430 MHz FOR WIND PROFILE RADAR

G. Guru Prasad
Asst Professor
Department of Electronics and Communication Engineering
Sree Vidhyanikhaten College of Engineering, Tirupathi.
E-mail id: guru.p6@gmail.com

T. Rama Sree
Associate Professor
Department of Electrical and Electronics Engineering
S. V. University College of Engineering, Tirupathi.
E-mail id: rama.japee@gmail.com

P. Srinivasulu
RADG- director, NARL-Gadanki
E-mail id: pslu@narl.gov.in

## ABSTRACT

A Microstrip patch antenna is a low-profile antenna that has a number of advantages over other antennas. It is lightweight, inexpensive, and easy to integrate with accompanying electronics. While the antenna can be 3-D in structure (wrapped around an object, for example), the elements are usually flat; hence their other name, planar antennas. Microstrip patch Antennas has been received tremendous attention since the last two decades and now it becomes a major component in the development of UHF Wind profile RADAR. National Atmospheric Research Laboratory Developed 8x8,16x16 Array UHF Wind Profile Radar with Microstrip Patch Antennas operating at 1280 MHz.

The aim of the project is to Design and test Rectangular Microstrip patch Antenna of 4x4 array operating at 430 MHz. In this design aluminum plates are used for patch and ground plate, air is used as Dielectric material. Coaxial Probe technique is used for feeding Antenna. IE3D software is for Design and Simulation of Antenna. The Simulated results are in good agreement with those measured for the Return Loss, VSWR and Radiation Pattern.

With single Microstrip Antenna we get 8.6 dBi Directivity and 7 MHz Band Width .With 2 X 2 Array Microstrip Antenna we get about 15 dBi Directivity and 7 MHz Band width Using this 4x4 antenna array 19.82 dBi gain and 10 MHz bandwidth were obtained These results show that significant improvements in the Antenna Efficiency. This is sufficient for data processing for the system of Wind Profiler Radar applications.

***Key Words:*** *Microstrip, Antenna Array, Dielectric, Patch, IE3D, Radiation Pattern*

## 1. INTRODUCTION

In radar and space communication applications patch antennas have attracted much interest due to their compactness and dual-frequency operation. They are inexpensive to fabricate, light in weight, and can be made conformable with planar and nonplanar surfaces. Unfortunately, they have some shortcomings, including relatively low gain, narrow bandwidth, and sensitivity to fabrication errors [1-2]. Microstrip antenna is printed type of antenna consisting of a dielectric substrate sandwiched in between a ground plane and a patch [1]. The concept of Micro strip antenna was first proposed in 1953, twenty years before the practical antennas were produced. Since the first practical antennas were developed in early 1970's, interest in this kind of antennas was held in New Mexico[6]. The microstrip antenna is physically very simple and flat, these are two of the reasons for the great interest in this type of antenna.

Microstrip antennas have several advantages compared to other bulky type of antennas. Some of the main advantages of the microstrip antennas are that it has low fabrication cost, its lightweight, low volume, and low profile configurations that it can be made conformal, it can be easily be mounted on rockets, missiles and satellites without major modifications and arrays of these antennas can simply be produced. However, microstrip antennas have some drawbacks including narrow bandwidth, low power handling capability and low gain. But with technology advancement and extensive research into this area these problem being gradually overcome.

In many practical designs, the advantages of microstrip antennas far outweigh their advantages. With continuing research and development it is expected that microstrip antennas will replace conventional antennas for most applications. Some of the notable applications for microstrip antennas are in the areas of mobile satellite communication, the Direct Broadcast Satellite (DBS) system and Global Position System (GPS). Microstrip antennas also found useful in non-satellite based application such as remote sensing and medical hypothermia application.

## 2. LITERATIVE REVIEW

In this paper I have chosen Microstrip antenna technology for the designing of the antenna because it is most widely used in the field of antennas technology because of its commercial reality with applications in wide variety of microwave systems. These are using in Personnel Communication systems (PCS), mobile satellite communication, wireless local area networks (WLANs) and intelligent vehicle highway systems(IVHS) etc.. These are preferred over other types of radiators because of its low profile and are light in weight and they can be mad e conformal and they are well suited to integration with microwave integrated circuits(MICs).these are low cost when compared to traditional antenna elements such as reflectors, horns, slots, or wire antennas.

In this paper Aluminum sheet is used as material and air is used as dielectric substrate. IE3D software is used to design and simulation of antenna array.

## 3. RESULTS AND DISCUSSIONS

**Simulated Results for Single patch Antenna:**

### 3.1. RETURN LOSS MEASUREMENT

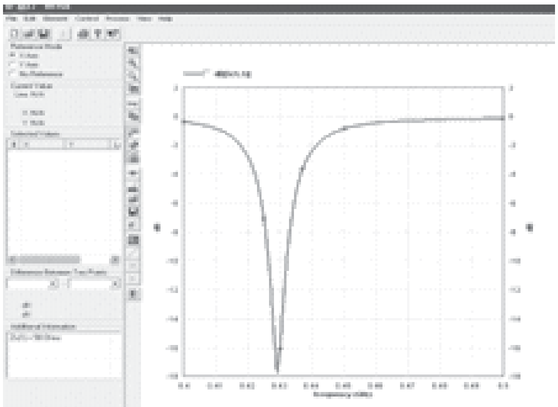

***Figure: 1***

From Fig 1,The Return loss obtained at 430 MHZ is -18 dB and band width obtained at -10 dB is about 7 MHZ.

### 3. 2 DIMENSIONAL RADIATION PATTERN

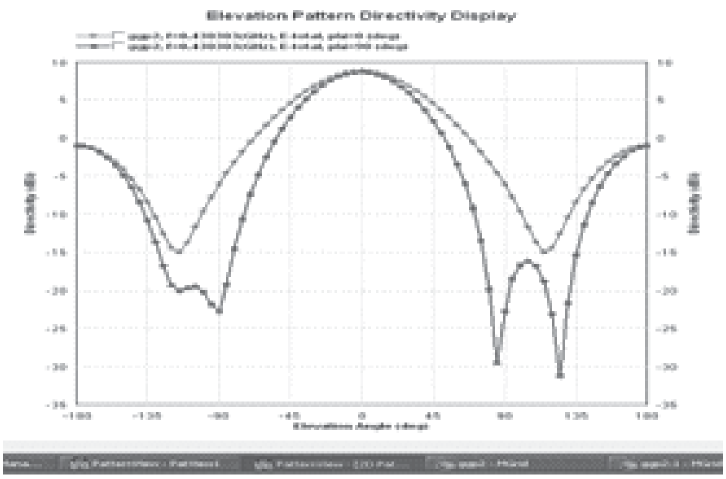


***Figure 2***

From figure 2, the 3 dB Beam Width obtained at pi=00 is 1050 and at 900 is 950

### 3.3 INPUT IMPEDANCE AT 430 MHZ

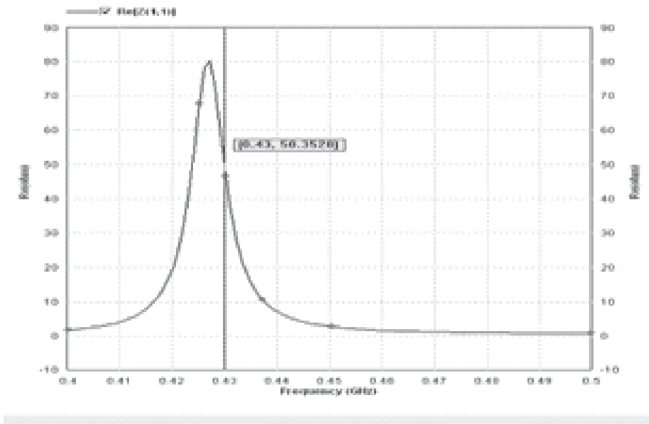


***Figure 3***

From figure 3, the Input Impedance at 430 MHZ is 50 ohm

### 3.4 VSWR MEASUREMENT

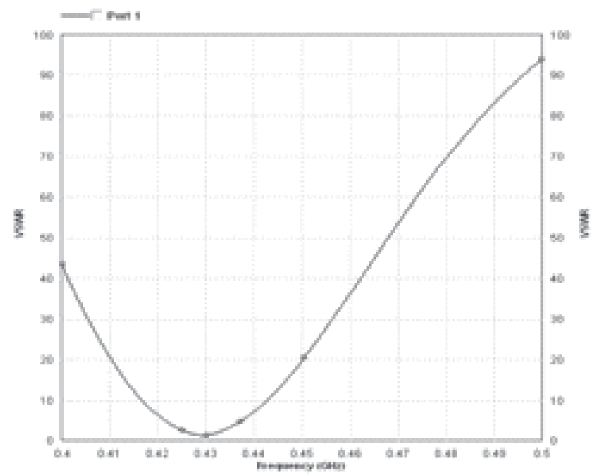


***Figure 4***

From the figure 4, the VSWR obtained at 430 MHZ is about 1.35

### 3.5 ANTENNA EFFICIENCY VS. FREQUENCY

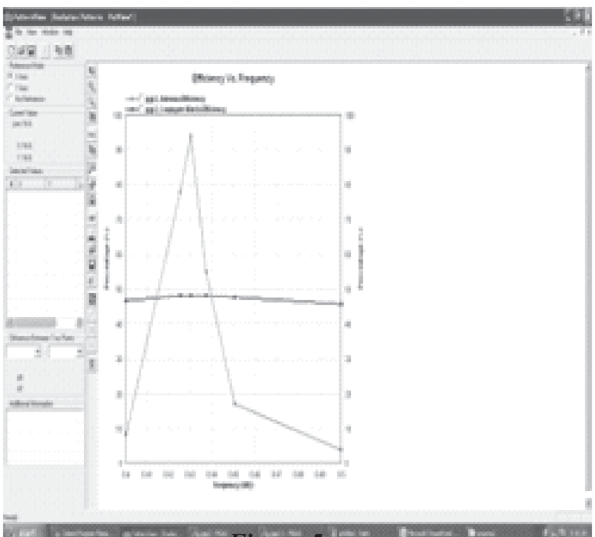


***Figure 5***

From the figure 5, the Antenna Efficiency is about 95%

### 3.6 RADIATION PATTERN FOR SINGLE PATCH ANTENNA

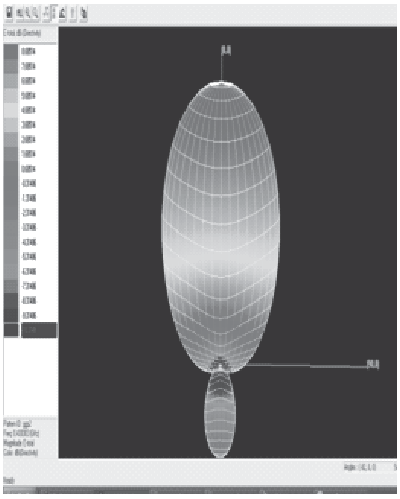

*Figure 6*

From the figure 6, the directivity of 3-Dimensional radiation pattern is about 8.6 dBi

### 3.7 MEASURED RESULTS FOR SINGLE MICROSTRIP ANTENNA USING NETWORK ANALYZER :

Fabricated Microstrip Antenna using Aluminum sheet and air as dielectric Material shown in figure 7

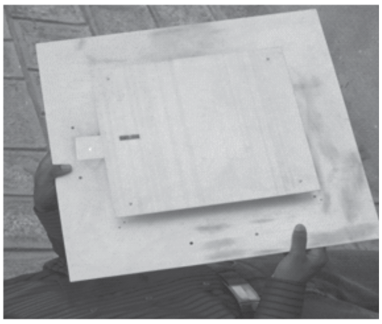

*Figure 7*

### 3.8 RETURN LOSS MEASUREMENT

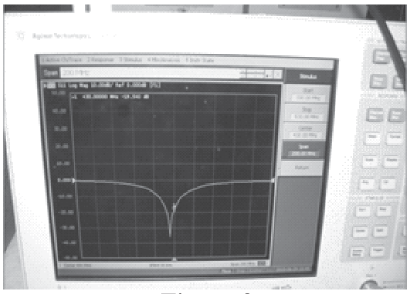

*Figure 8*

The Return loss obtained from Network Analyzer when Antenna placed inside the room at 430 MHZ is -19.5 db

### 3.9 RETURN LOSS MEASURED WHEN ANTENNA PLACED AT FREE SPACE

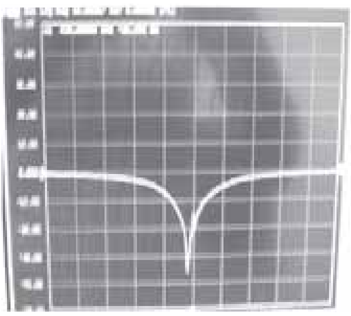

*Figure 9*

Measured return loss at 430 MHZ is -30 dB

IE3D Plots for 2 x 2 arrays

**3.10 RETURN LOSS**

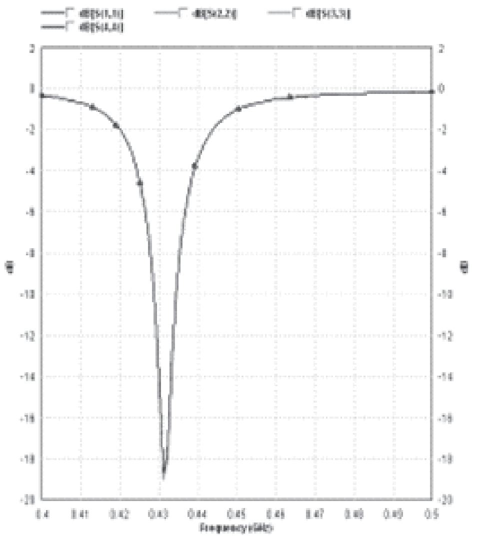

*Figure 10*

From figure 10, the simulated return loss obtained for 2 x 2 arrays at 430 MHZ is -19 dB and the Band Width at -10 dB is about 7 MHZ.

**3.11 RADIATION PATTERN FOR 2 X 2 ARRAYS**

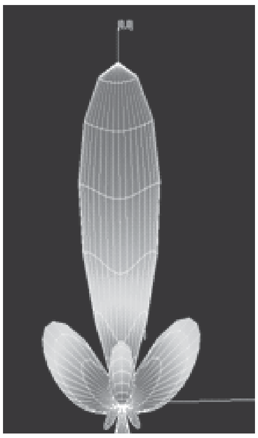

*Figure 11*

From figure 11, the Directivity of the 3-dimensional Radiation Pattern is 15 dBi

IE3D Plots for 4 x 4 Arrays

**3.12.1 DESIGNED 4 X 4 ARRAY MICROSTRIP ANTENNA**

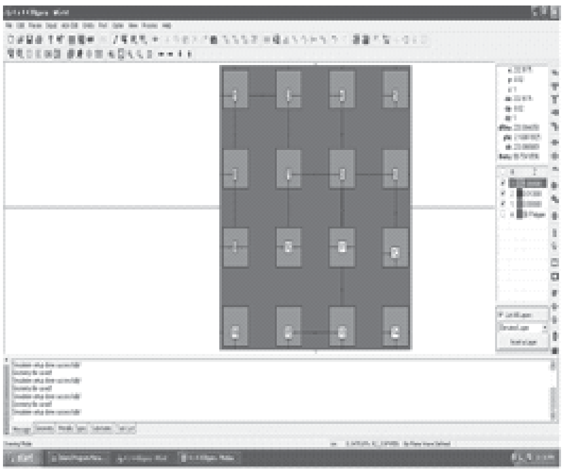

*Figure 12*

The 4 x 4 array Microstrip Patch Antenna Array shown in figure 12

### 3.13 RADIATION PATTERN FOR 4 X 4 ARRAYS

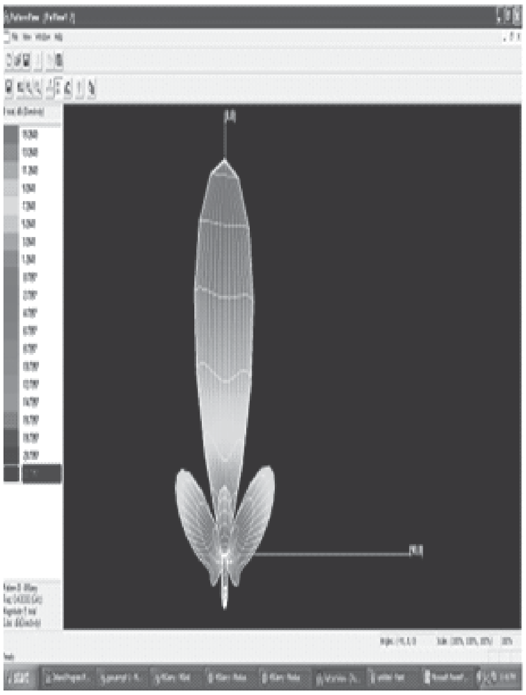

*Figure 13*

The 3-Dimensional Radiation Pattern is shown in figure 13 and 19.3 dBi

## 4. CONCLUSION

The aim of this project is to design a 4x4 Micro strip patch antenna array for atmospheric Wind Profile Radar application. Hence the designed must be able to fit in such application. As demonstrated by the design and the results obtained for a single patch antenna, at 430 MHz has been successfully designed and simulated . 2 x 2 Antenna Array, 4 x 4 Antenna Array and a 1x8 Antenna Array has been simulated using IE3D.

From the radiation pattern, it is observed that use of amplitude taper maintained the SLL within the maximum scan angle limit, which is an added advantage for Atmospheric Wind Profile Radar application.

With single microstrip Antenna we get 8.6 dBi Directivity and 7 MHZ Band Width are obtained.

With 2 X 2 Array Microstrip Antenna we get about 15 dBi Directivity and 7 MHZ Band Width. With 4X4 Array Microstrip Antenna Array about 19 dBi Directivity and 10 MHZ Band Width are achieved, which is sufficient for data processing for the system. These results are better when we compare with the existing system at NARL. So we can establish a new RADAR with Microstrip Antenna operating with 430 MHZ.

The future work of this Project is to extend the design to 8x8 Antenna Array and later 16x16 Antenna Array.

## REFERENCES


[1] John D. Kraus and Ronald J. Marhefka, "Antennas for All Applications, 3rdEdition", McGraw-Hill, 2002.

[2] C. A Balanis, "Antenna Theory Analysis and Design, 2nd Edition", John Wiley & Sons, New York, 1996.

[3] R. Garg, P. Bhartia, I. Bahl and A. Ittipiboon, "Microstrip Antenna Design Handbook", Artech House Antennas & Propagation Library,Nov 2000

[4] D.M Pozar, "Microstrip Antennas", IEEE Proceedings, vol.80, pp.79-91 Jan1992

[5] Leo G. Maloratsky "Reviewing the Basics of Microstrip Lines" Microwaves & RF March 2000

# THE UNUSED BANDWIDTH RECYCLING IN WIRELESS COMMUNICATION TECHNOLOGY

V. MARUTHI PRASAD
Asst. Professor, Dept of MCA, MITS, Madanapalle,
Chitoor Dist. Andhra Pradesh
Email: maruthi_vv@yahoo.co.in, Mobile: 9885259496

V. RAGHAVENDRA PRASAD
HOD of CSE, MNR College of Eng. Sangareddy,
Medak Dist. Andhra Pradesh
Email: meetraghu5@gmail.com, Mobile: 9440983701

## ABSTRACT

Bandwidth demanding applications was designed by using of IEEE 802.16 standard with quality of services (QoS).The quality of service (QoS) refers to several related aspects of telephony and computer networks that allow the transport of traffic with special requirements. N particular, much technology has been developed to allow computer networks to become as useful as telephone network for audio conversations, as well as supporting new applications with even more strict service demands. 4G is the fourth generation of cellular wireless standards. It is a successor to the 3G and 2G families of standards. Bandwidth is reserved for each application to ensure the QoS for variable bit rate (VBR) applications and difficult for subscriber stations to predict the amount of incoming data. The QoS guaranteed services to ensure subscriber station may reserve more bandwidth than its demand. In this paper, we propose a scheme, named Bandwidth Recycling, to recycle the unused bandwidth without changing the existing bandwidth reservation the idea of the proposed scheme is to allow other SSs to utilize the unused bandwidth when it is available. Thus, the system throughput can be improved while maintaining the same QoS guaranteed services. By analyzing factors affecting the recycling performance, three scheduling algorithms are proposed to improve the overall throughput. The simulation results show that our proposed algorithm improves the overall throughput by 40% in a steady network..

***Key Words:*** QoS, VBR, WiMAX, IEEE 802.16, Bandwidth Recycling

## 1. INTRODUCTION

The Worldwide Interoperability for Microwave Access (WiMAX), based on IEEE 802.16 standard standards, is designed to facilitate services with high trans-mission rates for data and multimedia applications in metropolitan areas. The physical (PHY) and medium access control (MAC) layers of WiMAX have been specified in the IEEE 802.16 standard. Many advanced communication technologies such as Orthogonal Frequency-Division Multiple Access (OFDMA) and multiple-input and multiple-output (MIMO) are embraced in the standards. Supported by these modern technologies, WiMAX is able to provide large service coverage, high data rates and QoS guaranteed services. Because of these features, WiMAX is considered as a promising alternative for last mile broadband wireless access (BWA).

In order to provide QoS guaranteed services, the subscriber station (SS) is required to reserve the necessary bandwidth from the base station (BS) before any data transmissions. In order to serve variable bit rate (VBR) applications, the SS tends to keep the reserved bandwidth to maintain the QoS guaranteed services. Thus, the amount of reserved bandwidth transmitted data may be more than the amount of transmitted data and may not be fully utilized all the time. Although the amount of reserved bandwidth is adjustable via making bandwidth requests (BRs), the adjusted bandwidth is applied as early as to the next coming frame. The unused bandwidth in the current frame has no chance to be utilized. Moreover, it is very challenging to adjust the amount of reserved bandwidth precisely. The SS may be exposed to the risk of degrading the QoS requirements of applications due to the insufficient amount of reserved bandwidth.

To improve the bandwidth utilization while maintaining the same QoS guaranteed services, our research objective is twofold:

1. The existing bandwidth reservation is not changed to maintain the same QoS guaranteed services.
2. Our research work focuses on increasing the bandwidth utilization by utilizing the unused bandwidth.

We propose a scheme, named Bandwidth Recycling, which recycles the unused bandwidth while keeping the same QoS guaranteed services without introducing extra delay. The general concept behind our scheme is to allow other SSs to utilize the unused bandwidth left by the current transmitting SS. Since the unused bandwidth is not supposed to occur regularly, our scheme allows SSs with non-real time applications, which have more flexibility of delay requirements, to re-cycle the unused bandwidth. Consequently, the unused bandwidth in the current frame can be utilized. It is different from the bandwidth adjustment in which the adjusted bandwidth is enforced as early as in the next coming frame. Moreover, the unused bandwidth is likely to be released temporarily (i.e., only in the current frame) and the existing bandwidth reservation does not change. Therefore, our scheme improves the overall throughput while providing the same QoS guaranteed services.

1. According to the IEEE 802.16 standard, SSs scheduled on the uplink (UL) map should have transmission opportunities in the current frame. Those SSs are called transmission SSs (TSs) in this paper. The main idea of the proposed scheme is to allow the BS to schedule a backup SS for each TS. The backup SS is assigned to standby for any opportunities to recycle the unused bandwidth of its corresponding TS. We call the backup SS as the complementary station (CS). In the IEEE 802.16 standard, BRs are made in per-connection basis. However, the BS allocates bandwidth in per-SS basis. It gives the SS flexibility to allocate the granted bandwidth to each connection locally. Therefore, the unused bandwidth is defined as the granted bandwidth which is still available after serving all connections running on the SS. In our scheme, when a TS has unused bandwidth, it should transmit a message, called releasing message (RM), to inform its corresponding CS to recycle the unused band-width. However, because of the variety of geographical distance between TS and CS and the transmission power of the TS, the CS may not receive the RM. In this case, the benefit of our scheme may be reduced. In this research, we investigate the probability that the CS receives a RM successfully. Our theoretical analysis shows that this probability is least 42%, which is confirmed by our simulation.

## 2 BACKGROUND INFORMATION

The IEEE 802.16 standard specifies three types of trans-mission mediums supported as the physical layer (PHY): single channel (SC), orthogonal frequency-division multiplexing (OFDM) and Orthogonal Frequency-Division Multiple Access (OFDMA). We assume OFDMA as the PHY in our analytical model since it is employed to sup-port mobility in IEEE 802.16e standard and the scheme working in OFDMA should also work in others. There are four types of modulations supported by OFDMA: BPSK, QPSK, 16-QAM and 64-QAM.

This paper is focused on the point-to-multipoint (PMP) mode in which the SS is not allowed to communicate with any other SSs but the BS directly. Based on the transmission direction, the transmissions between BS and SSs are classified into downlink (DL) and uplink (UL) transmissions. The former are the transmissions from the BS to SSs. Conversely, the latter are the trans-missions in the opposite direction.

There are two transmission modes: Time Division Duplex (TDD) and Frequency Division Duplex (FDD) supported in IEEE 802.16. Both UL and DL transmissions cannot be operated simultaneously in TDD mode but in FDD mode. In this paper, our scheme is focused on the TDD mode. In WiMAX, the BS is responsible for scheduling both UL and DL transmissions. All scheduling behavior is expressed in a MAC frame.

The structure of a MAC frame defined in IEEE 802.16 standard contains two parts: UL and DL subframe. The UL subframe is for UL transmissions. Similarly, the DL subframe is for DL transmissions. In IEEE 802.16 net-works, the SS is coordinated by the BS. All coordinating information including burst profiles and offsets is in the DL and UL maps, which are broadcasted at the beginning of a MAC frame.

The IEEE 802.16 network is connection-oriented. It gives the advantage of having better control over net-work resource to provide QoS guaranteed services. In order to support wide variety of applications, the IEEE 802.16 standard classifies traffic into five scheduling classes: Unsolicited Grant Service (UGS), Real Time Polling Service (rtPS), Non-real Time Polling Service (nrtPS), Best Effort (BE) and Extended Real Time Polling Service (ertPS). Each application is classified into one of the scheduling classes and to establish a connection with the BS based on its scheduling class. The BS assigns a connection ID (CID) to each connection. The bandwidth reservation is made based on the CID via sending a BR. When receiving a BR, the BS can either grant or reject the BR depending on its available resources and scheduling policies.

There are two types of BRs defined in the IEEE 802.16 standard: incremental and aggregate BRs. The former allow the SS to indicate the extra bandwidth required for a connection. Thus, the amount of reserved bandwidth can be only increased via incremental BRs. On the other hand, the SS specifies the current state of queue for the particular connection via a aggregate request. The BS re-sets its perception of that service's needs upon receiving the request. Consequently, the reserved bandwidth may be decreased.

## 3 MOTIVATION AND RELATED WORK

Bandwidth reservation allows IEEE 802.16 networks to provide QoS guaranteed services. The SS reserves the required bandwidth before any data transmissions. Due to the nature of VBR applications, it is very difficult for the SS to make the optimal bandwidth reservation. It is possible that the amount of reserved bandwidth is more than the demand. Therefore, the reserved bandwidth cannot be fully utilized. Although the reserved band-width can be adjusted via BRs, however, the updated reserved bandwidth is applied as early as to the next coming frame and there is no way to utilize the unused bandwidth in the current frame. In our scheme, the SS releases its unused bandwidth in the current frame and another SS pre-assigned by the BS has opportunities to utilize this unused bandwidth. This improves the bandwidth utilization. Moreover, since the existing bandwidth reservation is not changed, the same QoS guaranteed services are provided without introducing any extra delay.

Many research works related to bandwidth utilization improvement have been proposed in the literature. In [4], a dynamic resource reservation mechanism is proposed. It can dynamically change the amount of reserved re-source depending on the actual number of active connections. The investigation of dynamic bandwidth reservation for hybrid networks is presented in [3]. The authors evaluated the performance and effectiveness for the hybrid network, and proposed efficient methods to ensure optimum reservation and utilization of bandwidth while minimizing signal blocking probability and signaling cost. In [5], the authors enhanced the system throughput by using concurrent transmission in mesh mode. The authors in [6] proposed a new QoS control scheme by considering MAC-PHY cross-layer resource allocation. A dynamic bandwidth request-allocation algorithm for real-time services is proposed in [7]. The authors predict the amount of bandwidth to be requested based on the information of the backlogged amount of traffic in the queue and the rate mismatch between packet arrival and service rate to improve the bandwidth utilization. The research works listed above improve the performance by predicting the traffic coming in the future. Instead of prediction, our scheme can allow SSs to accurately identify the portion of unused bandwidth and provides a method to recycle the unused bandwidth. It can improve the utilization of bandwidth while keeping the same QoS guaranteed services and introducing no extra delay.

## 4. PROPOSED SCHEME

The objectives of our research are twofold: 1) The same QoS guaranteed services are provided by maintaining the existing bandwidth reservation. 2) the bandwidth utilization is improved by recycling the unused band-width. To achieve these objectives, our scheme named Bandwidth Recycling is proposed. The main idea of the proposed scheme is to allow the BS to pre-assign a CS for each TS at the beginning of a frame. The CS waits for the possible opportunities to recycle the unused bandwidth of its corresponding TS in this frame. The CS information scheduled by the BS is resided in a list, called complementary list (CL). The CL includes the mapping relation between each pair of pre-assigned CS and TS. As shown in Fig. 1, each CS is mapped to at least one TS. The CL is broadcasted followed by the UL map. To reach the backward compatibility, a broadcast CID (B-CID) is attached in front of the CL. Moreover, a stuff byte value (SBV) is transmitted followed by the B-CID to distinguish the CL from other broadcast DL transmission intervals.

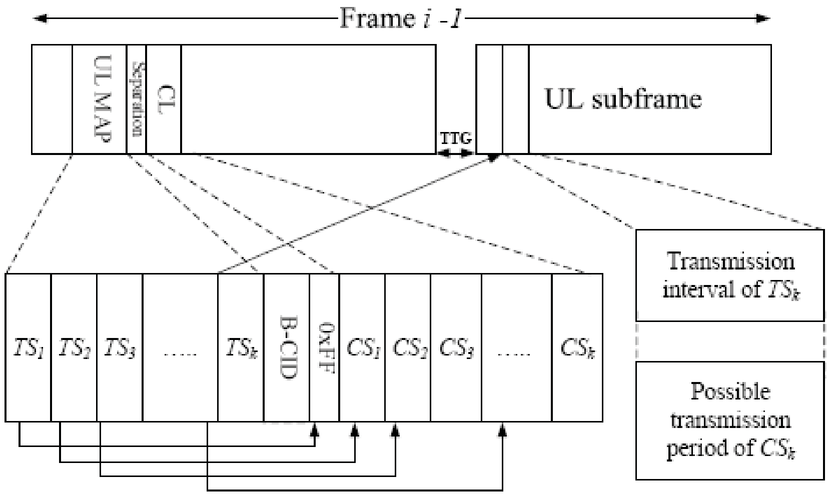


***Fig 1.*** The mapping relation between CSs and TSs in a MAC frame

The UL map including burst profiles and offsets of each TS is received by all SSs within the network. Thus, if a SS is on both UL map and CL, the necessary information (e.g., burst profile) residing in the CL may be reduced to the mapping information between the CS and its corresponding TS. The BS only specifies the burst profiles for the SSs which are only scheduled on the CL. For example, as shown in Fig. 1, CSj is scheduled as the corresponding CS of TSj, where $1 \leqslant j \leqslant k$. When TSj has unused bandwidth, it performs our protocol introduced in Section 4.1. If CSj receives the message sent from TSj, it starts to transmit data by using the agreed burst profile. The burst profile of a CS is resided on either the UL map if the CS is also scheduled on the UL map or the CL if the CS is only scheduled on CL. Our proposed scheme is presented into two parts: the protocol and the scheduling algorithm. The protocol describes how the TS identifies the unused bandwidth and informs recycling opportunities to its corresponding CS. The scheduling algorithm helps the BS to schedule a CS for each TS.

**4.1 PROTOCOL** According to the IEEE 802.16 standard, the allocated space within a data burst that is unused should be initialized to a known state. Each unused byte should be set as a padding value (i.e., 0xFF), called stuffed byte value (SBV). If the size of the unused region is at least the size of a MAC header, the entire unused region is initialized as a MAC PDU. The padding CID is used in the CID field of the MAC PDU header. In this research, we intend to recycle the unused space for data transmissions.

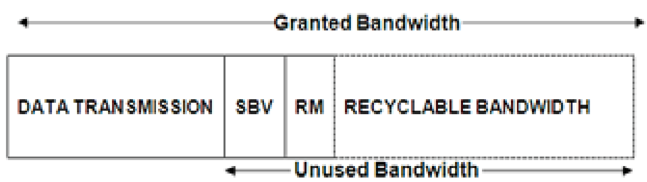


***Fig2:*** Messages to release the unused bandwidth Within a UL transmission interval

<table>
<tr><td>HT</td><td>EC</td><td>TYPE</td><td>REV</td><td>CI</td><td>EKS</td><td>RSV</td><td>LEN<br>MSB</td></tr>
<tr><td colspan="3">LEN<br>LSB</td><td colspan="5">CIS<br>MSB</td></tr>
<tr><td colspan="3">CID<br>LSB</td><td colspan="5">HCS</td></tr>
</table>

| | | |
|---|---|---|
| HT : Header Type | CI : CRC Indicator | MSB: Most Significant Bit |
| EC : Encryption Control | EKS: Encryption Key Sequence | LSB : Least Significant Bt |
| CID : Connection ID | LEN : Length | HCS: Header Check Sequence |

***Fig. 3.*** The format of RM

Since both UL map and CL can be received by the CS, the CS knows the UL transmission period of its corresponding TS. This period is called the UL transmission interval. The CS monitors this interval to see if a RM is received from its corresponding TS. Once received, the CS starts to recycle the unused bandwidth by using the burst profile residing in either UL map (if the CS is scheduled on the UL map) or CL (if the CS is only scheduled on the CL), until using up the rest of the TS's transmission interval. If the CS does not have any data to transmit, it simply pads the rest of the transmission interval.

**4.2 SCHEDULING ALGORITHM** Assume Q represents the set of SSs serving non-real time connections (i.e., nrtPS or BE connections) and T is the set of TSs. Due to the feature of TDD that the UL and DL operations cannot be performed simultaneously, we cannot schedule the SS which UL transmission interval is overlapped with the target TS. For any TS, St, let Ot be the set of SSs which UL transmission interval overlaps with that of St in Q. Thus, the possible corresponding CS of St must be in Q−Ot. All SSs in Q−Ot are considered as candidates of the CS for St. A scheduling algorithm, called Priority based Scheduling Algorithm (PSA), shown in Algorithm 1 is used to schedule a SS with the highest priority as the CS. The priority of each candidate is decided based on the scheduling factor (SF) defined as the ratio of the current requested bandwidth (CR) to the current granted bandwidth (CG). The SS with higher SF has more demand on the bandwidth. Thus, we give the higher priority to those SSs. The highest priority is given to the SSs with zero CG. Non real time connections include nrtPS and BE connections. The nrtPS connections should have higher priority than the BE connections because of the QoS requirements. The priority of candidates of CSs is concluded from high to low as: nrtPS with zero CG, BE with zero CG, nrtPS with nonzero CG and BE with non-zero CG. If there are more than one SS with the highest priority, we select one with the largest CR as the CS in order to decrease the probability of overflow.

## 5 ANALYSES

The percentage of potentially unused bandwidth occupied in the reserved bandwidth is critical for the potential performance gain of our scheme. We investigate this percentage on VBR traffics which is popularly used today. Additionally, in our scheme, each TS should transmit a RM to inform its corresponding CS when it has 6 bandwidth to total reserved bandwidth in N frames, Ru can be presented as:

Algorithm 1 Priority-based Scheduling Algorithm

Input: T is the set of TSs scheduled on the UL map.
Q is the set of SSs running non-real time applications.

Output: Schedule CSs for all TSs in T.
For i =1 to $\| T \|$ do
a. St $\leftarrow$ TSi.
b. Qt $\leftarrow$ Q−Ot:
c. Calculate the SF for each SS in Qt.
d. If Any SS $\in$ Qt has zero granted bandwidth,
If Any SSs have nrtPS traffics and zero granted bandwidth,
Choose one running nrtPS traffics with the largest CR.

else
Choose one with the largest CR.
else
Choose one with largest SF and CR.
e. Schedule the SS as the corresponding CS of St.
End For

However, the transmission range of the TS may not be able to cover the corresponding CS. It depends on the location and the transmission power of the TS. It is possible that the unused bandwidth cannot be recycled because the CS does not receive the RM. Therefore, the benefit of our scheme is reduced. In this section, we analyze mathematically the probability of a CS to receive a RM successfully. Obviously, this probability affects the bandwidth recycling rate (BBR). BBR stands for the percentage of the unused bandwidth which is recycled. Moreover, the performance analysis is presented in terms of throughput gain (TG). At the end, we evaluate the performance of our scheme under different traffic load.

$$R_U = \frac{\sum_{i=0}^{N-1} E(i)}{\sum_{i=0}^{N-1} W_i}$$

**5.2 THE PROBABILITY OF RMS RECEIVED BY THE CORRESPONDING CSS SUCCESSFULLY** Assume a BS resides at the center of a geographical area. There are n SSs uniformly distributed in the coverage area of the BS. Since PMP mode is considered, the transmissions only exist between BS and Ss. Moreover, each SS may be in different locations. The transmission rate of each SS may be variant depending on the PHY transmission technology and transmission power. For a given SS, St, let Rt (B), Rt

(Q), Rt (16) and Rt (64) denote as the transmission range of BPSK, QPSK, 16-QAM and 64- QAM, respectively. In our scheme, the RM should be transmitted via the most robust modulation (i.e., BPSK) since it has the largest coverage of RMs among all modulations supported by the IEEE 802.16 standard without adjusting the transmission power. Based on the fixed transmission power, the relation of transmission range b etween modulations is expressed as:

$$\mathbf{Rt(B) = kt(Q)Rt(Q) = kt(16)Rt(16) = kt(64)Rt(64)}$$

where kt (Q), kt (16) and kt (64) are constants depending on the transmission power of St and kt (64) $\geqslant$ kt (16) $\geqslant$ kt (Q) $\geqslant$ 1. Again, the RM should be transmitted via BPSK. In the rest of the paper, we use Rt to represent the BPSK transmission range of St. Moreover, SB and R are denoted the BS and its transmission range of BPSK, respectively.

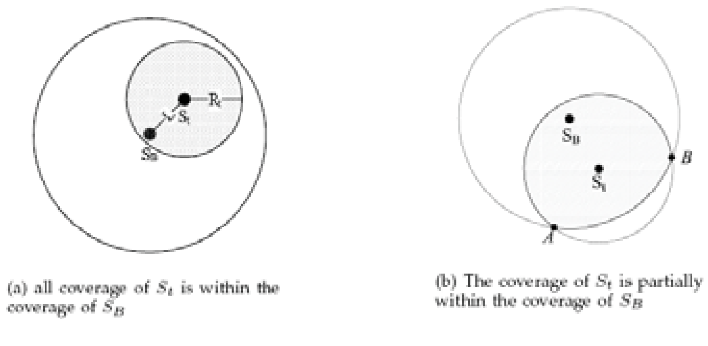


***Fig. 4.*** Possible geographical relationship between St and SB

**5.3 PERFORMANCE ANALYSIS OF PROPOSED SCHEME** Assume Qn represents a set of SSs running non-real time connections and QCL is a set of SSs in Qn scheduled as CSs. Thus, // QCL // is at most // T //, where T is the set of all TSs. For any SS, Sn $\in$ Qn, the probability of Sn scheduled on the CL, PCL(n), is derived as:

$$PCL(n) = \frac{//QCL//}{//Qn//}$$

It is possible that the CS fails to recycle the unused bandwidth due to the lack of no-real time data to be transmitted. Thus, it is necessary to analyze this probability.

**5.4 OVERHEAD ANALYSIS OF PROPOSED SCHEME** The overhead introduced by our scheme resides in both DL and UL subframes. In DL subframe, the separation and CL are considered as the overhead. As shown in Fig. 1, the separation contains a broadcast CID (B-CID) and a SBV (0xFF). It costs 3 bytes of overhead (16 bits for B-CID and one byte for SBV). In addition, The CL is composed by the CL information elements (CL-IEs). The CL-IE contains the basic CID of the CS. If the CS is not scheduled on the UL map, the burst profile and offset must be specified in the CL-IE of this CS. Therefore, the size of CL-IE is at most the size of UL-MAP IE which is 7 bytes defined in the IEEE 802.16 standard. In summary, the total overhead in a DL subframe can be concluded As:

$$OHDL \leqslant 3 + 7BTS$$

Where BTS is the number of TSs scheduled on the UL map.

According to the IEEE 802.16 standard, the SBV is inevitable when the SS has unused bandwidth. Therefore, only RMs are considered as the overhead in UL sub frame. Each TS transmits at most one RM in each UL sub frame. A RM comprises a generic MAC Header (GMH). The size of a GMH is 6 bytes defined in the IEEE 802.16 standard. Thus, the total overhead in an UL sub frame is calculated as:

$$OHUL \leqslant 6BTS$$

where BTS is the number of TSs scheduled on the UL map. From equation (27) and (28), the total overhead introduced by our scheme in a MAC frame is concluded as:

$$OH = OHDL + OHDL \leqslant 3 + 7BTS + 6BTS$$

# 6. SIMULATION RESULTS

Our simulation is conducted by using Qualnet In this section; we first present our simulation model followed by introducing the definition of performance metrics used for measuring the network performance. The simulation results are shown as the third part of this section. At the end, we provide the validation of theoretical analysis and simulation results.

**6.1 SIMULATION MODEL** Our simulation model comprises one BS residing at the center of geographical area and 50 SSs uniformly distributed in the service coverage of BS. The parameters of PHY and MAC layers used in the simulation are summarized in Table 1. PMP mode is employed in our

model. Since our proposed scheme is used to recycle the unused bandwidth in UL subframe, the simulation only focuses on the performance of UL transmissions.

***Table 1 :*** System parameters used in our simulation

| Parameters | Values |
|---|---|
| Node number | 51 |
| Frame duration | 20MS |
| UL/DL subframe duration | 10MS |
| Modulation scheme | BPSK ,QPSK,16QAM,64QAM |
| DCD/UCD broadcast interval | 5S |
| TTG/RTG | 10US |
| SS transition gap (SSTG) | 4US |

CBR is a typical traffic type used to measure the performance of networks in WiMAX research. However, it may not be able to represent the network traffic existing in real life. Moreover, the IEEE 802.16 network aims to serve both data and multi-media applications. Most of the modern streaming videos are encoded by industrial standards (e.g., H.264 or MPEG 4) which generate data in variant rates. In this research, we include VBR traffics to illustrate H.264 and MPEG 4-encoded videos.

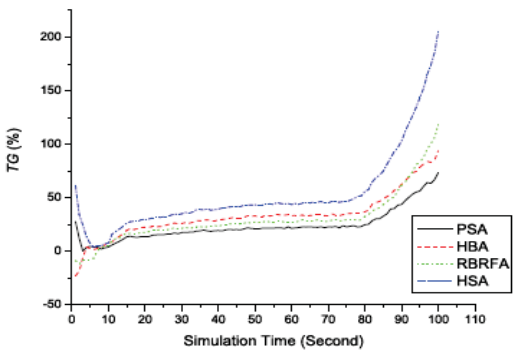


***Fig 5:*** Simulation results of TG among all scheduling Algorithms

**6.2 SIMULATION RESULTS** In This section presents the percentage of the unused bandwidth in our simulation traffic model (i.e., UBR). It shows the room of improvement by implementing our scheme. From the simulation results, we conclude that the average UBR is around 38%. In the beginning, the UBR goes down. It is because each connection still requests bandwidth from the BS. As time goes on, the UBR starts to increase when the connection has received the requested bandwidth. After 75th second of simulation time, UBR increases dramatically due to the inactivity of real time connections. The purpose to have inactive real time connections is to simulate a network with large amount of unused bandwidth and evaluate the improvement of the proposed scheme in such network status. The evaluation is presented in the later of this section.

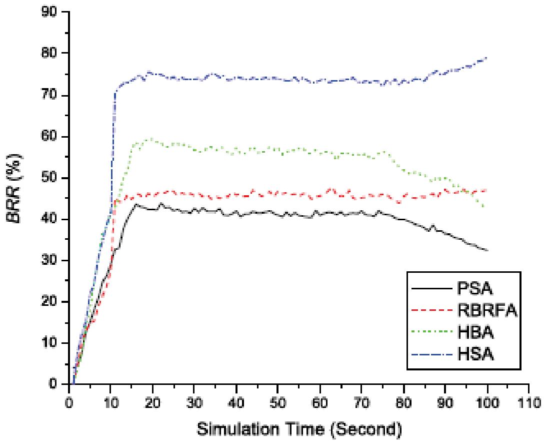


***Fig 6:*** Simulation results of BBR among all scheduling algorithms

The simulation results of recycling rate are presented in this section. From the figure, we observe that the recycling rate is very close to zero at the beginning of the simulation. It is because that only a few connections transmit data during that time and the network has a light load. Therefore, only few connections need to recycle the unused bandwidth from others. As time goes on, many active connections join in the network. The available bandwidth may not be able to satisfy the needs of connections. Therefore, there is a high probability that the CS recycles the unused bandwidth. It leads a higher BRR. It shows the total bandwidth demand requested by SSs during the simulation. In the figure, the dashed line indicates the system bandwidth capacity. During the simulation, the BS always allocates the bandwidth to satisfy the demand of real time connections due to the QoS requirement.

## 7. FURTHER ENHANCEMENTS

As our investigation, one of the factors causing recycling failures is that the CS does not have data to transmit while receiving a RM. To alleviate this factor, we propose to schedule SSs which have rejected BRs in the last frame because it can ensure that the SS scheduled as CS has data to recycle the unused bandwidth. This scheduling algorithm is called Rejected Bandwidth Requests First Algorithm (RBRFA). It is worth to notice that the RBRFA is only suitable to heavily loaded networks with rejected BRs sent from non-real time connections (i.e., nrtPS or BE). Notice that only rejected BRs sent in the last frame are considered in the RBRFA for scheduling the current frame. The RBRFA is summarized in. The BS grants or rejects BRs based on its available resource and scheduling policy. In RBRFA, if the BS grants partially amount of bandwidth requested by a BR, then this BR is also considered as a rejected BR. Similarly, Ot represents the set of SSs which transmission period overlaps with the TS, St, in QR. All SSs in Qt are considered as possible CSs of St.

Algorithm2: Rejected Bandwidth Requests
Input: T is the set of TSs scheduled on the UL map.
QR is the set of SSs which have rejected BRs
sent from non-real time connections in the last
frame.
Output: Schedule a CS for each TS in T.
For i =1 to // T // do
a. St ← TSi.
b. Qt ← QR−Ot:
c. Randomly pick a SS ∈ Qt as the
corresponding CS of St
End For

A rejected BR shows that the SS must have extra data to be transmitted in the next frame and no bandwidth is allocated for these data. The RBRFA schedules those SSs as CSs on the CL, so the probability to recycle the unused bandwidth while the CS receives the RM is increased. The other factor that may affect the performance of bandwidth recycling is the probability of the RM to be received by the CS successfully. To increase this probability, a scheduling algorithm, named history-Based Scheduling Algorithm (HBA), is proposed.

Algorithm 3: History-Based Scheduling Algorithm
Input: T is the set of TSs scheduled on the UL map.
Q is the set of SSs running non-real time applications
BL is the set of black lists of TSs.
Output: Schedule a CS for each TS in T.

For i =1 to // T // do
a. St ← TSi.
b. Qt ← Q − Ot − BLi
c. Randomly pick a SS ∈ Qt as the corresponding CS of St
d. IF the scheduled CS did not transmit data or SBV
Then put this CS in the BLi
End For

For each TS, the BS maintains a list, called Black List (BL). The basic CID of a CS is recorded in the BL of the TS if this CS cannot receive RMs sent from the TS. According to our protocol, the CS transmits data or pad the rest of transmission interval if a RM is received. The BS considers that a CS cannot receive the RM from its corresponding TS if the BS does not receive either data or padding information from the CS. When the BS schedules the CS of each TS in future frames, the BS only schedules a SS which is not on the BL of the TS as the CS. After collecting enough history, the BL of each TS should contains the basic CID of all SSs which cannot receive the RM sent from the TS. By eliminating those SS, the BS should have high probability to schedule a CS which can receive the RM successfully. Therefore, HBA can increase the probability of scheduling a SS which is able to receive the RM as the CS. To support the mobility, the BL of each TS should be updated periodically. Moreover, the BS changes the UL burst profile of the SS when it cannot listen to the SS clearly. There are two possible reasons which may make the BS receive signals unclearly: 1) the SS has moved to another location. 2) the background noise is strong enough to interfere the data transmissions. Since those two factors may also affect the recipient of RMs, therefore, the BL containing this SS should be updated as well.

The two algorithms described above focus on mitigating each factor that may cause the failure of recycling. The RBRFA increases the probability that the CS has data to transmit while receiving the RM. The HBA increases the probability that the CS receives the RM. However, none of them can alleviate both factors at the same time. By taking the advantages of both RBRFA and HBA, an algorithm called Hybrid Scheduling Algorithm (HSA) is proposed. HSA can increase not only the probability of CSs to transmit data while receiving the RM but also the probability of CSs to receive the RM. The detail of HSA is summarized in Algorithm 4

Algorithm 4: Hybrid Scheduling Algorithm
Input: T is the set of TSs scheduled on the UL map.
QR is the set of SSs which have rejected BRs sent for non-real time applications.
BL is the set of black lists of TSs.
Output: Schedule a CS for each TS in T.
For i =1 to // T// do
a. St ← TSi.
b. Qt ← QR−Ot − BLi
c. Randomly pick a SS € Qt as the corresponding CS of St
d. IF the scheduled CS did not transmit data or SBV
Then put this CS in the BLi
End For

When the BS schedules the CS for each TS, only the SS with rejected BRs is considered. As mentioned before, it increases the probability of CSs to transmit data while receiving the RM. Moreover, the BS maintains a BL for each TS. It can screen out the SSs which cannot receive the RM so that those SS cannot be scheduled as the CSs. The probability of receiving RMs can be increased. Again, the BL of each TS should be updated periodically or when the UL burst profile of the SS has been changed. By considering those two advantages, HSA is expected to achieve higher TG and BBR comparing to RBRFA and HBA.

## 8 CONCLUSION AND FUTURE WORK

Variable bit rate applications generate data in variant rates. It is very challenging for SSs to predict the amount of arriving data precisely. Although the existing method allows the SS to adjust the reserved bandwidth via bandwidth requests in each frame, it cannot avoid the risk of failing to satisfy the QoS requirements.

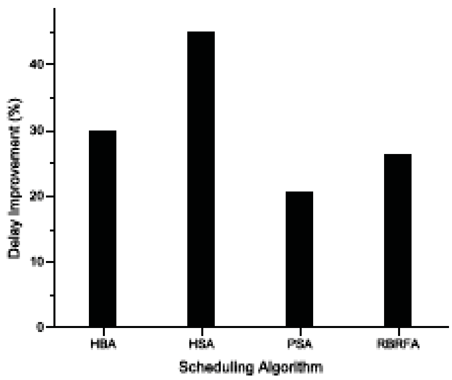


***Fig 7:*** Simulation results of delay improvement

Moreover, the unused bandwidth occurs in the current frame cannot be utilized by the existing bandwidth adjustment since the adjusted amount of bandwidth can be applied as early as in the next coming frame. Our research does not change the existing bandwidth reservation to ensure that the same QoS guaranteed services are provided.

We proposed bandwidth recycling to recycle the unused bandwidth once it occurs. It allows the BS to schedule a complementary station for each transmission stations. Each complementary station monitors the entire UL transmission interval of its corresponding TS and standby for any opportunities to recycle the unused bandwidth. Besides the naive priority-based scheduling algorithm, three additional algorithms have been proposed to improve the recycling effectiveness. Our mathematical and simulation results confirm that our scheme can not only improve the throughput but also reduce the delay with negligible overhead and satisfy the QoS requirements.

## REFERENCES


[1] IEEE 802.16 WG,"IEEE Standard for Local and Metropolitan Area Network Part 16: Air Interface for Fixed Boardband Wireless Access Systems" IEEE Std 802.16-2004 p.1 - p.857

[2] IEEE 802.16WG, "IEEE standard for local and metropolitan area networks part 16: Air interface for fixed and mobile broadband wireless access systems, Amendment 2," IEEE 802.16 Standard, December 2005.

[3] Jianhua He, Kun Yang and Ken Guild "A Dynamic BandwidthReservation Scheme for Hybrid IEEE 802.16 Wireless Networks" ICC'08 p.2571-2575.

[4] Kamal Gakhar, Mounir Achir and Annie Gravey, "Dynamic resource reservation in IEEE 802.16 broadband wireless networks", IWQoS, 2006. p.140-148

[5] J. Tao, F. Liu, Z. Zeng, and Z. Lin, Throughput enhancement in WiMax mesh networks using concurrent transmission, In Proc. IEEE Int. Conf. Wireless Commun., Netw. Mobile Comput., 2005, p. 871V874.

[6] Xiaofeng Bai, Abdallah Shami and Yinghua Ye "Robust QoS Control for Single Carrier PMP Mode IEEE 802.16 Systems",IEEE TRANSACTIONS ON MOBILE COMPUTING, VOL. 7, NO. 4, APRIL 2008, p.416-429

[7] Eun-Chan Park, Hwangnam Kim, Jae-Young Kim, Han-Seok Kim"Dynamic Bandwidth Request-Allocation Algorithm for Real-time Services in IEEE 802.16 Broadband Wireless Access Networks", INFOCOM 2008,p.852 - 860.

[8] Thomas G. Robertazzi "Computer Networks and Systems: Theory and Performance Evaluation." Springer-Verlag 1990

[9] Kamal Gakhar, Mounir Achir and Annie Gravey, "How Many Traffic Classes Do We Need In WiMAX?," WCNC 2007, p.3703-3708.

[10] Giuseppe Iazeolla, Pieter Kritzinger and Paolo Pileggi, "Modelling quality of service in IEEE 802.16 networks,"SoftCOM 2008. p.130-134.

[11] Frank H.P. Fitzek, Martin Reisslein, "MPEG–4 and H.263 Video Traces for Network Performance Evaluation", IEEE Network, Vol. 15, No. 6, p.40-54, November/December 2001.

# SOURCE ENCODING IN NETWORKS BY IMPLEMENTING LOSSLESS DATA COMPRESSION

Vishal Bharti
Ph.D. Research Scholar, Department of Computer Science & Engineering
NIMS University, Shobha Nagar, Jaipur, Rajasthan
Email: mevishalbharti@yahoo.com

B.M.K.Prasad
Principal & Professor, Department of Electronics & Communication Engineering
Dronacharya College of Engineering, Gurgaon -123506
Email: principal@dronacharya.info

## ABSTRACT

Data compression is, in the perspective of computer science, the science and art in lieu of information in a compacted form. It has been one of the significant enabling technologies for the continuing digital multimedia uprising for decades. Most people repeatedly use data compression software such as zip, gzip and WinZip (and many others) to diminish the file size before storing or transferring it in media. Compression techniques are rooted in more and more software and data is time and again compressed without people knowing it. The idea of compression by reducing redundancy suggests the general law of data compression, which is to “assign short codes to common events (symbols or phrases) and long codes to rare events.” This paper mainly focus on the lossless type of data compression techniques such as Huffman Coding, Lempel-Ziv-Welch [LZW] Algorithm and Adaptive Huffman Coding, and finally proposed an algorithm, which is a combination of the two schemes. The algorithm is finally analyzed with various inputs and the result is a clear cut increase in compression ratio than the traditional compression algorithms.

***Key Words:*** Huffman, LZW, Adaptive Huffman, Statistical Modeling, Dictionary Modeling.

## 1. INTRODUCTION

Data compression essentially includes the following steps

**1.1 COMPRESSION** Data compression can be viewed as a means for proficient depiction of a digital source of data such as text, image, sound or any grouping of all these types such as video. The objective of data compression is to symbolize a source in digital form with a small amount of bits possible while gathering the minimum prerequisite of re-enactment of the original [2].

We can examine data compression as algorithms to accomplish the compression goals on the source data. Behind each algorithm there are ideas, mathematical models or accomplishment techniques to accomplish compression.

When functioning on compression troubles, we need to reflect on the efficiency portion of the algorithms as well as the usefulness of compression. Spontaneously, the performance of a compression algorithm would depend on the data and their inner structure. The more redundancy the source data has, the more effective a compression algorithm may be [10].

**1.2 DECOMPRESSION** Any compression algorithm will not work but for a means of decompression is also provided due to the nature of data compression. When compression algorithms are discussed in general, the word compression alone essentially implies the perspective of both compression and decompression [10].

In several realistic cases, the efficiency of the decompression algorithm is of further anxiety than that of the compression algorithm. For example; movies, photos, and audio data are over and over again compressed once by the artist but the similar version of the compressed files is decompressed countless times by millions of viewers. On the added hand, the efficiency of the compression algorithm is occasionally more significant. For example, the recording audio or video data from several real-time programs may need to be recorded straightforwardly to inadequate computer storage, or transmitted to a far-flung destination through a narrow signal channel. Depending on specific problems, we occasionally think about compression and decompression as two separate synchronous or asynchronous processes [2]. Figure 1 shows a platform based on the relationship between compression and decompression algorithms.

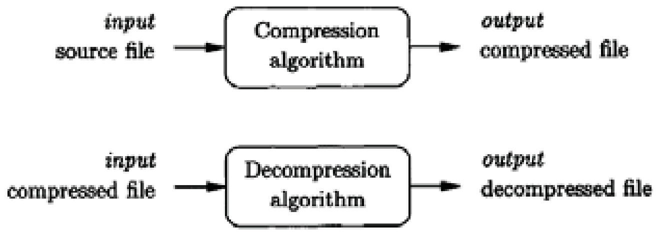


*Figure 1:* Compressor and Decompressor

A compression algorithm is often called compressor and the decompression algorithm is called decompressor.

**1.3 COMPRESSION TECHNIQUES** There are two foremost families of compression techniques when taking into consideration the prospect of reconstructing precisely the original source. They are called lossless and lossy compression [2, 10].

**1.3.1 LOSSLESS COMPRESSION** A compression approach is lossless only if it is promising to precisely reconstruct the original data from the compressed version. There is no loss of any information during the compression process. For example, in Figure 2, the input string AABBBA is reconstructed after the execution of the compression algorithm followed with the decompression algorithm. Lossless compression is called reversible compression as the novel data may be recovered absolutely by decompression. Lossless compression techniques are used when the novel data of a source are so important that we cannot meet the expense of losing any details. Examples of such source data are medical images, text and images conserved for legal reason, some computer executable files, etc [11].

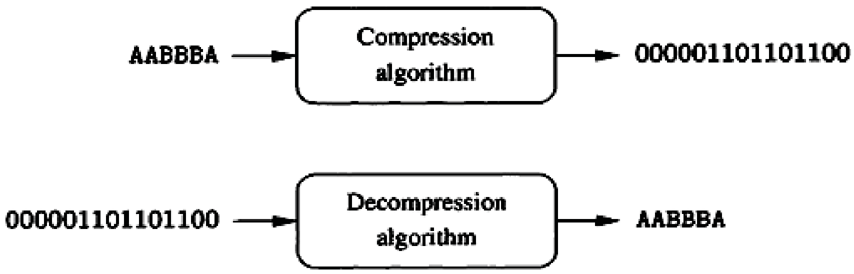


*Figure 2:* Lossless Compression Algorithms

**1.3.2 LOSSY COMPRESSION** A compression routine is lossy if it is not possible to reconstruct the original exactly from the compressed version. There are some inconsequential details that may get mislaid during the process of compression. The word inconsequential here implies certain necessities to the quality of the reconstructed data. Figure 3 shows an example where a long decimal number becomes a shorter approximation after the compression-decompression process [2, 10, 11].

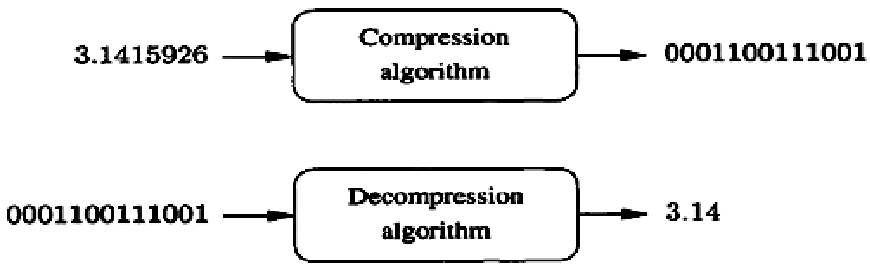


*Figure 3:* Lossy Compression Algorithms

Lossy compression is called irreversible compression because it is unfeasible to recover the original data precisely by decompression. Approximate restoration might be enviable since it could lead to more effectual compression. However, it often requires a good balance between the visual eminence and the computation complexity. In many applications, this lack of precise reconstruction is not a problem. Depending on the quality required of the reconstructed speech, varying amounts of loss of information about the value of each sample can be tolerated. If the quality of the reconstructed speech is to be analogous to that heard on the telephone, a significant loss of information can be tolerated. However, if the reconstructed speech needs to be of the quality heard on a compact disc, the quantity of information loss that can be tolerated is comparatively low. Likewise, when screening a rebuilding of a video sequence, the fact that the reconstruction is distinct from the original is commonly not significant as long as the differences do not result in annoying artifacts. Thus, video is generally compressed using lossy compression. Data compression has become a widespread requirement for most application software as well as a significant and vigorous research area in computer science [10, 11].

## 2. TYPES OF MODELING FOR LOSSLESS DATA COMPRESSION

Lossless data compression is usually implemented using one of two diverse types of modeling: statistical or dictionary-based. Statistical modeling reads in and encodes a single symbol at an instance using the probability of that character's manifestation. Dictionary-based modeling uses a single code to surrogate strings of symbols. In dictionary-based modeling, the coding problem is reduced in significance, leaving the model supremely important [13].

**2.1 STATISTICAL MODELING** The simplest forms of statistical modeling employ a static table of probabilities. In the earliest days of information theory, the CPU cost of analyzing data and building a Huffman tree was considered significant, so it wasn't often performed. As an alternative, representative blocks of data were analyzed once, giving a table of character-frequency counts. Huffman encoding/decoding trees were then built and stored. Compression programs had admittance to this static model and would compress data using it [11].

For an order-0 compression table, the authentic statistics used to form the table may take up as little as 256 bytes—not a very large amount of overhead. But trying to accomplish better compression through use of a higher order table will make the statistics that need to be passed to the decoder grow at an alarming rate. Just moving to an order 1 model can boost the statistics table from 256 to 65,536 bytes. Nevertheless compression ratios will indisputably progress when moving to order-1, the overhead of passing the statistics table will probably wipe out any gains [13].

For this motive, compression research in the last 10 years has concerted on adaptive models. When using an adaptive model, data does not need to be scanned once prior to coding in order to generate statistics. Instead, the statistics are continually customized as new characters are read in and coded. The broad flow of a program using an adaptive model looks something like that shown in Figures 4 and 5.

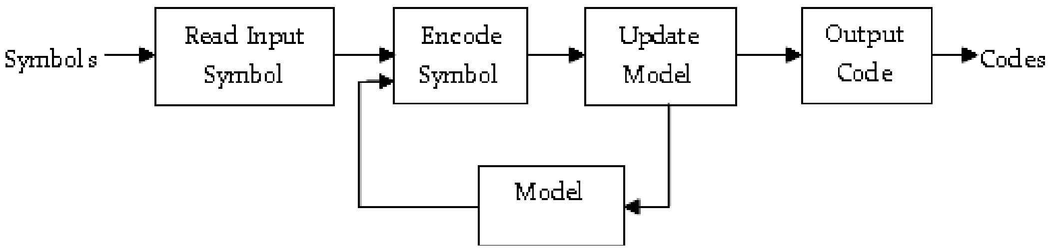


***Figure 4:*** General Adaptive Compression

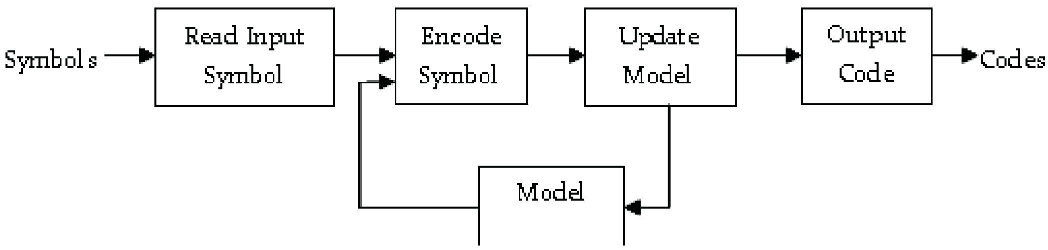


Figure 5: General Adaptive Decompression

**2.2 DICTIONARY-BASED MODELING** Statistical compression methods use a statistical model of the data, and the eminence of compression they achieve depends on how good that model is. Dictionary-based compression methods do not use a statistical model, nor do they use variable-size codes. As an alternative they select strings of symbols and encode each string as a codeword using a dictionary. The dictionary holds strings of symbols and it may be static or dynamic (adaptive). The former is permanent, occasionally allowing the addition of strings but no deletions, while the latter holds strings formerly originate in the input stream, allowing for additions and deletions of strings as new input is being read [3, 6, 7].

Given a string of 'n' symbols, a dictionary-based compressor can, in opinion, compress it down to 'nH' bits where 'H' is the entropy of the string. As a result, dictionary-based compressors are entropy encoders, but only if the input file is very large. For most files in realistic applications, dictionary-based compressors produce results that are good enough to make this type of encoder extremely accepted. Such encoders are also general purpose, performing on images and audio data as well as they achieve on text [8].

## 3. BRIEF OVERVIEW

This section gives a concise indication of the diverse lossless techniques, based on which our proposed algorithm is based. A Study of the following Lossless Algorithms:

- Huffman Coding
- Lempel-Ziv-Welch [LZW] Algorithm
- Adaptive Huffman Coding

**3.1 THE HUFFMAN CODING ALGORITHM** This algorithm is used to compress data. An example of Huffman encoding is given in. The foremost property of Huffman Coding Algorithm is that the codes for more feasible characters are shorter than the ones for less probable characters. Each code can be distinctively decoded. A basic intricacy in decoding Huffman codes is that the decoder cannot identify at first the length of an incoming codeword [1, 2, 14].

The main steps of the Algorithm are

Step 1: First count the number of times each character appears and assign this as a weight to each character or node. Add all these nodes to a LIST.
Step 2: Then repeat the steps until one node is left.
Step 3: Find the two nodes with the lowest weights.
Step 4: Create a Parent Node for these two nodes. The weight of this parent node will be the sum of the individual weights of the two nodes.
Step 5: Replace the two nodes from the list by a single parent node.

### 3.2 THE LZW {LEMPEL-ZIV-WELCH} ALGORITHM

The main steps in the algorithm [4, 5, 9] are as follows:

Step 1: Uses a dictionary of single characters
Step 2: The dictionary expands as new strings are encountered
Step 3: Higher Compression Ratio is achieved.
Step 4: Utilizes the redundancies in the input data very efficiently.
Step 5: Memory Intensive Algorithm

### 3.3 ADAPTIVE HUFFMAN CODING

To get the code for every node, in case of binary tree we could just traverse the entire path from the root to the node, writing down (for example) "1" if we go to the right and "0" if we go to the left [2, 12].

For every symbol transmitted both the transmitter and receiver execute the update procedure:

Step 1: If current symbol is NYT (not yet transmitted), add two child nodes to NYT node. One will be a new NYT node the other is a leaf node for our symbol. Increase weight for the new leaf node and the old NYT and go to step 4. If not, go to symbol's leaf node.
Step 2: If this node does not have the highest number in a block, swap it with the node having the highest number, except if that node is its parent
Step 3: Increase weight for current node
Step 4: If this is not the root node go to parent node then go to step 2. If this is the root, end.

Note: swapping nodes means swapping weights and corresponding symbols, but not the numbers.

## 4. PROPOSED ALGORITHM

The Strategies/Methods based on which we have proposed our scheme is based on the following parameters:
1. Choose the Best Acceptor
2. The Greedy Strategy
3. Grouping

Our approach is based on the combination of LZW algorithm and Adaptive Huffman Coding to achieve maximum compression ratio and a Dictionary Updating System.

**ASSUMPTIONS:** The proposed algorithm is based on the following three main assumptions and the proposed scheme is depicted with the help of a block diagram shown in Figure 6

1. This dictionary updating system is run in a loop until n1>=n2. Thus, this will ensure longer strings to be present in the dictionary.
2. n1=Size of largest word in the dictionary
3. n2=Size of largest word in the text file (Sample Data)

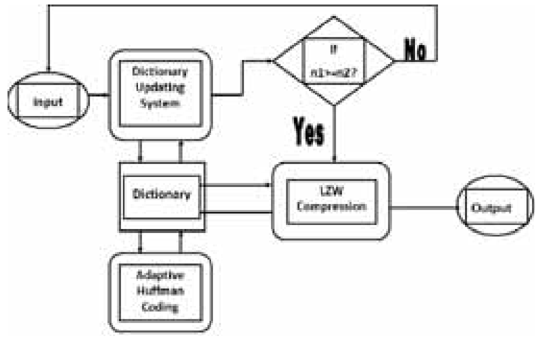


***Figure 6:*** Block diagram of the Proposed Scheme

**The Algorithm:**
Step 1: Input Character data
Step 2: Run Dictionary Updating System
Step 3: Simultaneously when each new word is found, perform Adaptive Huffman Coding on it and store it in the dictionary
Step 4: if n1>=n2
Run LZW algorithm to compress the sample data and output the compressed data
else
goto: Step 1

//**Dictionary updating system**
Step 5: Set w = NIL
Step 6: read a character k
Step 7: if wk exists in the dictionary
w = wk
else
add wk to the dictionary
w = k
Step 8: goto: Step 2
Step 9: end if no more characters

## 5. PERFORMANCE EVALUATION

### 5.1 USING A SAMPLE STRING "ASSESS" WE APPLY THE LZW ALGORITHM ON IT FIRST.

***Table 1:*** Simple LZW Compression

| K | W | WK | O/P | Found? | Dictionary |
|---|---|---|---|---|---|
| A | Nil | A | - | YES | |
| S | A | AS | - | NO | AS 91 |
| S | S | SS | - | NO | SS 92 |
| E | S | SE | - | NO | SE 93 |
| S | E | ES | - | NO | ES 94 |
| S | S | SS | - | YES | |

### 5.2 COMPRESSING THE SAME INPUT STRING USING THE PROPOSED ALGORITHM

***Table 2*** n1=1, n2=6

| K | W | WK | O/P | Found? | Dictionary |
|---|---|---|---|---|---|
| A | Nil | A | - | YES | |
| S | A | AS | - | NO | AS 91 |
| S | S | SS | - | NO | SS 92 |
| E | S | SE | - | NO | SE 93 |
| S | E | ES | - | NO | ES 94 |
| S | S | SS | - | YES | |

***Table 3*** n1=2, n2=6

| K | W | WK | O/P | Found? | Dictionary |
|---|---|---|---|---|---|
| A | Nil | A | - | YES | |
| S | A | AS | - | NO | AS 91 |
| S | AS | ASS | - | NO | SS 92 |
| E | S | SE | - | NO | SE 93 |
| S | SE | SES | - | NO | ES 94 |
| S | S | SS | - | YES | |

***Table 4*** n1=3, n2=6

| K | W | WK | O/P | Found? | Dictionary |
|---|---|---|---|---|---|
| A | Nil | A | - | YES | |
| S | A | AS | - | YES | |
| S | AS | ASS | - | YES | |
| E | ASS | ASSE | - | NO | ASSE 97 |
| S | E | ES | - | YES | |
| S | ES | ESS | - | NO | ESS 98 |

***Table 5*** n1=4, n2=6

| K | W | WK | O/P | Found? | Dictionary |
|---|---|---|---|---|---|
| A | Nil | A | - | YES | |
| S | A | AS | - | YES | |
| S | AS | ASS | - | YES | |
| E | ASS | ASSE | - | YES | |
| S | ASSE | ASSES | - | NO | ASSES 99 |
| S | S | SS | - | YES | |

***Table 6*** n1=5, n2=6

| K | W | WK | O/P | Found? | Dictionary |
|---|---|---|---|---|---|
| A | Nil | A | - | YES | |
| S | A | AS | - | YES | |
| S | AS | ASS | - | YES | |
| E | ASS | ASSE | - | YES | |
| S | ASSE | ASSES | - | YES | |
| S | ASSES | ASSESS | - | NO | ASSESS 100 |

## 6. RESULT

From the above analysis and implementation of the proposed work, for the input:
n1=6, n2=6, i.e. n1=n2
when the proposed algorithm is run, the dictionary already has the word "ASSESS", therefore it will substitute the word "ASSESS" (42 bits) by the code index 100 (7 bits) achieving a compression ratio of ((42-7)/42)*100=83.33%, unlike the conventional LZW where the output result found was 6583698392 (35 bits) and compression ratio of ((42-35)/42)*100)=16.67%.

## 7. CONCLUSION

Based on the implementation and analysis of the outcome, we can conclude that the compression ratio achieved by the proposed algorithm is much higher as compared to the traditional one. In a nutshell, we can conclude that the proposed algorithms compression ratio is around 5 times higher than the traditional one. Some other features of the proposed algorithm, based on analysis are:

- High Compression Ratio
- Less Memory Intensive
- High CPU Intensive

# 8. FUTURE ASPECTS

The algorithm can be further enhanced for compressing Data Packets in Networks using packet switching technology. Also further research can be extended to increase throughput (data rate). Also better congestion control can be achieved by limiting the number of data packets sent across the network.

# REFERENCES


[1] Suri Pushpa R. and Goel Madhu, “Ternary Tree and Memory-Efficient Huffman Decoding Algorithm”, IJCSI International Journal of Computer Science Issues, Vol. 8, Issue 1, January 2011

[2] Abdelfattah Eman, Mohiuddin Asif, “Performance analysis of multimedia compression algorithms”, International journal of computer science & information Technology (IJCSIT) Vol.2, No.5, October 2010

[3] S. Subathra, M. Sethuraman and J. V. B. James, “Performance Analysis of Dictionary based Data Compression Algorithms for High Speed Networks”, IEEE Indicon Conference, Dec 2005.

[4] N. Zhang, T. Tao, R. V. Satya and A. Mukherjee, “Modified LZW Algorithm for Efficient Compressed Text Retrieval”, Computer Science Dept., Univ. of Central Florida, 2004.

[5] R. N. Horspool, “Improving LZW”, Research, Dept. of Computer Science, University of Victoria, Victoria, B.C, Canada.

[6] Y. Matias, N. M. Rajboot and S. C. Sahinalp, “The Effect of Flexible Parsing for Dynamic Dictionary Based Data Compression”, Proceedings of the Data Compression Conference, 1999.

[7] C. L. Yu and J. L. Wu, “Hierarchical dictionary model and dictionary management policies for data compression”, Signal Processing, Sept 1999.

[8] K. Sadakane, "Improvements of Speed and Performance of Data Compression Based on Dictionary and Context Similarity", Master Thesis, The Graduate School of Infornation Science, The University of Tokyo, 1997.

[9] R. N. Horspool, “The Effect of Non-Greedy Parsing in Ziv-Lempel Compression Methods”, IEEE Data Compression Conference, 1995.

[10] J.Ziv and A.Lempel, "Compression of Individual Sequences via Variable-Rate Coding", IEEE Trans on Information Theory, Vol. IT-24, No. 5, Sept 1978, pp 530-536.

[11] J.Ziv and A.Lempel, "A universal Algorithm for sequential Data Compression", IEEE Transactions on Information Theory, Vol IT-23, No.3, May 1977, pp 337-343.

[12] Wiseman, J., “A quick tutorial on generating a Huffman tree,” http://www.siggraph.org/education/materials/HyperGraph/video/mpeg/mpegfaq/huffman_tutorial.html

[13] D. Salomon, “Data Compression - The Complete Reference”, 2nd Ed, Springer- New York, Inc., New York, 2001.

# DERIVING AND MINIMIZING TEST CASES FROM DECISION BASED MODULES

Mahamaya Mohanty
Department of Information Technology
Dronacharya Group of Institutions, 27 Knowledge Park-III, Greater Noida
Email- mahamayamohanty@yahoo.co.in

## ABSTRACT

The use of formal specifications themselves is still seen by many as a barrier to the widespread industrial usage of formal methods. For the benefits of formal methods in Verification & Validation to be fully exploited in industry there is a need to "disguise" the formality in some way. Recent work [5] has shown that formal specifications and the corresponding proof obligations for specification validation can be generated from more intuitive engineering notations with mathematical underpinnings. These restrictions, coupled with the subset of data types used for particular domains can be exploited to develop powerful targeted heuristics for automating the Verification and Validation activities. The approaches discussed in this paper are assumed to be undertaken in the context of formal specifications generated for deriving the test cases from the decision based modules in the manner of completeness and determinism. In this paper data coupling and functional cohesion is considered within the modules and the approach is entirely focused on dynamic testing .

***Key Words:*** Cohesion, Coupling, Module Specification, Verification, Validation, Test Data,, Test Case

## 1. INTRODUCTION

Testing starts from the early requirement analysis phase and goes till the last phase i.e maintenance phase. During requirement analysis and designing we do static testing wherein the Software Requirement Specification is tested to check and the techniques used are code reviews, code inspection, walkthroughs and software Technical Reviews to do static testing. Dynamic testing starts when the code or module is ready in the coding phase and this plays the vital role for the entire software that is under testing. The various testing techniques used for this are black box, gray-box and white box testing. In this paper emphasis is given on the interdependent or independent modules having different conditions from which decision can be derived and respective actions takes place. It has been named as module categorization. From these decisions number of test cases can be derived and are put into a decision table .All test cases within a test suite will not be good, so they must be selected. From this it will be easy for us to derive the number of test cases, prioritize the test cases and finally reduce them. The dependencies of test cases within the module is traced out and these test cases affecting the test cases of other module is also found and thus can be reduced. Good design consists of a number of stages which progressively elaborate the design. Good test design consists of number of stages which progressively elaborate the design of tests: Test strategy, Test planning, Test specification and Test procedure.

The test case identification includes the following benefits :

- Optimize test coverage of critical functions
- Establish the baseline for regression testing
- Reduce the number of errors going into production
- Reduce the time required to execute tests
- Increase reusability of test across related projects
- Increase the quality of the final deliverable
- Test the quality of business requirements before development

## 2. RELATED WORK

Most of the work presents either testing theories or testing frameworks. Few testing techniques for deriving test cases are presented. Testing theories are methodologies to handle testing. Testing frameworks involve a test plan or a test strategy used as an aid in transforming the testing theory into a testing technique. Imperative testing techniques are incorporated into modules concentrated on features like categorization and prioritization[2,3]. In testing frameworks or theories are addressed. Overall, these efforts lack experimentation and robust features to test inheritance. Formal specifications are a good basis for testing. They allow for a concise and unambiguous representation of the requirements and are amenable to proof and automated analysis. Test generation techniques for model-based formal specifications [4,7, 8].

## 3. BASIC CONCEPTS

1. Test data are the input values to a set of test inputs or test cases and observing if the program behaves as expected.

2. Test case has an identity and is associated with program behavior. Test case has a set of inputs and a list of expected outputs.The test case template includes:

Test Case ID
Purpose
Preconditions
Inputs
Expected Outputs
Post conditions
Execution History

3. Test Suite is a collection of test cases used for validating bug fixes (or finding new bugs) .

4. Coupling is the measure of the degree of interdependence between modules. (Loosely coupled is always good). The different types of coupling includes data coupling, stamp coupling control coupling external coupling, common coupling and content coupling. Data coupling is best than all other types of coupling.

5. Cohesion is the measure of the degree to which the elements of a module are functionally related.
Cohesion= strength of relations within modules
The different types of cohension include functional cohesion, sequential cohesion, communicational cohesion, procedural cohesion, temporal cohesion, logical cohesion and coincidential cohesion. Functional cohesion is best of all the cohensions.

6. Verification is a static process of verifying documents, design and code. It generally answers the question—Are we building the product right?.It does not involve executing the code.It uses the methods like walkthroughs, desk-checking etc.

7. Validation is a dynamic process of testing or validating the actual product. It generally answers the question—Are we building the right product?. It involves executing the code. It uses the methods like black box testing, white box testing ,gray box testing etc.

8. Decision Tables describes situations in which a number of combinations of actions are taken under varying sets of conditions. It represents analyze complex logical relationships. There are four portions of a decision table namely, Condition Stub, Action Stub, Condition entries and Action entries .If the conditions are true respective action takes place .Conditions are represented by True or False as 'T' or 'F' and when Action takes place for certain conditions it is represented as a cross' X'. The format of this is given in Fig.1.

| | **RULE1** | **RULE2** | **RULE3** | **RULE4** |
|---|---|---|---|---|
| **CONDITION STUB**<br>C1:CONDITION 1<br>C2:CONDITION 2 | **T**<br>**T** | **T**<br>**F** | **F**<br>**T** | **F**<br>**F** |
| **ACTION STUB**<br>A1:ACTION 1<br>A2:ACTION 2<br>A3:ACTION 3<br>A4:ACTION 4 | **X**<br>**--**<br>**--**<br>**--** | **--**<br>**X**<br>**--**<br>**--** | **--**<br>**--**<br>**X**<br>**--** | **--**<br>**--**<br>**--**<br>**X** |

***Fig.1***

## 4. PROPOSED APPROACH

Step 1: Module Specification includes the number of test cases in 'm' number of modules present in a program.

Module 1 [Test Case1, Test Case 2, Test Case3, Test Case4 Test Case5…………………. Test Case n1]
Module 2 [Test Case1, Test Case 2, Test Case3, Test Case4 Test Case5…………………. Test Case n2]
Module 3[Test Case1, Test Case 2, Test Case3, Test Case4 Test Case5……………………Test Case n3]
:
:
Module m[Test Case1, Test Case 2, Test Case3, Test Case4 Test Case5…………………. Test Case nX]

With 'm' number of modules we will have n1,n2,n3…….nx number of test cases in total.

Total number of test cases in 'm' number of modules = n1+n2+n3…….+nX .

Step 2: Secondly we find the number of dependencies among the modules .

Step 3: Now the number of test data for each module is found .

Step 4: Now the total number of test data used in the entire program is found.

Step 5: With these test data for each module we design number of test cases like n1 number of test cases for module 1, n2 test cases for module 2……nX test cases for module m.

Step 6: Next we find the number of test cases dependent on each other in a single module.

Step 7: Now we have the number of modules dependent on each other, so we can find the number of test cases similar among these dependent modules , so that we can reduce them into single test case .

Step 8: In this way we can have unique number of test cases from all the modules in a program.

Step 9: Finally we put them in the decision table and enter all the possible test data to get certain action/result.

Step 10: So if this program can be a subroutine for a large program with kilo lines of codes (KLOC) then its test cases and test data would be predefined for the new program without any error.

Let us consider an example of triangle where the triangle is classified into Scalene, Isoscales, Equilateral and Not a triangle. The classification depends on the inputs of positive integers(say a, b, c) from the interval [1,100].

Source Code for the above problem is:

```
1   int main( )
2   {
3   int a, b, c, validInput=0;
4   printf("Enter the side 'a' value:");
5   scanf("%d", &a);
6   printf("Enter the side 'b' value:");
7   scanf("%d", &b);
8       printf("Enter the side 'c' value:");
9       scanf("%d", &c);
10      if ( (a>0)&&(a<=100) && (b>0) && (b<=100) && (c>0) && (c<=100) )
        {
11          if ( (a+b) > c) && ( (c+a) > b) && ((b+c)>a) )
                {
12                 validInput=1;
13              }
14      }
15      else{
16          validInput=  -1;
17          }
18      if (validInput==1){
19              if ( (a==b)&&(b==c)){
20                  printf("The triangle is equilateral");
21                                  }
22              elseif ((a==b) || (b==c) || (c==a) ){
23                  printf("The triangle is isoscales");
24                                  }
25              else{
26                  printf("The triangle is scalene");
27                  }
28                          }
29          else if(validInput==0){
30              printf("The values do not constitute a Triangle ");
31                              }
32     else{
33          printf("The inputs belong to invalid range");
34        }
35     getch();
36     return 1;
37     }
```

Line number 10 to 33 completely denotes all the possible conditions and corresponding actions are taken.

The sequence moves to line 11 only when line number 10 is satisfied. Once line number 11 is satisfied and validInput is 1 then we would test whether the triangle is equilateral, scalene or isosceles. So the data a, b, c are strongly depended on each other, change in one variable would affect the other. Similarly if we divide the condition into modules then these modules are interdependent on each other.

The following decision Tables in Fig 2 have all the conditions and its respective action taken.

| Conditions | | | | | | | | | | | |
|---|---|---|---|---|---|---|---|---|---|---|---|
| C1:a< b+c? | F | T | T | T | T | T | T | T | T | T | T |
| C2:b< a+c? | -- | F | T | T | T | T | T | T | T | T | T |
| C3:c< a+b? | -- | -- | F | T | T | T | T | T | T | T | T |
| C4:a=b? | -- | -- | -- | T | T | T | T | F | F | F | F |
| C5:a=c? | -- | -- | -- | T | T | F | F | T | T | F | F |
| C6:b=c? | -- | -- | -- | T | F | T | F | T | F | T | F |
| Actions | | | | | | | | | | | |
| A1:Not a triangle | X | X | X | | | | | | | | |
| A2:Scalene | | | | | | | | | | | X |
| A3:Isoscales | | | | | | | X | | X | X | |
| A4:Equilateral | | | | X | | | | | | | |
| A5:Impossible | | | | | X | X | | X | | | |

***Fig. 2***

Now we have 11 number of test cases with 3 test data that is a, b, c, where we enter them as input to check the conditions and obtain the expected output.

| **Test Case** | **a** | **b** | **c** | **Expected Output** |
|---|---|---|---|---|
| 1 | 5 | 1 | 2 | Not a triangle |
| 2 | 1 | 5 | 2 | Not a triangle |
| 3 | 1 | 2 | 5 | Not a triangle |
| 4 | 7 | 7 | 7 | Equilateral |
| 5 | ? | ? | ? | Impossible |
| 6 | -1 | 3 | 4 | Invalid input |
| 7 | 3 | 3 | 4 | Isoscales |
| 8 | 3 | -1 | 4 | Invalid input |
| 9 | 3 | 4 | -1 | Invalid input |
| 10 | 2 | 0 | 3 | Invalid input |
| 11 | 2 | 3 | 0 | Invalid input |
| 12 | 0 | 2 | 3 | Invalid input |
| 13 | 3 | 4 | 3 | Isoscales |
| 14 | 4 | 3 | 3 | Isoscales |
| 15 | 3 | 4 | 5 | Scalene |

***Fig. 3***

Similarly we can also derive number of other test cases in terms of domain based classes but all the test cases in the above table are prioritized.

## 5. CONCLUSION

In this paper it has been shown the judicious use of testing and proof to support one another can lead to significant benefits for the software Verification and Validation processes, both in terms of increased automation and integrity irrespective of kilo lines of Codes. The paper is focused morely on test modules, testing strategies, testing levels and testing processes. Testing modules, represents the relationships between elements of a representation or an implementation of a software component. Testing levels, specifying the different scopes of the tests to be run, i.e., the collections of components to be tested. Testing strategies, defining heuristics or algorithms to create test cases from software representation models, implementation models or test models. Testing processes, defining the flow of testing activities, and other decisions regarding when testing should be started, who should perform testing, how much effort should be used, and similar issues. The use of counterexample generation can save much wasted proof effort and the use of proof to support test case design can be used to demonstrate the correctness of the test partitioning techniques as well as offering a means of automation in itself. In future it is aimed for the proof of correctness of the number of test cases present in all the modules of a program so that effort and cost can be estimated and can be reduced accordingly. Module-based testing can be combined with source-code level test coverage measurement, and functional models can be based on existing source code in the first place. Module-based testing for complex software systems is still an evolving field.The most effective result of this approach is test case reuse without focusing on the dependencies of the modules in a program.

## REFERENCES

[1] M. Alles, D. Crosby, C. Erickson, B. Harleton, M. Marsiglia, G. Pattison, C. Stienstra. Presenter First: Organizing Complex " GUI Applications for Test-Driven Development." Agile 2006. Minneapolis, MN. July 2006.

[2] Michael Karlesky, William Bereza, and Carl Erickson. "Effective Test Driven Development for Embedded Software." IEEE EIT2006. East Lansing, Michigan. May 2006.

[3] Steve Freeman, Nat Pryce, Tim Mackinnon, Joe Walnes. "Mock Roles, not Objects." OOPSLA 2004. Vancouver, British Columbia.

[4] Wolfgang Schmitt. "Automated Unit Testing of Embedded ARM Applications." Information Quarterly, Volume 3, Number 4, p. 29,2004.

[5] B. Jones, H. Sthamer, and D. Eyres, "Automatic structural testing using genetic algorithms," Software Engineering J., vol. 11, no. 5, September 1996, pp. 299 – 306

[6] Mark Harman, Chris Fox, Rob Hierons, Lin Hu, Sebastian Danicic, Joachim Wegener, "VADA: A Transfor mation-Based System for Variable Dependence Analysis," scam, pp.55, Second IEEE International Workshop on Source Code Analysis and Manipulation (SCAM'02), 2002

[7] Simon Burton, John Clark and John McDermid." Automated generation of tests from Statechart specifications," Proceedings of Formal Approaches to Testing Software, 2001.

[8] Sergiy A. Vilkomir and Jonathon P. Bowen. Reinforced Condition/Decision Coverage (RC/DC): "A new criterion for software testing" In Didier Bert, Jonathon P. Bowen, Martin C. Henson, and Ken Robinson, editors, ZB2002 Formal Specification and Development in Z and B, Lecture Notes in ComputerScience, vol. 2272, pages 291–308. Springer, 2002.

[9] Simon Burton, John Clark, Andy Galloway, and John McDermid. "AutomatedV&V for high integrity systems, a targeted formal methods approach." In Proceedings of the 5th NASA Langley Formal Methods Workshop, June 2000.

[10] Anitha Goel, S.C Gupta. S.K Wasan ;"Controllability mechanism for object-oriented software testing" Software Engineering Conference, 2003. Tenth Asia-Pacific 2003 Page(s):98 – 107

[11] M. Prutkina and A. Windisch, "Evolutionary structural testing of software with pointers," Proc. 2008 IEEE Int'l Conf. Software Testing Verification and Validation Workshop (ICSTW 08), p. 231, doi:10.1109/ICSTW.2008.15

[12] M. Harman et al., "Testability transformation," IEEE Trans. Software Eng., vol. 30, no. 1, 2004, pp. 3-16, doi:10.1109/TSE.2004.1265732.

[13] P. McMinn, D. Binkley, and M. Harman, "Empirical evaluation of a nesting testability transformation for evolutionary testing," ACM Trans. Software Eng. and Methodology, in press .

[14] A. Baresel, D. Binkley, M. Harman, and B. Korel, " Evolutionary testing in the presence of loop-assigned flags, a testability transformation approach," Proc. 2004 ACM SIGSOFT Int'l Symp. Software Testing and Analysis (ISSTA 04), 2004, pp. 108-118.

[15] A. Arcuri, D.R. White, J. Clark, and X. Yao, "Multi-objective improvement of software using co-evolution and smart seeding," Proc. 7th Int'l Conf. Simulated Evolution and Learning (SEAL 08), 2008, pp. 61-70, doi:10.1007/978-3-540-89694-4_7.

# EVOLUTION OF MANAGEMENT ACROSS DOMAINS OF COALITION NETWORK

Somnath S. Banerjee
Director IEM Mathura, Mob - 09818319793
drssbanerjee@gmail.com, ssb1950@yahoo.com

## ABSTRACT

Strategies of coalition operations dictate Inter Domain Coalition Information Management and Communication System The present Network is Combined Enterprise Regional Information Exchange System (CENTRIXS). Aims of CENTRIXS operations are yet to be met demanding new objectives of coalition Network and its management. Terminology and Fundamental Concepts for Inter Domain Coalition Network management and Reference model for Inter Domain Coalition Network and its Physical topology is undertaken before embarking on Evolution of management across Inter domain Coalition Networks wherein Simple Network Management Protocol (SNMP) and Common Management Information Protocol (CMIP), Object Management Group (OMG) Common Object Request Broker Architecture (CORBA), JIDM (Joint Inter Domain Management ) and ITU CORBA have been briefly enunciated. Qualitative Requirements (objectives) have been mapped on TCP/IP layers of Coalition Network Management. A modus operandi of Policy-enabled Network, Service oriented architecture (SOA), and Bandwidth Brokering is presented. Lastly Inter Domain Coalition Manager Physical Topology is depicted.

***Key Words:*** ***coalition operations, Inter Domain Coalition Network, Evolution of management, Policy-enabled Network, Service oriented architecture & Bandwidth Brokering***

## 1. INTRODUCTION

1. In the present Network centric Warfare, it is of paramount importance that the Commanders of Coalition partners (COCOM) be provided with mission, decision support and analysis of nontraditional operational needs. Domain commanders have an area of influence and an area of Interest. Based on these requirements, access to information base is provided. Therefore, Coalition Networking is to have inclusive and dynamic membership while maintaining appropriate security and dissemination control required by national policy. Multi coalition partner or communities of interest are assumed to assure swift, sure and secure network with commensurate Network Management system. Strategies of coalition operations dictate that it should be fully integrated ( functions and capabilities to ensure the desired mission).expeditionary (rapidly deployable, employable and sustainable), networked (linked and synchronized), decentralized ( integrated capabilities working jointly at lower echelon), decision superiority; (analysis of information in real time) and lethality ( destroy enemy system in all condition).

2. Coalition Network shall consist of multiple domains. Each domain shall have Network supporting operations in the area of influence called Intra domain Network. Inter Domain Coalition Operations Network operating over area of Interest must commensurate with coalition operation. The interoperable Networks are

- Surveillance Grid consists of Early Warning systems including AWACs., RADARS, UAV and satellite..
- Engagement grid consists Artillery, Armed Heptrs, Air force and Strategic Weapons.
- Electronic warfare grid. Basic aim is to deny enemy electromagnetic spectrum whereas allow own forces its exploitation.
- Hierarchical grid is omnipresent, it provides Hotlines, Networked voice and data communication.
- Logistic Grid is also omnipresent provides wireline and mobile communication for provisioning of ammunition, ration, water and other logistic requirements for operations.
- Command control and decision grid provides communication brain . It includes Network Management Systems at all levels together with intelligent agents.

## 3. AN INTER DOMAIN COALITION INFORMATION MANAGEMENT AND COMMUNICATION SYSTEM

The primary objectives of an Inter domain Coalition information management and Communication system 1 is to improve the capacity of commanders to take needed action by highlighting the key knowledge, responsibilities, and tasks which can enable Inter domain Coalition commanders to make informed decisions about the information system they manage, and the type of communications system which is most appropriate to their particular needs. An effective information system provides selective information relevant to the user's needs, clarifies particular problems and available options, and helps the user to make reasonable choices. It does not drown the commanders in a sea of information but, rather, adds value and coherence to the decision maker's activities. Such a system may be viewed as a cycle (fig. 1) starting with the identification of coalition partners needs and continuing through the feedback of lessons learned into program design or modification. The Inter domain Coalition manager responsible for the information management system must ensure that each of these five components of the system is funded, well staffed, and coordinated with the other components. Neglect of any parts can bring the cycle to a halt with potentially devastating results.

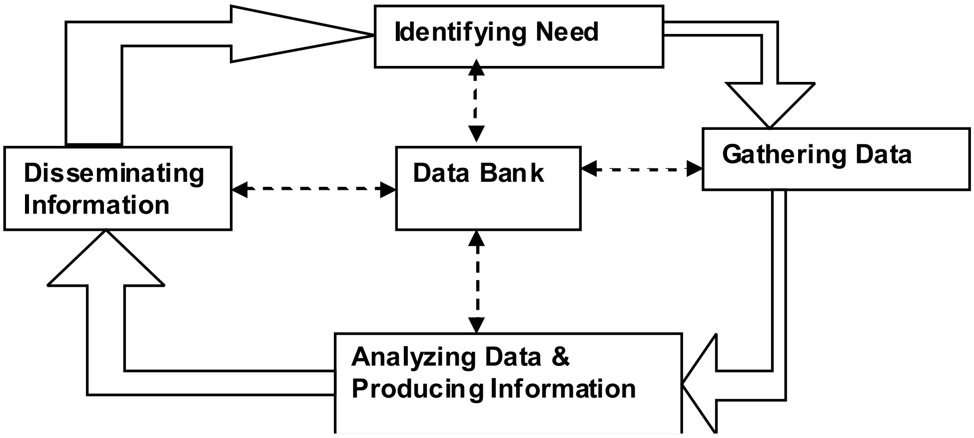


**Fig 1. INFORMATION MANAGEMENT SYSTEM FOR COALITION NETWORK**

**3.1 IDENTIFICATION OF INFORMATION NEEDS** The starting point in the design of any information management system is the identification of the eventual users of the system and their particular needs. Coalition Managers should beware requests for information of a type not considered during the system design stage are often extremely difficult, if not impossible, to satisfy by that system. Information needs for contingency planning. Contingency planning is defined as: a forward planning process, in a state of uncertainty, in which scenarios and objectives are agreed, managerial and technical actions defined, and potential response systems put in place to prevent, or better respond to, an emergency or critical situation.

**3.2 DATA GATHERING AND COALITION MANAGEMENT** Data-gathering is a continuous coalition management function, it is conducted before (warning,) during (assessment and monitoring) and after (evaluation) the coalition operation to ensure that decision makers can stay abreast of changing conditions. There is a wide range of data-gathering techniques available to coalition managers, from highly sophisticated satellite and remote sensing systems to one-on-one interviews with key informants. There is a wide range of tools available to assist coalition managers with their data-gathering needs.

**3.3 DATA ANALYSIS AND INFORMATION PRODUCTION** What decision makers clearly need is not sheer volume, but well reasoned, insightful finding and conclusions accompanied by recommendations for action and clear statements from data analysts on how particular conclusions were drawn. The early stages of a Coalition response are often characterized by very fast moving events and high levels of stress on operational staff. Mechanisms for Filtering and prioritization information are essential.

**3.4 INFORMATION DISSEMINATION** The gathering and analysis of data to produce information which consequently does not reach decision maker is an unfortunately waste of scarce resources-with potentially life-threatening consequences. Coalition managers should never assume that information finds its way to those who need it. Procedures for the dissemination of information to the decision makers and media who are positioned to set the wheels of the coalition response in motion should be planned in advance. Planning should take into account the geographical, political, and organizational location of those eventual users.

**3.4 DATA BANK** At the heart of effective information management is a capacity to use "institutional memory"-i. e., the recording and feedback into program design of the Coalition response experience.

## 4. COMBINED ENTERPRISE REGIONAL INFORMATION EXCHANGE SYSTEM (CENTRIXS 2)

It is the existing system supporting coalition efforts worldwide, to ensure readiness of Coalition command, control, communications, computers and intelligence (C4I) assets, the Coalition forces supports the following:

- War fighter Information Network-Tactical (WIN-T)
- Homeland Security Package
- Secret Internet Protocol Router Network (SIPRNet) for battalion infrastructure
- Standard Information Technology (IT) package
- Sensitive Compartmented Information Facilities (SCIFs) in every Domain
- Army Space Support Team (ARSST) equipment sets Space Battalion
- Availability Anti-Spoofing Module (SAASM) to all compatible Single Channel Ground and Airborne Radio Systems (SINCGARS) to ensure 100 percent Global Positioning System (GPS) capability in the SINCGARS radio

**4.1 AIMS OF CENTRIXS OPERATIONS ARE YET TO BE MET , SOME OF THESE ARE3:**

- Evolution of the technical support required to enable effective and efficient coalition operations in a net-centric environment is taking too long. COCOMs are forced to build multiple separate networks to support coalition warfare.
- Requirement for a single global coalition network that enables secure exchanges with multiple, separate communities of interest from a single workstation was jointly articulated by the combatant commands remains unmet.
- Seamless secure interconnected information environment
- Labeled data – metadata tagging
- Recognizes who you are: limits access based on who/where you are
- Secure interoperability within/across DoD (Department of Defence) and international partners
- Common infrastructure

**4.2 . CAPABILITIES OF GLOBAL INFORMATION GRID (GIG) FORMED BY CENTRIX.** The main features are provisioning of secured email over SIPRNet, Message and Imagery with Radient Mercury Guard and Order of Battle database with MLDBR:Multi level data base Replication and Security Bridge as shown in fig 2. The GIG as on March 2008 4 consists of 7 million DOD (Department of Defense) personnel, 1000 war fighting and support appliances and 120 thousand commercial telecom circuits. With presence in 88 countries it deploys 21 Satellite Communication gateways, 3544 Base stations and 15000 Networks. There are 1.1billion Internet Subscribers with 80 Gigabit bandwidth (70Gigabit NIPRNet +10 Gigabit SIPRNet), In Recce and Surveillance it undertakes 6 million probes / scans. Management across Inter Domain Coalition Network is colossal and challenging.

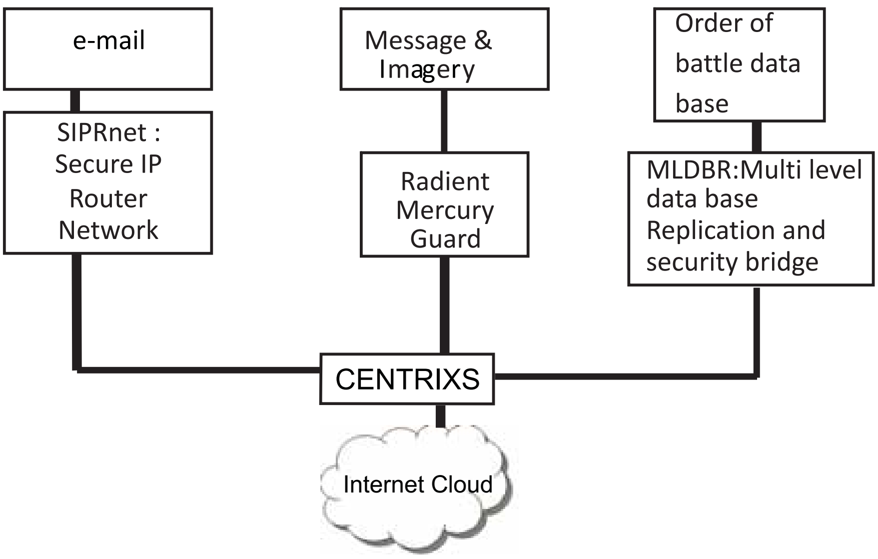


*Fig 2* Functional diagram of CENTRI

## 5. QUALITATIVE REQUIREMENT ON COALITION NETWORK MANAGEMENT

The Objectives of Coalition Network are

- Improve command Mission Assurance planning and execution capabilities and procedures, integrated and technology-enabled planning across information assurance, continuity of operations, anti-terrorism/force protection and critical infrastructure protection.
- Provide an enhanced interoperable Situation Awareness capability,
- Scalable in time, scope and bandwidth within and between information domains.
- Provide solutions to facilitate Information Sharing across Multiple Information Domains.
- Provide solutions and offer techniques and procedures that enable Collaborative Planning Across Bandwidth Constrained Operational Environment.
- Provide solutions to permit Enhanced Sharing And Dissemination Of Intelligence, Surveillance, And Reconnaissance (ISR)
- Provide solutions to address In-Transit Security of Information being exchanged between fixed domains and mobile users.
- Provide solutions for Responsive Effective Logistics within and between multiple information domains.

**6. In Feb 2008, the Air Force Research Laboratory 5issued qualitative requirement on Coalition Network management . The new scope include**

- Policy –enabled Network control
- Integrating different bearer service
- Management and security across different security domain
- Routing strategies, Bandwidth Brokering
- Policy control Quality of service
- Service oriented architecture
- Performance optimization
- Information Assurance.

## 7. REFERENCE MODEL FOR INTER DOMAIN COALITION

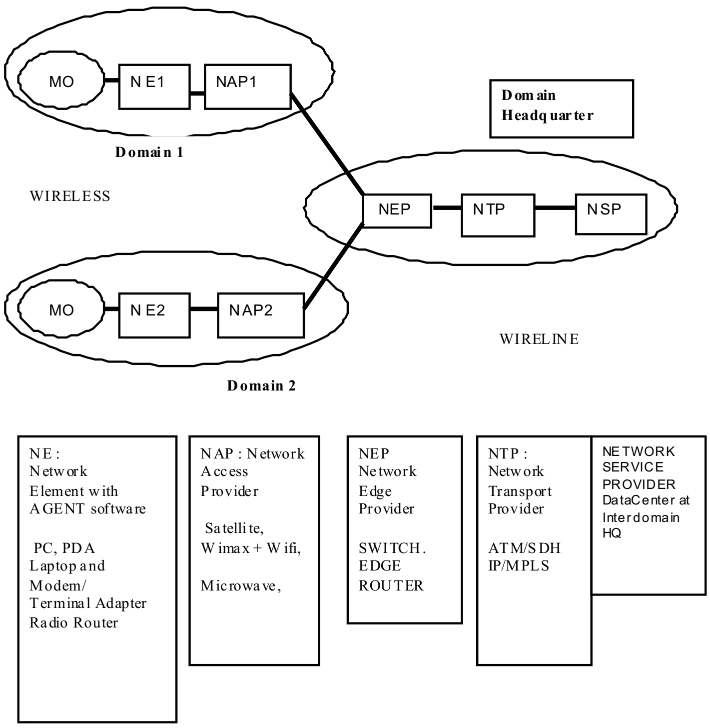

**NETWORK**


*Fig 3* REFERENCE MODEL INTER DOMAIN COALITION NETWORK

**7.1.** The reference model for Inter Domain Coalition Network is extension of broadband system model. The network elements are classified as per their functions into : Managed objects (MO), Network elements (NE), Network access provider (NAP), Network Edge provider, Network Transport Provider(NTP) and Network service Provider(NSP). The MO are sensors or Customer Premise Equipments (CPE) , these are managed by network Elements . NAP, NEP and NSP are Networks that connects the NE to Manager.

**7.2 TWO CASES ARE CONSIDERED IN FIG 3.** Case 1: MO is connected by wireless/ copper wire to NE. NE is accessed by NAP utilising WIMAX/WIFI or Radio. The inputs from these are aggregated by Edge routers or ATM switch. NTP is the transport network essentially SDH or IP/MPLS . NSP is the service provider at Data Center Inter Domain Headquarter,

Case 2: Network Element is directly connected to Manager by Satellite using PAMA (Pre assigned Multiple Access)or DAMA (Dynamic Assigned Multiple Access**)**

## 8. THE PHYSICAL TOPOLOGY

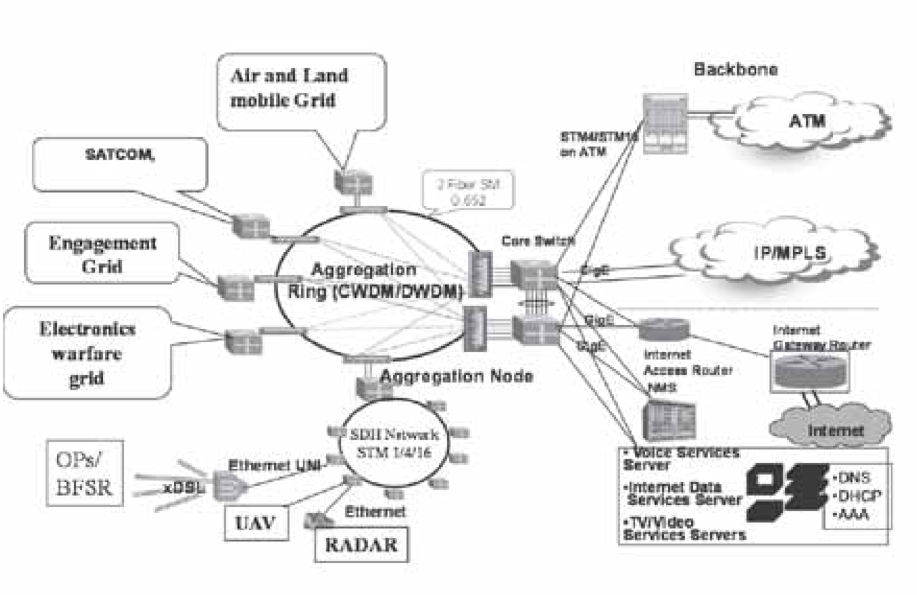


*Fig 4.* Physical topology of Reference Model

One of the various configuration 6 is shown in Fig. 4, in which inter Domain coalition network may be configured. The Digital subscriber line (DSL) of Observation Post(OP)/ Battle field Surveillance Rader (BFSR) are aggregated by Ethernet or UNI of ATM (depends on DSLAM used) and led to SDH ring. The SDH ring also supports UAV and RADARs . These are examples of NAP, NAP of Air and Land mobile, Engagement grid and Electronic Warfare grid shall be similarly configured. The Edge provider is depicted by CWDM (Coarse Wavelength Division Multiplexing) & DWDM (Dense wavelength Division multiplexing), The transport Network Provider is shown as ATM and IP clouds. NSP highlights Internet Access Router(IAR) and Internet Gateway Router (IGR) together with NMS with host of Servers for Voice, data, and video. Domain Name Server,(DNS), Dynamic Host control protocol (DHCP) servers with AAA (Authorization ,authentication and accounting) servers. The software of these servers shall be modified to produce better and efficient functionality.

## 9. EVOLUTION OF MANAGEMENT FOR INTER DOMAIN COALITION NETWORKS

Convergence of Voice, data and Video transport over a number of diverse architectural and technological domains e.g. Time Division Multiplexing (TDM),Asynchronous Transfer mode(ATM),Synchronous Optical Network (SONET), Synchronous Digital hierarchy (SDH),Frame Relay (FR), Dense Wavelength Division Multiplexing (DWDM), Internet Protocol (IP) led to formalization of Management Interface Standards. Apart from Geographical separate domains several vendors provide different technologies. Technology providers supply Network Elements and network Management Systems to manage their Technologies. The network management situation is further complicated by Multivendor support even within a single Technology and a service provider needs to partition the management of its growing Network

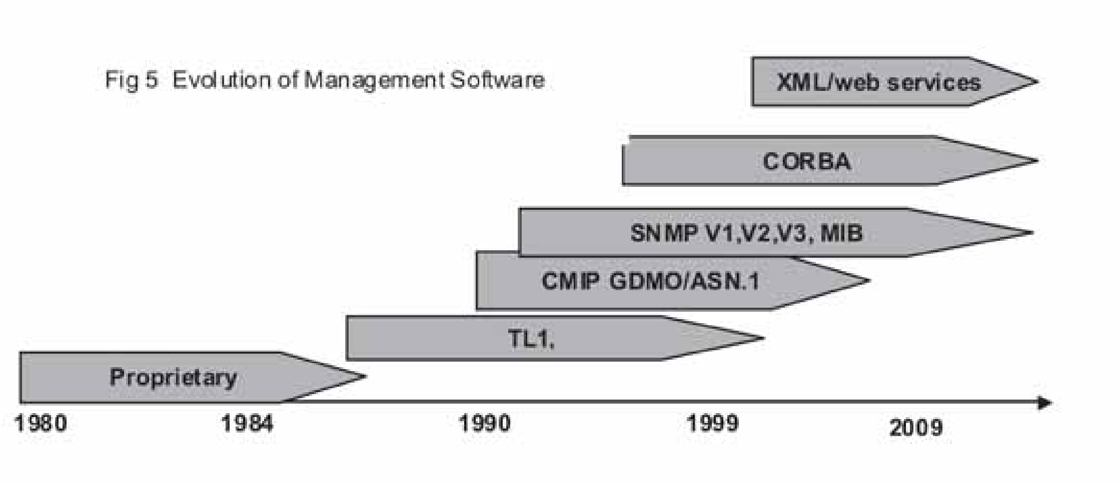


**9.1.** Network management involves a distributed database, auto polling of network devices, and high-end workstations generating real-time graphical views of network topology changes and traffic. In general, network management is a service that employs a variety of tools, applications, and devices to assist human network managers in monitoring and maintaining networks. In the early 1980s, the staffing requirements alone for managing large, heterogeneous networks created a crisis for many organizations. An urgent need arose for automated network management integrated across diverse environments. Most network management architectures (Fig 6)use the same basic structure and set of relationships. End stations (managed devices), such as computer systems and other network devices, run software that enables them to send alerts when they recognize problems (for example, when one or more user-determined thresholds are exceeded). Upon receiving these alerts, management entities are programmed to react by executing one, several, or a group of actions, including operator notification, event logging, system shutdown, and automatic attempts at system repair. NMS were Proprietary like TL1 of Micromuse.

**9.2.** Management entities also can poll end stations to check the values of certain variables. Polling can be automatic or user-initiated, but agents in the managed devices respond to all polls. Agents are software modules that first compile information about the managed devices in which they reside, then store this information in a management database, and finally provide it (proactively or reactively) to management entities within network management systems (NMSs) via a network management protocol. Well-known network management protocols include the Simple Network Management Protocol (SNMP) and Common Management Information Protocol (CMIP). In CMIP each managed system has a Management Information Base (MIB) . MIB represents the resources in a managed system that has been externalized for communication with the managing system. CMI P is not privy to internal data structure of the managed system, however the managing system has ability to retrieve information about the resources and to provision, reconfigure or inhibit the capabilities of the resources within the managedsystem. It performs its operations (as per ISO/IEC 9595) by attribute orientation, object orientation and notification. CMIP does not allow requests or messages as such it is not dynamic' The SNMP management framework is based on Internet – standard Mangement framework (sec 7 of RFC 3410). Here the managed objects are accessed via a Virtual Management Information base (MIB). MIB objects are accessed by SNMP. The mechanism is defined in the structure of management Information (RFC 2578, RFC 2579 & RFC 2580) .

**9.3. CMIP STANDARDS (FIG 6)** were the first to be formalized as management interface standards ITU-T,
M.3010: Defines the architecture for management systems.
G.805: Defines the representation of the network topology
X.7xx: Defines basic protocol and functions, such as object management and event reporting.
M.3100: Defines a generic set of objects for modeling networks and network elements

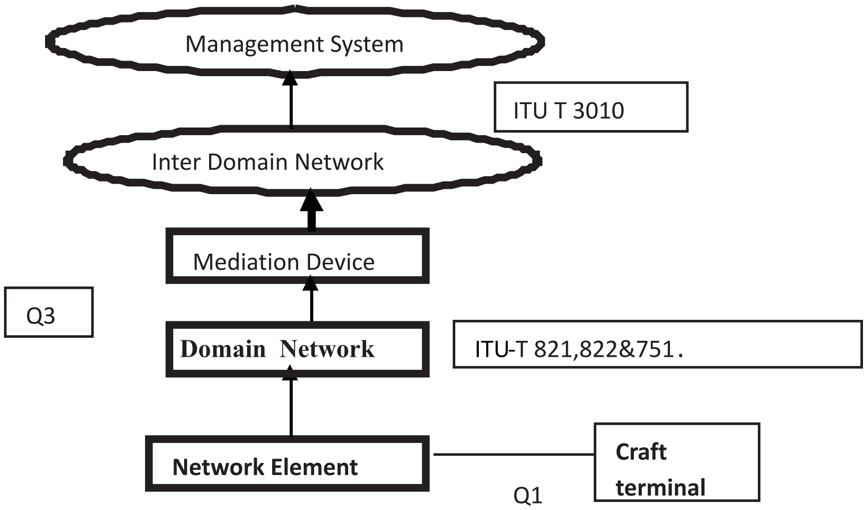


*Fig 6.* CMIP standard

Standards such as Q.821 and Q.822 define objects and functions for fault and performance management. The base standards have also been used for technology-specific models by the ITU (e.g. G.774), the TeleManagement Forum (e.g. TMF 038), and the ATM Forum (e.g. M4).These standards covered almost every aspect of network management, but failed to gain general acceptance because of the perceived complexity of the Q3 protocol and the Guidelines for the Definition of Managed Objects (GDMO)/ASN.1 modeling language. Another problem was the proliferation of different standards, each with its own "following" in the industry.

**9.4 OMG CORBA** 7(Object Management Group (OMG) Common Object Request Broker Architecture) The Object Management Group (OMG) Common Object Request Broker Architecture (CORBA) is a generic object-oriented middleware architecture that is not restricted to telecommunication applications. Interfaces are defined in the object-oriented Interface Description Language (IDL), which can be mapped directly to software programming languages. The protocol is simpler than Q3, but is complemented by CORBA services (defined in IDL), which can implement most middleware functions. This concept was successful and CORBA has thrived as the Q3 protocols were being undermined by the Simple Network Management Protocol (SNMP), Transaction Language 1 (TL1) and proprietary command line interfaces. The base CORBA specifications do not address telecommunication management, so various standards bodies have tried to preserve the enormous body of object definitions drawn up within the Q3 framework by adapting them to CORBA.

**9.5** JIDM (Joint InterDomain Management ) Specifications. The Joint InterDomain Management (JIDM) specifications are "a technology that defines how network management components based on Open Systems Interconnection (OSI) and SNMP can interoperate with CORBA-basedcomponents". JIDM was seen as a bridge between Q3 and pure CORBA implementations, and was developed to be a CORBA "veneer" on top of an existing implementation based on the Common Management Information Protocol (CMIP). It defines:
Translation algorithms between TMN or SNMP information models and the CORBA IDL.
CORBA interfaces for all possible interactions in CMIP or SNMP.

**9.6. ITU CORBA FRAMEWORK (FUTURE MANAGEMENT SYSTEM)** The IDL resulting from automatic translation is complex and JIDM is not widely accepted in the industry. In response to this situation, the Alliance for Telecommunications Industry Solutions (ATIS) and ITU introduced a new CORBA framework to permit GDMO/ASN.1 object definitions to be reused.
The ITU CORBA suite includes:
X.780, X.780.1 – modeling guidelines;
Q.816, Q.816.1 – interface support functions;
M.3120 – core object definitions;
Q.821.1, Q.822.1 – additional support services.
For example, the GDMO "managed object class" concept is more sophisticated than a CORBA object. The ITU CORBA framework restores this feature abundance so that existing managed object classes can be rewritten in IDL: ITU-T X.721 becomes X.780; M.3100 generic network model becomes M.3120, etc.
XML : XML is everywhere. It is the most common tool for data transmissions between all sorts of applications, and is becoming more and more popular in the area of storing and describing information

## 10. MAPPING OF QUALITATIVE REQUIREMENTS ON TCP/IP LAYERS OF COALITIO NETWORK MANAGEMENT (FIG 7)

**Fig 7. Mapping of Qualitative Requirements on TCP/IP layers of Coalition Network Management**

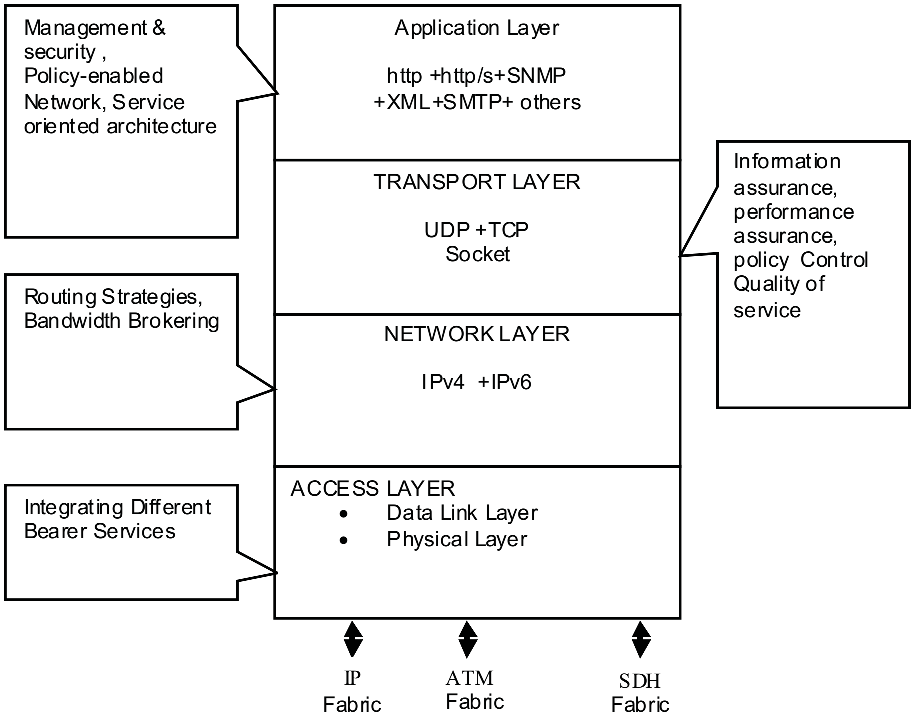


**10.1** Multiple Layers are involved in implementation of the QR (qualitative requirements)

- Access Layer has the physical layer and data link layer. Here the various Transport technologies are integrated.
- The data link layer has to deal with the frames where the MAC address resides. Message switching is in this layer. Access layer removes the frame address and forwards it to the Network layer.
- Network layer is the IP layer . It has twin stack of IPv4 + IPv6. Built into every router are the management table, Routing Table and Filter table which are programmable to provide IP security and routing strategy.
- Transport layer ; Two main protocol User Datagram Protocol (UDP) and Transmission Control protocol (TCP). Socket management , Information assurance, performance assurance, policy Control and Quality of service are in its ambit
- Application Layer has host of services providing Secure and non secure Hyper Text Transfer Protocol (SIPNet & NIPNet), Extended Mark up Language (XML) Simple Network management Protocol and others. Management & security, Policy-enabled Network, and Service oriented architecture function in this layer.

**11. POLICY-ENABLED NETWORK, 8** A policy- directed system operates under a set of guidelines (policies) that constrain its behavior relative to its current state and perceived operating environment. Such systems are composed of functional components for

- Sensing environmental conditions,
- Specifying and interpreting policies,
- Distributing and mediating the resultant behavioral constraints, and
- Accommodating the behavioral constraints. Resident in the higher layer of Management agent consists of policies, Policy manager agent, Policy repository and event.

**12.** Service oriented architecture (SOA) 9 is a design for linking computational resources (principally applications and data) on demand to achieve the desired results for service consumers (either end users or other services). OASIS (the Organization for the advancement of structured Information standard) defines SOA as the following: 'A paradigm for organizing and utilizing distributed capabilities that may be under the control of different ownership domains. It provides a uniform means to offer, discover, interact with and use capabilities to produce desired effects consistent with measurable preconditions and expectations'

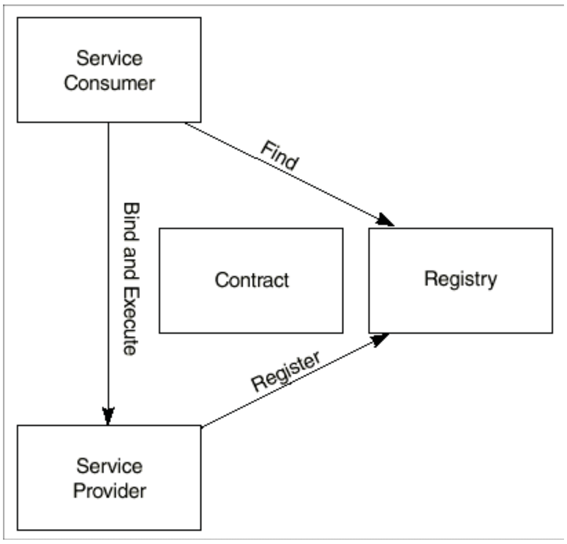


***Fig 9*** Service oriented architecture (SOA)

**12,1.** The "find, bind, and execute" paradigm as shown in Fig 9 allows the consumer of a service to ask a third-party registry for the service that matches its criteria. If the registry has such a service, it gives the consumer a contract and an endpoint address for the service. SOA consists of the following six entities configured together to support the find, bind, and execute paradigm

- **Service Consumer :** The service consumer is an application, service, or some other type of software module that requires a service.
- **Service Provider :** The service provider is the service, the network-addressable entity that accepts and executes requests from consumers.
- **Service registry** is a network-based directory that contains available services. It is an entity that accepts and stores contracts from service providers and provides those contracts to interested service consumers.
- **Service Contract :** A contract is a specification of the way a consumer of a service will interact with the provider of the service. It specifies the format of the request and response from the service.
- **Service Proxy :** The service provider supplies a service proxy to the s ervice consumer. The service consumer executes the request by calling an API function on the proxy.
- **Service Lease :** The service lease, which the registry grants the service consumer, specifies the amount of time the contract is valid: only from the time the consumer requests it from the registry to the time specified by the lease . When the lease runs out, the consumer must request a new lease from the registry.

## 13. INFORMATION , PERFORMANCE ASSURANCE, & POLICY CONTROL QUALITY OF SERVICE

These form part of Performance management. The purpose of performance management is to enable analysis and supervision of the quality of the network. Some of the parameters that give a picture of the network quality are: BER, pointer justification counts (PJC), protection switch counts (PSC), and slip rate (SLR). The Manager can order collection of parameter values at a particular point in time or at specified intervals. The parameter values are stored in the Managers database and can be used for various purposes. The Manager can give a graphical picture of the quality of the network (or of a leased line) and search for lines of a particular type and quality. The operator may wish to know the number of lines between two points - and the capacity and quality of these lines. The Manager can use a search profile to obtain this information and then provide it in response to the operator's question.

## 14. BANDWIDTH BROKERING 10

In ATM the hierarchy of Virtual Path (VP) and Virtual Channel (VC) allows designers to set up a dynamically configurable logical network . In MPLS this is carried out by means of Label Switch Paths (LSP). In this we use the term Logical Path (LP) to refer to any kind of logical path (e.g. VP, LSP, etc). One of the main objectives of bandwidth management is to minimise Call Blocking Probability (CBP), i.e. the probability that a call offered is rejected due to insufficient capacity being available for the allocation of the new call. Two actions are usually performed for the bandwidth management system: bandwidth re-allocation and path rerouting. There are four typical cases,

(a) If there is enough spare bandwidth in the link, then the congested LP is expanded using this bandwidth.

(b) If there is not enough spare bandwidth and other LPs going through the same link are under-utilised, it is possible to transfer resources from one LP to the other.
If (a) and (b) fail, then a re-routing is needed:

(c) If the congested LP finds another path with enough resources then it can be re-routed. Otherwise,

(d) other LPs may be re-routed through other links in order to free enough capacity to expand the congested LP

**14.1** Integrating Different Bearer Services . All Edge and core Routers have the interface and associated Network Input cards for the purpose.

## 15. INTER DOMAIN COALITION MANAGER PHYSICAL TOPOLOGY (FIG 10)

Inter Domain Coalition Manager Physical Topology has been suggested in following The ITU CORBA suite which includes X.780, X.780.1 – modeling guidelines; Q.816, Q.816.1 – interface support functions; M.3120 – core object definitions; Q.821.1, Q.822.1 – additional support services and US Patent No 7197546B1 dated 2007 . Heterogeneous Managed objects are connected to Network element(NE) which comprises the Management Information base and Agent with management Protocols. NE is connected to Intra Domain Manager and Inter Domain Coalition Manager utilizing IP/ATM/SDH Fabric.

**15.1.** Inter Domain Coalition Manager interfaces with functional managers through published CORBA API (Application Specific Interface). Four managers have been highlighted they are Fault manager, configuration manager, Tree manager and Service manager, system is complex and is under development.

- Inter Domain Fault Manager . The Physical connection to Agent and Domain manager is led to Correlation Manager . Correlation Manager is connected to Topology Manager which has its own Data Base, It is also connected to View Manager (part of Tree manager. The correlation manager is connected to Trouble Ticket Manager. The process of fault rectification is initiated.
- Inter Domain Configuration Manager. It uses Inter domain Provisioning Manager, Implementation Manager and Tree Manager. Inter domain Design Manager together with design Data base forms the Provisioning Maneger which is connected to logical tree manager accessing connectivity data base. The directions are sent for implementation .
- Service Manager comprises of order Manager, Trouble Manager, Customer service Manager and service level Manager

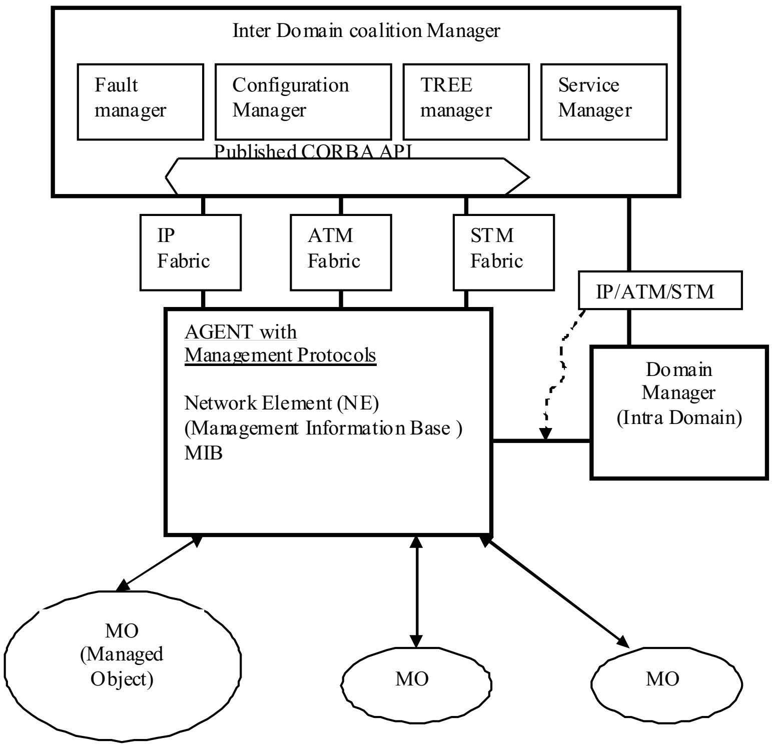


***Fig 10.*** Inter Domain Coalition Manager Physical Topology

**15.2** The trials and developments are being conducted in America, Canada, Australia and United Kingdom By 2012 the result of implementation shall affect globally the Inter Domain Coalition Network. The Defense Information Systems Agency (DISA) is a combat support agency responsible forconnecting the force by linking processes, systems, and infrastructure to people during last three years 2009-2011 has made significant progress in the following areas 11

- Transition to Net Centric Environment
- Eliminate Bandwidth Constraints
- GIG Network Operations and Defense
- Exploit the GIG for Improved Decision Making
- Deliver Capabilities Effectively/Efficiently
- Advanced Concept Technology Demonstration
- Special Missions Coalition Warrior Interoperability Demonstration

**15.3. SIMPLIFIED MULTICAST FORWARDING DRAFT-IETF-MANET-SMF-12A** In july 2011 MANET WORKING GROUP12 has provided Simplified Multicast Forwarding (SMF) mechanism that provides basic IP multicast forwarding suitable for limited wireless mesh and mobile ad hoc network (MANET) use. It is mainly applicable in situations where efficient flooding represents an acceptable engineering design trade-off. It defines techniques for multicast duplicate packet detection (DPD), to be applied in the forwarding process, for both IPv4 and IPv6 protocol use. It shall help in Identity Management and configuration management. It is in experimental stage.

# 16. CONCLUSION

An Inter Domain Coalition Information Management And Communication System is essential for Coalition Operation. Presently capability of Combined Enterprise Regional Information Exchange System (CENTRIXS) is global but aims of CENTRIXS operations are yet to be met. The Objectives of coalition Network and its management has been revised. To achieve the objectives the Terminology and Fundamental Concepts and Reference model for Inter Domain Coalition Network have been restated. A Physical topology is suggested. Evolution of management for Inter domain coalition Networking is then taken up discussing Simple Network Management Protocol (SNMP) and Common Management Information Protocol (CMIP). Object Management Group (OMG) Common Object Request Broker Architecture (CORBA) JIDM (Joint InterDomain Management ) ITU CORBA. Qualitative Requirements is mapped on TCP/IP layers of Coalition Network Management explaining methodology for Policy-enabled Network, Service oriented architecture (SOA ), Bandwidth Brokering. Physical Topology Inter Domain Coalition Manager is presented. The shall be useful for both hardware and software engineers who would be developing the systems independently. has envisaged to analyze, evaluate and suggest initiatives in understanding of inter domain coalition Network management .

# REFERENCES


1. Jeffrey S. Klenk, Emergency Information Management and Telecommunications,1st Edition, Inter Works,Disaster Management Training Programme 1997.
2. Jill L. Boardman and Donald W. Shuey,Combined Enterprise Regional Information Exchange System (Centrixs); Supporting Coalition Warfare World-Wide, Lockheed Martin Information Technologies, Department of the Air Force, USCENTCOM, April 2004
3. Peter J Fitzgerald, Coalition Network Management system,2008,In house Interim Technical Memorandum , Air Force Research Laboratory.
4. Information America's Greatest Weapon System, Lt Gen Charlie Croom, Defense Information Systems Agency, JTF-GNO 13 March 2008
5. M. Sloman: Network and Disributed Systems Management, Addison Wesley, 1994.
6. S. S. Banerjee & Vikas Kumar, Architectural Aspects of Present Day Network Management System for Military Communication , The Icfai Journal of Systems Management, Vol. 5, No. 3, pp. 7-13, August 2007
7. Object Management Group (OMG). CORBABasics. mwww.omg.org/gettingstarted/corbafaq.htm, accessed October 2002.
8 Ritu Chadha, Cho-Yu Jason Chiang, Mike Little, & Sunil Samtani, Agent-Based Policy-Enabled Network Management Architecture For Mobile Ad Hoc Networks, Applied Research, Telcordia Technologies 2003.
9. Stevens, M. Service-Oriented Architecture Introduction, Part 2. Developer.com, http://softwaredev.earthweb.com/msnet/article/0,,10527_1014371,00.html, accessed October 2002.
10. Ken Young,Research challengesfor Military Networking,Telcordia Technologies, 2002.

11. Defense Information Systems Agency (DISA ,Fiscal Year 2011 Budget Estimates ,February 2010.
12. Ian Chakeres (ian.chakeres ,Active Internet-Draft (manet WG), July 11, 2011


## STANDARDS

ISO-IEC 9595
CMIP
ITU-T M3010,G805,X7XX,M3100Q831,Q832,G774.
CORBA
ITU-T X780, Q616,M3120,Q821,Q8221
SNMP
RFC 3410,2578,2579,2580

## WEB RESOURCES

- The Simple Times http://www.simple-times.org/
- The Simple Web http://www.simpleweb.org/
- CMIP Run! http://wwwsnmp.cs.utwente.nl/Docs/iso/cmip-run/
- The Smurfland NM Web Server http://netman.cit.buffalo.edu/
- Organisations:
- Internet Engineering Task Force (IETF) http://www.ietf.org/
- Internet Research Task Force (IRTF) http://www.irtf.org/
- International Organization for Standardisation (ISO) http://www.iso.ch/
- International Telecommunication Union (ITU) http://www.itu.ch/
- Tele Management Forum (TMF) http://www.tmforum.org/
- Disributed Management Task Force (DMTF) http://www.dmtf.org/
- Object Management Group (OMG) http://www.omg.org/
- The Open Group http://www.opengroup.org/

# MICRO PULSE LIDAR: A TOOL FOR ANALYZING INTERACTIVE RELATION BETWEEN AEROSOL AND CLOUD FORMATION

Minakshi Devi
Department of Physics, Gauhati University, Guwahati-781014, India
Email: md555@sify.com, Tel: 03612676607

Ananda Kumar Barbara
Department of Physics, Gauhati University, Guwahati-781014, India Tel: 03612676607

Manoj Saikia, Bandita Choudhury
Department of Physics, Gauhati University, Guwahati-781014, India Tel: 03612676607

Hemanta Sarmah
Department of Physics, Gauhati University, Guwahati-781014, India Tel: 03612676607

## ABSTRACT

The paper gives in brief some basic technical aspects of the Micro Pulse Lidar (MPL) operated at Gauhati University (26º N and 92º E) and alludes to suitability of the system in examining aerosol and cloud interactions in temporal resolution of seconds to minutes. The lidar transmits 532 nm pulses of width 10 ns at peak repetition frequency of 1 KHz and is capable of receiving back scatter from aerosols and clouds up to heights of 5 and 15 km respectively, at a resolution of 15 m. With bin time of 100 ns and average integrating time of 20s for one profile, the system provides inputs for understanding variations of aerosol concentration in fine temporal scale. The transition pattern of aerosol backscatter counts has been adopted as a tracer of cloud formation process. The paper demonstrates this with relevant echograms.

***Key words:*** lidar; aerosol; cloud

## 1. INTRODUCTION

The Micro Pulse Lidar (MPL) or aerosol lidar has the ability to provide continuous data related to aerosols and clouds. It can offer both geometric and microphysical properties especially of clouds1,2 of different types. Further, since aerosol particles serve as Cloud Condensation Nuclei (CCN), lidar observations can be used for understanding aerosol-cloud radiative association3,4. These results are used in framing of atmospheric models for estimation of cloud radiative forcing5. Reports on detection of cloud base and hydrometeor information from lidar echograms are also available6.

In this paper the basic configuration of GU lidar is given along with corrections applied to data retrieval process on backscatter counts, to focus on the efficacy of the lidar in extraction of aerosol and cloud interactive process in fine temporal structure of seconds. Attempt is made to utilize the back scatter information during interactive transition process between aerosol and cloud as a tracer of cloud seeding process culminating in development of a new cloud structure.

## 2. OBSERVATION AND ANALYSIS

**2.1 GU LIDAR: BASIC CONFIGURATION AND ERROR CORRECTION FOR DATA RETRIEVAL** The basic configuration of GU MPL system, designed after Spinhirne (1993)7 and Spinhirne et al., (2000)8, is presented in Figure 1. It is composed of (a) laser transmitter, transmitting 532 nm wavelength signal, (b) beam expander, (c) Schmidt Cassegrain type telescope, fitted with a PMT at the focus of a pinhole size (iris) of 0.2mm diameter, (d) scalar for controlling trans-receiving signal, (e) monitor, data storage and computing units, (f) necessary optical system for working the lidar in co- axial mode and (g) the cooling system.

The lidar transmits 532 nm μj pulses of width 10 ns at Peak Repetition Frequency (PRF) of 1 KHz 9,10 and for achieving eye safety suitable for continuous operation, the transmitted beam width is expanded from 3 μ-rad to 80 μ-rad . The back scatter counts from aerosols and cloud structures are collected by a telescope of diameter 20 cm , falls on a PMT , placed near to the focus of a convex lens of 15 mm focal length . The input received in photon counting mode, is filtered by a 2.28 nm optical filter for reducing background illumination. The amplified signal from the PMT after conversion to TTL level is passed to the scalar for averaging and processing. A PMT has the advantage of low dark count of a few tens of counts/sec, thus it works within a broad dynamic range, suitable for handling widely varying backscatter counts.

The output is processed in LabView environment by a software developed10,11 for obtaining aerosol and cloud features. One bin-time is generally 100 ns and average integrating time of one profile is kept at 20 s, thus the maximum time of a scan may be 64000 s. The output is available as intensity- time profile for a single sounding from where, the height-time-intensity plot is obtained. The system is capable of receiving back scatter counts from aerosol and clouds up to a height of 5 and 15 km respectively, at a resolution of 15 m. This coaxial unit is thus capable of detecting fraction of one photon, after error corrections and normalization. Details of subsystems will not be discussed further.

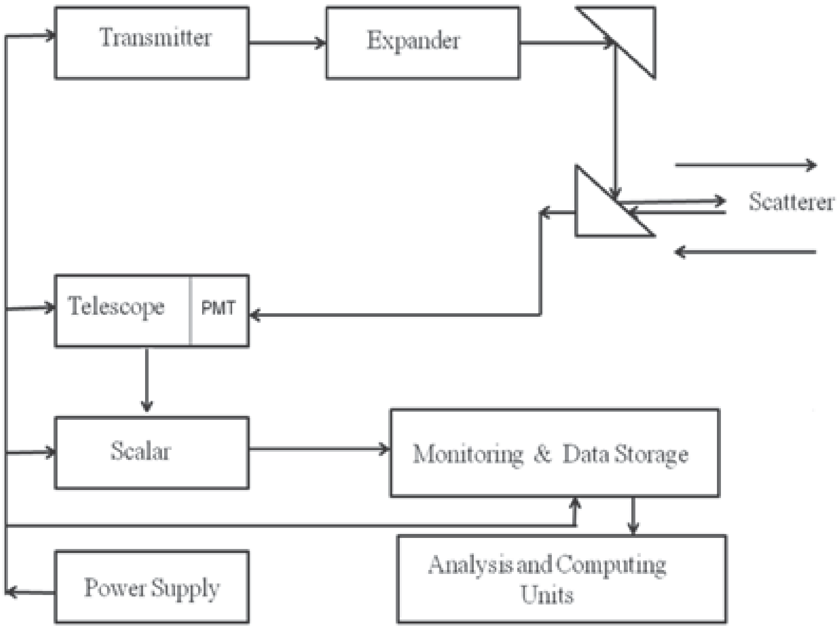


$$n_r(r) = \left[(O_c(r)CP_0\beta(r)T^2/r^2) + n_b(r) + n_{ap}(r)\right]/DTC[n(r)] \quad (1)$$

***Figure 1:*** The basic building blocks of the GU lidar

**2.2 RETRIEVAL OF SIGNAL FROM COUNTS AND ERROR CORRECTIONS** The intensity of received signal from a lidar is dependent in a complex way on the properties of the constituents of atmosphere i.e. on backscatter cross-sections of aerosols and molecules, as well as on other parameters as defined by Eq. (1).

Where,

| | |
|---|---|
| nr(r) | Raw signal recorded as photoelectrons per micro second (µs) |
| Oc(r) | Optical overlap correction (dimensionless) |
| C | Dimensional system calibration constant |
| E | Laser pulse energy (µj) |
| (r) | Backscatter cross section (both of aerosol and molecule) |
| T2 | Atmospheric transmittance |
| nb | Background signal (photoelectrons/µs) |
| nap(r) | After pulse correction counts (photoelectrons/µs) |
| DTC[n(r)] | Detector dead time correction (dimensionless) |
| P0 | Transmitter power |

In general, the equation (1) is rewritten in the form of equation (2 ) that gives normalized received power P(R ) and is available in real-time for MPL units.

$$\{n_r(r)DTC[n(r)] - n_b - n_{ap}(r)\}/O_c(r) = CP_0\beta(r)T^2/r^2 = P(R) \quad (2)$$

This equation requires correction for errors due to overlap, dead-time and after-pulse factor, for eliciting error-free information and also for realizing system sensitivity in temporal and spatial scales; the corrective measures taken here are described below

**Overlap correction**

At a very close field range, the laser beam does not come in to the Field Of View (FOV) of the telescope, thus the two beams will not overlap and signal from laser will not be viewed by the telescope and with increase of heights or distances, telescope will have partial or full view of the laser beam. It is thus important to calculate the overlap height, defined by a parameter called overlap factor. For evaluation of the overlap factor, a computer algorithm is developed by the group. The main aim of our exercise is to receive overlap factor for the GU MPL system, therefore, the configurations of this lidar i.e., laser beam divergence of 80 radian, telescope diameter 20 cm, FOV divergence 100 radian and laser -telescope axes distance of 15 cm are considered, while calculating this factor. As indicated in Figure 2, the overlap factor at the three characteristic regions which are shadow zone, partial view and full view zones are now discussed as separate cases. The overlapping distance R is calculated from laser divergence 1 (Figure 3a), FOV of the telescope 2 and distance between axes of transmitter and the telescope D, by using trigonometric Eq. ( 3).

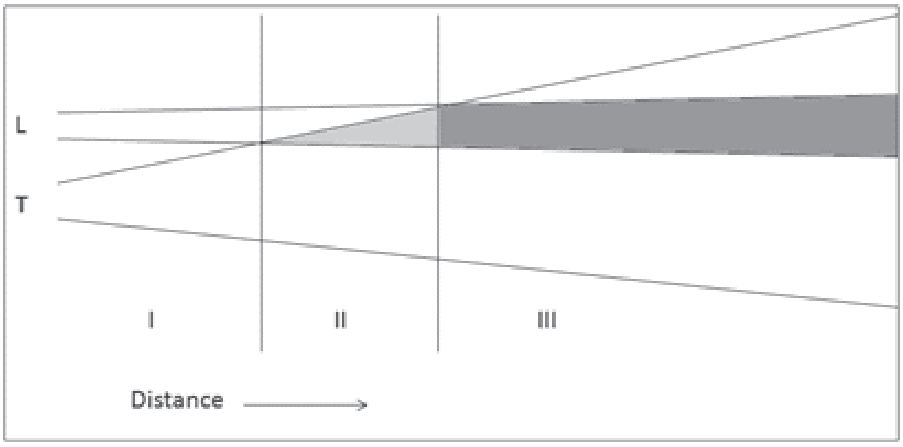


***Figure 2:*** Overlap factor analysis by trigonometric approach

Here L stands for laser transmitted beam, T signifies telescope FOV. The regions I, II and III are the shadow zone, partial view zone and full view zone respectively (details are given in the text).

$$R = [2D - (S_1 + S_2)] / 2(Tan\theta_1 + Tan\theta_2) \tag{3}$$

Here, S1 is diameter of the opening of the laser beam i.e., of the beam expander and S2 is diameter of the telescope.I. The shadow zone: In this region the laser beam and FOV of the telescope does not touch (region I of Figure 2), and therefore, the telescope cannot receive any signal. This shadow zone is defined by the condition (Figure 3a): D >AR1+AR2, where AR1 and AR2 are radii respectively of laser beam and telescope FOV cross-section. Here the overlap factor is zero.

II. Partial overlap zone: This is region II of Figure 2, where the laser beam illuminates some area of telescope. The intersection boundary illuminated by the laser and FOV of the telescope is shown in Figures 3(b, c). From geometry of the diagram, the overlap area ($\Lambda$) is given by the Eq. (4) as:

$$\Lambda = a^2 / 2[\phi - Sin\phi] \tag{4}$$

This gives the area formed by a semi cord that makes an angle at center of a circle, where 'a' is radius of the circle. The overlap areas for the two conditions as shown in Figures 3(b) and 3© are:

(I) $\Lambda$ = AR1+AR2, when both 1 and 2 are less than 180o (Figure 3b), and
(ii ) $\Lambda$ = AP-(AR1+AR2) When 1is greater than 180o, (Figure 3c)

Here, AP = $\pi$Ab2 is total area covered by the laser beam where, Ab is radius of the boundary of the laser beam illuminated area. Now, to calculate the overlap area [Eq. (4)], we evaluate coordinates of the intersecting point of the two circles. Numerical approach is adopted to solve the parametric equations of the two circles and by putting the value of in equation (4), we obtain the value of $\Lambda$, for different partial overlap conditions.

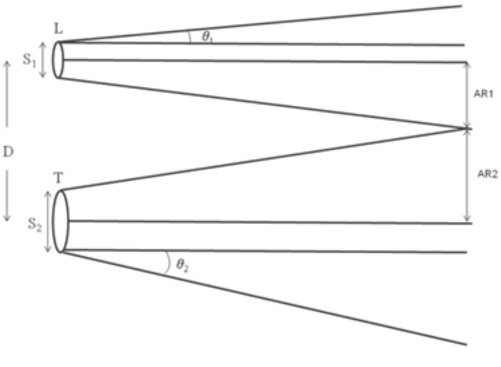

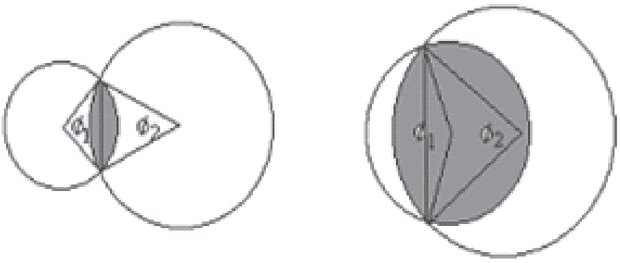

***Figure 3:*** (a) Gives the geometrical configuration for measuring overlap factor; (b) and (c) show the conditions of partial overlap

III. Full view zone: In this zone the telescope view covers the entire area illuminated by the laser beam, the overlap factor is thus unity (section III of Figure 2).

The exercise on evaluation of overlap region is done extensively for identifying the lowest possible altitude from which backscatter counts of GU lidar is possible . The software is thus made versatile so that it can be used to calculate overlap factor for the system at fine height resolution of about 15 meter. The results show that the shadow region comes below 100 m, a convenient height limit for measurement of aerosol and cloud very near to the surface.

**Dead time Correction:** This correction factor compensates the inability of photon detector to compile accurately a high data rate due to dead time of the detector. The 'dead time correction chart', provided by the manufacturer was used in case of GU lidar.

**After-pulse Correction:** This correction subtracts a residual signature that occurs due to leakage of photons in to the detector. This can be evaluated on receiving the signature of the laser pulse shape after the signal is blocked near to the transmitter. A non-linear decay of the return signal is an indicator of residual signature of the pulse.

Along with the corrections defined above, it is also required to eliminate range offset factor from raw lidar counts. This error occurs due to a time lag between the laser trigger and start of counting mechanism. The largest spike seen in the first point of range bin plot refers to the trigger of laser pulse. Therefore, time difference of the trigger mark and appearance of the first bin is an estimate of how many bins are off from the trigger event. This correction is effected by allowing the laser signal to strike on a hard target at a known distance.

Once all the corrections are incorporated into raw backscatter counts, the lidar Eq.(2) is written as

$$P(r) = P_0 C \beta(r) T^2(r) / r^2 \tag{5}$$

$$P(r) = CE \beta(r) T^2 / r^2 \tag{6}$$

Finally, normalized backscatter count is calculated by dividing P(r) by the dimensional calibration constant 'C' and the laser power. After correcting the quotient for the distance square attenuation10,11, we can write the final equation as :

$$P(r) r^2 / CE = \beta(r) T^2 \tag{7}$$

Next, the most important requirement for reliable interpretation of data from a system is its calibration i.e. the process of conversion of raw counts to optical parameters of aerosols and clouds. The details of lidar calibration process adopted by us are however given elsewhere10 along with the description of the software that is developed for this purpose under LabVIEW environment 11. This user friendly software also offers parameters like system constant, bin time, save length, average time and the output in appropriate format. We will discuss here only a few salient points of the software to highlight resolution capability of the system.

The lidar files are in 2D array of 32-bit single precision number (SGL) and therefore the 'read SGL function' is used to read these files. It gives the file data in one or two-dimensional array depending on the number of rows and columns supplied as input. The output data from this function include all the parameters as defined above and from the SGL function, the lidar setting parameters, i.e. bin time, save length, trigger frequency are first extracted and are used for calculating the other variabilities such as dimension of array in the remaining programme. To plot backscattered count P(r) in 2D and 3D graphs, the dimension is calculated from save length (L) and bin width (b). The average time which is software selectable, is normally kept at 20 second. Thus the system receives 2 x 105 data during one hour (at normal setting). The data of each hour is stored in separate files in 2D array of 32 bit single precision number at a specific format. From this 2D-array, we extract the sub array containing only the backscattered count P(r) and plot these in a 3D intensity graph. A control for extracting a single frame (a row of the array) is also introduced for plotting in a 2D graph.

Flexibility of the software is that all the corrections can be put into the main programme in a user friendly mode and therefore, one can resolve less than one back-scatter count, suitable for identifying a micro-scale temporal structure in the process of cloud formation, which is one of the aims of the paper. We will display a few aerosol-cloud echograms in normal mode, before fine-scale features are presented.

**2.2.1 CLOUD AND AEROSOL FEATURES SEEN BY GU LIDAR** Typical echograms of evening cloud structure with aerosols in the background are shown in Figure 4(a,b). In Figure 4 (a), white signatures seen within 2.2 km to 3.0 km altitude are strong back scatter from layered clouds and the green images are average signals returned from aerosols. The counts in brown, give strong scatter zones of aerosols within the average background. Similarly Figure 4(b) displays cloud structure with aerosols in background. These figures however will not offer in-depth details of cloud and of aerosol,

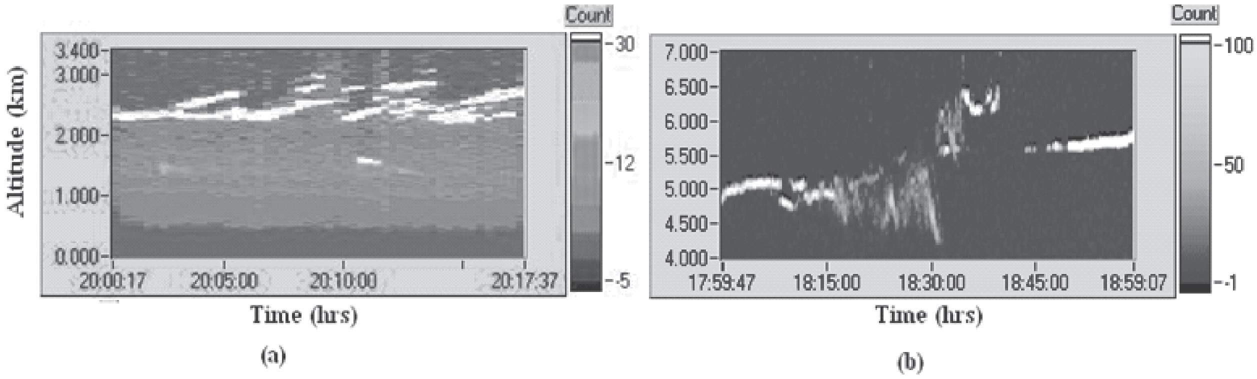


***Figure 4:*** Displays typical aerosol and cloud structures obtained from GU lidar

except that there is marginal enhancement of aerosol counts in the vicinity of cloud structure. Therefore, in Figure 5, we present echograms for a short period of sounding time (integrated for 1 minute) for vernal equinoxial days. Here, enhancement of aerosol (marked by arrow head) is noted in the vicinity of cloud layer. It does not however show any development process of cloud or interaction phenomenon with ambient aerosols because of relatively large integration time. Next, we analyze events in finer temporal resolution of 20s profile time. In Figure 6, a series of such echograms is presented to look for cloud development process in context of Figure 5.

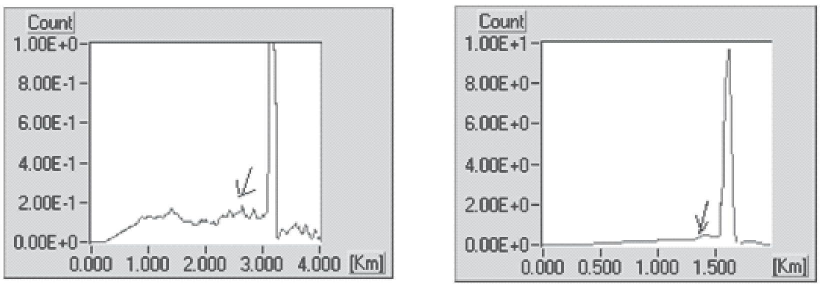


***Figure: 5*** Enhancement of aerosol (marked by arrow head) counts in the vicinity of cloud, obtained from GU lidar for two different events.

In Figure 6, we present a few representative lidar profiles taken over a 3 minute period. In all the frames (a, b, c, d) backscatter groups show a small build up of counts at 3km altitude, prior to the appearance of a cloud (frame d). It is important to note that though there is only a marginal increase in aerosol counts in the vicinity of a cloud development height, the pre-cursive aerosol count slightly decreases after the event. This characteristic feature is normally observed to be maintained during the cloud formation process in vernal equinoxial condition for low precipitating. The important point we like to focus is that, with proper calibration of aerosol lidar, the system is capable of providing even 1% enhancement in aerosols counts associated with the appearance of cloud. This coupling process can be implemented in future modeling of cloud seeding mechanism.

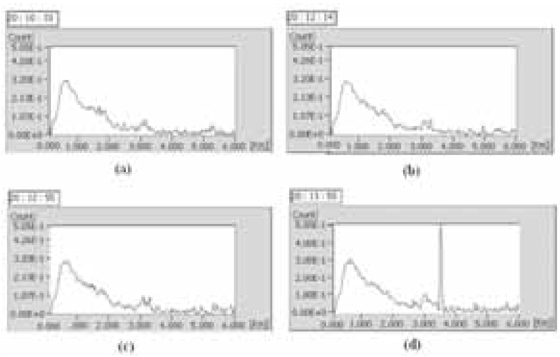


***Figure 6:*** Cloud growth and aerosols relation for a vernal equinoxial month (8.2.2001). Figures show aerosol counts and development of cloud within a 3 minute period starting from 20:10:33 hrs. It is seen that aerosol counts show a marginal but detectable enhancement at 3km prior to the growth of cloud layer.

## 3 CONCLUSION

The paper offers calibration approaches of aerosol lidar in determination of optical properties of aerosol in a suburban environment and their role in cloud formation in fine time resolution. The finding shows that it is possible to identify aerosol character in resolution at 1% relevant to growth of cloud structure. The information will be an input for future modeling of cloud seeding process which may be further extended to prediction of growth and development of fog specially applicable to safe landing of aircraft.

## ACKNOWLEDGMENT

The authors acknowledge with thanks the Department of Electronics (DOE), New Delhi, for funding the lidar project of Gauhati University.

## REFERENCES

1. Stokes G.M. & Schwartz, S.E., The Atmospheric Radiation Measurement (ARM) Program: Program background and design of cloud and radiation test bed. Bull. Amer. Meteorol. Society, 75, 1994, p.1201.

2. Campbell, J.R., Dennis, L.H., Spinhirne, J.D., Scott,III, V.S. & Turner, D.D., Operational processing and cloud boundary detection from Micro Pulse Lidar data, Presented in 19th International Laser Radar Conferences, 1998, p. 119.

3. Graβl, H., Albedo reduction and radiative heating of clouds by absorbing aerosol particles, Contributions Atmospheric Physics, 48, 1975, p.199.

4. Bian, H., Chin, M., Rodriguez, J., Yu, H., Penner, J. E. & Strahan, S., Sensitivity of aerosol optical thickness and aerosol direct radiative effect to relative humidity, Atmos. Chem. Phys, 9, 2009, p. 2375.

5. Hobbs, P.V., Aerosol cloud climate interactions, Academic Press Inc., New York, 1993

6. Clothiaux, E.E., Mace, G.G., Ackerman, T.P., Kane, T.J., Spinhirne J.D & Scott, V.S., An automated algorithm for detection of hydrometeor returns in micro pulse lidar data, J Atmos and Ocean Techn, 15, 1998, p. 1035.

7. Spinhirne, J.D., Micro Pulse Lidar, IEE Transaction on Geoscience and Remote Sensing, 13, 1993, p. 48

8. Spinhirne, J.D., Campbel, J.R. & Dennis, L., Autonomous, fulltime cloud profiling at arm sites with Micro Pulse Lidar, Symposium on lidar atmospheric monitoring, 2000. (http://www.ams.confex.com/ams/annual2000/lidar/index.htm).

9. Devi M. & Barbara, A.K., Development of a Portable lidar, Ministry of Information Technology, India, 2004, final report.

10. Devi, M., Barbara, A. K., Saikia, M. and Chen, W., Vertical distribution of optical parameter of aerosol by using portable atmospheric lidar system of Gauhati University, Ind. Jr. Radio & Space Phys., 37(5), 2008, p. 333.

11. Devi, M., Barbara, A. K., Saikia, M. and Chen, W., Vertical distribution of optical parameter of aerosol by using portable atmospheric lidar system of Gauhati University, Ind. Jr. Radio & Space Phys., 37(5), 2008, p. 333.

12. Hegg, D. A., Radke, L. F., and Hobbs, P. V., Particle production associated with marine clouds, J Geophys. Res. 95, 1990, p. 13917.

13. Keil, A. and Wendisch, M., Bursts of Aitken mode and ultrafine particles observed at the top of continental boundary layer clouds, J. Aerosol Sci., 32, 2001, p. 649.

14. Twohy, C. H., Clement, C. F., Gandrud, B. W., Weinheimer, A. J., Campos, T. L., Baumgardner, D., Brune, W. H., Faloona, I., Sachse, G. W., Vay, S. A., and Tan, D., Deep convection as a source of new particles in the midlatitude upper troposphere, J. Geophys. Res., 107(D21), 2002, p. 4560.

15. Weigelt, A., Hermann, M., Van Velthoven, P. F. J., Brenninkmeijer, C. A. M., Schlaf, G., Zahn, A., and Wiedensohler, A.: Influence of clouds on aerosol particle number concentrations in the upper troposphere, J. Geophys. Res., 114, 2009, p. D01204.

# A TWO-STATE MARKOVIAN QUEUEING MODEL WITH ARRIVALS IN BATCHES OF VARIABLE SIZE

Vijay Kumar
School of Business Studies, Sharda University,
Knowledge Park-III, Plot No.-32-34, Greater Noida,U.P.
vijay.gahlawat@gmail.com, vijay.kumar@sharda.ac.in (+91-9868040718)

Indra
Department of Statistics and Operations Research
Kurukshetra University, Kurukshetra
Haryana-131001

## ABSTRACT

New results are obtained for the transient behavior of first-come-first-served queueing model with arrivals in batches of variable size. Inter-arrival time and service time are exponentially distributed. Arrivals occur in batches of variable size. Probabilities of exact number of arrivals and departures are obtained. Finally particular case of interest is derived therefrom.

***Key Words:*** Two-State Queuing Model, Batch Arrival, Laplace Transform

## 1. INTRODUCTION

In ordinary queueing problems it is assumed that customers arrive singly at a service facility. However, this assumption is violated in many real-world queueing situations. Letters arriving at a post office, ships arriving at a port in convoy, people going to a theatre, restaurant, and so on, are some of the examples of queueing situations in which customers do not arrive singly, but in bulk or groups. Also, the size of an arriving group may be a random variable or a fixed number. Mathematically and also from practical point of view, the cases when the size of an arriving group is a random variable, are more general, and also more difficult to handle.

The study of batch arrival queues may be said to have begun with Erlang's solution of M/Ek/1 queue since this gives, implicitly the solution of the Mk/M/1 queue [1]. The major contributions on bulk arrival queues are made by Gaver [2] Sharda [3], Yao [4], Chaudhry & Templeton[5], Madan et al. [6].

Indra and Sharda [7] obtained explicitly the probabilities of exact number of arrivals and departures of a batch arrival two-state M/M/1 queueing system with latest arrival run having maximum effective length one. Kim and Kim [8], Schleyer and Furmans [9], Ahmed [10], M.S. El-Paoumy [11], F. A. Maraghi, et.al.[12], Wei Li et.al. [13], Rehab F. Khalaf et.al. [14], C. J. Singh, et.al. [15] also studied bulk arrival queues. Vijay Kumar [16] has done a survey on bulk queues.

Much of the vast literature on queueing models is confined to results describing steady-state operation only. But in many potential application of queueing theory, the practitioner needs to know how the system will operate up to some instant t. Many systems begin operations and are stopped at some specified time t. Business or service operations such as barber shops, rental agencies or physician's offices which open & close, never operate under steady-state conditions.

The classical transient results for the M/M/1 queue provide little insight into the behavior of a queueing system through a fixed operation time t. The function Pn(t) give the distribution for the number in the system at time t, but provide no information on how the system has operated up until time t. The practitioner needs to know what will happen up to time t. Typical questions include

- How many customers will be processed by time 't'?
- What fraction of time will the server be busy during the first 't' time units of operation?

Furthermore, if the system begins operation empty, the fraction of time the server is busy, the expected queue length, and the initial state of output from the system will be below the steady-state values so that the use of steady-state results to obtain these measures is not appropriate. Thus, the investigation of the transient behavior of queueing processes is also important from the point of view of the theory and its applications.

Pegden and Rosenshine [17] have given the probability of exact number of arrivals and departures by a given time for the classical queueing model M/M/1. This measure provides better insight into the behavior of queueing system than the probability of an exact number of units in the system in a given time, studied in earlier literature on queues, in many practical situations and is therefore more justified.

In two state queueing models, the state of the system is given by $(i, j)$, where 'i' is the number of arrivals and 'j' is the number of departures until time t. In present work an attempt has been made to study a two-state queueing model where arrivals are occurring in batches of variable size. We obtain the transient probabilities of exact number of arrivals and departures by a given time and various other results.

## 2. THE MODEL

The queueing system investigated in this paper is described by the following assumptions:

1. Arrivals are occurring in batches of variable size according to a Poisson distribution and $\lambda a_i \, \Delta t$ $(i=1,2,3\ldots)$ is the first order probability of i arrivals in the short interval of time $\Delta t$ $P(X=i)=a_i, \sum a_i = 1$ and $\lambda>0$ is the mean arrival rate.
2. Service times are exponentially distributed with parameter $\mu$
3. Queue discipline is first-come-first-served.
4. The various stochastic processes involved in the system are statistically independent.

### 2.1 DEFINITIONS AND NOTATIONS

$P_{i,j}(t)$ =Probability that there are exactly i arrivals and j departures by time t; i $i \geq j \geq 0$

Laplace transform of $P_{i,j}(t)$ is as follows:

$$\bar{P}_{i,j}(s) = \int_0^\infty e^{-st} P_{i,j}(t)\, dt$$

1. $\sum\limits_{\sum_{t=1}^{u} r_t = n}^{1}$ The summation over all those permutations of n objects

taken u (=1, 2…n) at a time, such that $\sum_{t=1}^{u} r_t = n, r_t > 0$

For example, when n=3 $\sum\limits_{\sum_{t=1}^{u} r_t = 3}^{1}$ The summation over all those permutations of 3 is the

sum of permutation of 3 taken one (u=1) at a time i.e., $r_1 = 3$
permutations of 3 taken two (u=2) at a time i.e., $r_1 + r_2 = 3$
and permutations of 3 taken (u=3) at a time, i.e. $r_1 + r_2 + r_3 = 3$

2. The Laplace inverse-transform of $\frac{Q(p)}{P(p)}$ is

$$\sum_{k=1}^{n}\sum_{\ell=1}^{m_k} \frac{t^{m_k-\ell} e^{\alpha_k t}}{(m_k-\ell)!(\ell-1)!} \frac{d^{\ell-1}}{d^{\ell-1}p} \frac{Q(p)(p-\alpha_k)^{m_k}}{P(p)} \Bigg|_{p=\alpha_k} \alpha_i \neq \alpha_k \quad \text{for } i \neq k$$

where, $P(p) = (p-\alpha_1)^{m_1}(p-\alpha_2)^{m_2}(p-\alpha_3)^{m_3}\ldots\ldots(p-\alpha_n)^{m_n}$ and $Q(p)$ is

polynomial of degree $< m_1 + m_2 + m_3 + \ldots\ldots + m_n - 1 >$

3. If $L^{-1}\{f(s)\} = F(t)$ and $L^{-1}\{g(s)\} = G(t)$ then

$$L^{-1}\{f(s)g(s)\} = \int_0^t F(u)\, G(t-u)\,du = F*G,$$

$F*G$ is called the convolution of F and G

4. The Laplace inverse of $\bar{B}^{a,b}_{\alpha,\beta}(s) = \left(\frac{1}{(s+a)^\alpha (s+b)^\beta}\right)$ using 2 is

$$B^{a,b}_{\alpha,\beta}(t) = \left[ \frac{e^{-at}}{(b-a)^{\beta}} \left\{ \sum_{g=1}^{\alpha} \left( \frac{t^{\alpha-g}}{(\alpha-g)!} \right) \left( \frac{\frac{1}{(g-1)!} \left( \prod_{\ell=1}^{g-1} (\beta+\ell-1) \right)^{(1-\delta_{g,1})}}{(b-a)^{g-1}} \right) \right\} + \frac{e^{-bt}}{(a-b)^{\alpha}} \right.$$

$$\left. \left\{ \sum_{g=1}^{\beta} (-1)^{g+1} \left( \frac{t^{\beta-g}}{(\beta-g)!} \right) \left( \frac{\frac{1}{(\alpha-1)!} \left( \prod_{\ell=0}^{\alpha-2} (g+\ell) \right)}{(a\text{-}b)^{g-1}} \right) \right\} \right]$$

5. $\prod_{\alpha}^{\beta} = 1$ and $\sum_{\alpha}^{\beta} = 0$ for $\beta < \alpha$ and $\delta_{i,j} = \begin{cases} 1 & , i = j \\ 0 & , i \# j \end{cases}$

## 3. SOLUTION OF THE PROBLEM

Initially $$P_{0,0}(0) = 1 \tag{2}$$

Difference differential equations governing the system are

$$\frac{d}{dt} P_{i,i}(t) = -\lambda P_{i,i}(t) + \mu P_{i,i-1}(t)(1-\delta_{i,0}); i \geq 0 \tag{3}$$

$$\frac{d}{dt} P_{i,j}(t) = -(\lambda+\mu) P_{i,j}(t) + \lambda \sum_{\ell=1}^{i-j} a_{\ell} P_{i-\ell,j}(t) + \mu P_{i,j-1}(t)(1-\delta_{j,0}); i > j \geq 0 \tag{4}$$

Taking the Laplace transform of (3) & (4) along with (2) we get (see Appendix),

$$\overline{P}_{0,0}(s) = \left( \frac{1}{s+\lambda} \right) \tag{5}$$

$$\overline{P}_{i,0}(s) = \left\{ \sum_{\sum_{t=1}^{u} r_t = i}^{1} \prod_{t=1}^{u} a_{r_t} \left\{ \left( \lambda^{u} \right) \overline{B}^{\lambda,(\lambda+\mu)}_{1,u}(s) \right\} \right\} ; \quad i > 0 \tag{6}$$

$$\overline{P}_{i,i}(s) = \left( \frac{\mu}{s+\lambda} \right) \overline{P}_{i,i-1}(s); \quad i \geq 1 \tag{7}$$

$$\overline{P}_{i,j}(s) == \sum_{\ell=j}^{i} \left[ \left[ \left\{ \sum_{\sum_{t=1}^{u} r_t = i-\ell}^{1} \prod_{t=1}^{u} a_{r_t} \left\{ \left( \lambda^{u} \mu \right) \left( \frac{1}{(s+\lambda+\mu)^{u+1}} \right)^{(1-\delta_{\ell,j})} \left( \overline{B}^{\lambda,(\lambda+\mu)}_{1,u}(s) \right)^{\delta_{\ell,j}} \right\} \right\} \right] \right]^{(1-\delta_{i,\ell})}$$

$$\left[\left\{\frac{\mu}{s+\lambda+\mu}\right\}^{(1-\delta_{\ell,j})}\right]^{\delta_{i,\ell}}\Bigg]\overline{P}_{\ell,j-1}(s)\,;\ i>j>0 \tag{8}$$

Taking the Laplace inverse transforms of equations from (5) to (8), we have

$$P_{0,0}(t)=e^{-\lambda t}$$

$$P_{i,0}(t)=\left\{\sum_{\sum_{t=1}^{u} r_t=i}{}^{1}\prod_{t=1}^{u} a_{r_t}\left\{\left(\lambda^{u}\right)B_{1,u}^{\lambda,(\lambda+\mu)}(t)\right\}\right\};\ i>0 \tag{10}$$

$$P_{i,j}(t)=\left(\mu e^{-\lambda t}\right)*P_{i,i-1}(t)\,;\ i\geq 1 \tag{11}$$

$$P_{i,j}(t)=\sum_{\ell=j}^{i}\left[\left[\left\{\sum_{\sum_{t=1}^{u} r_t=i-\ell}{}^{1}\prod_{t=1}^{u} a_{r_t}\left\{\left(\lambda^{u}\mu\right)\left(\frac{e^{-(\lambda+\mu)t}t^{u}}{u!}\right)^{(1-\delta_{\ell,j})}\left(B_{1,u}^{\lambda,(\lambda+\mu)}(t)\right)^{\delta_{\ell,j}}\right\}\right\}\right]\right]^{(1-\delta_{i,\ell})}$$

$$\left[\left\{\mu\, e^{-(\lambda+\mu)t}\right\}^{(1-\delta_{\ell,j})}\right]^{\delta_{i,\ell}}\Bigg]*P_{\ell,j-1}(t)\,;i>j>0 \tag{12}$$

From equations (5) to (8), it is seen that

$$\sum_{i=0}^{\infty}\sum_{j=0}^{i}\overline{P}_{i,j}(s)=\frac{1}{s}\ \text{ and hence}$$

$$\sum_{i=0}^{\infty}\sum_{j=0}^{i}P_{i,j}(t)=1\ \text{ a verification.}$$

**3.1 RESULTS**

1. The Laplace transform $\overline{P}_{i,.}(s)$ of the probability $P_{i,.}(t)$ that exactly i units arrive by time t is

$$\overline{P}_{i,.}(s)=\sum_{j=0}^{i}\overline{P}_{i,j}(s)=\left(\frac{1}{s+\lambda}\right)\left\{\sum_{\sum_{t=1}^{u} r_t=i}{}^{1}\prod_{t=1}^{u} a_{r_t}\left(\frac{\lambda}{s+\lambda}\right)^{u}\right\}^{(1-\delta_{i,0})};\quad i\geq 0$$

and after substituting $a_k=1$, for $k=1$; $a_k=0$, for $k>1$, we have

$$\overline{P}_{i,.}(s)=\sum_{j=0}^{i}\overline{P}_{i,j}(s)=\left\{\frac{\lambda^{i}}{(s+\lambda)^{i+1}}\right\};\quad \mathbf{i\geq 0} \tag{13}$$

and hence

$$P_{i,.}(t)=\frac{(\lambda\, t)^{i}}{i!}e^{-\lambda t};\quad i\geq 0 \tag{14}$$

The arrivals follow a Poisson distribution

2. The Laplace transform of mean number of arrivals by time t is

$$\sum_{i=0}^{\infty} i\,\overline{P}_{i,.}(s) = \left\{\frac{\lambda}{s^2}\right\} \tag{15}$$

and the Laplace inverse of the mean number of arrivals by time t is

$$\sum_{i=0}^{\infty} i\,P_{i,.}(t) = \lambda t \tag{16}$$

3. The Laplace transform $\overline{P}_{.,j}(s)$ of the probability $P_{.,j}(t)$ that exactly j customers have been served by time t, we have

$$\overline{P}_{.,j}(s) = \sum_{i=j}^{\infty} \overline{P}_{i,j}(s)$$

For n=0

$$\overline{P}_{.,0}(s) = \sum_{i=0}^{\infty} \overline{P}_{i,0}(s) = \sum_{i=0}^{\infty}\left[\left\{\frac{1}{s+\lambda}\right\}^{\delta_{i,0}}\left\{\sum_{\sum_{t=1}^{u} r_t = i}^{1}\prod_{t=1}^{u} a_{r_t}\left\{(\lambda^u)\overline{B}_{1,u}^{\lambda,(\lambda+\mu)}(s)\right\}\right\}^{(1-\delta_{i,0})}\right]$$ and

$$P_{.,0}(t) = \sum_{i=0}^{\infty} P_{i,0}(t) = \sum_{i=0}^{\infty}\left[\left\{e^{-\lambda t}\right\}^{\delta_{i,0}}\left\{\sum_{\sum_{t=1}^{u} r_t = i}^{1}\prod_{t=1}^{u} a_{r_t}\left\{(\lambda^u)B_{1,u}^{\lambda,(\lambda+\mu)}(t)\right\}\right\}^{(1-\delta_{i,0})}\right]$$

For n>0

$$\overline{P}_{.,j}(s) = \sum_{i=j}^{\infty} \overline{P}_{i,j}(s) = \sum_{i=j}^{\infty}\left[\left[\sum_{\ell=0}^{\infty}\left\{\frac{\mu}{s+\lambda}\right\}^{\delta_{\ell,0}}\left\{\sum_{\sum_{t=1}^{u} r_t = \ell}^{1}\prod_{t=1}^{u} a_{r_t}\left\{(\lambda^u\mu)\overline{B}_{1,u}^{\lambda,(\lambda+\mu)}(s)\right\}\right\}^{1-\delta_{\ell,0}}\right]^{\delta_{i,j}}\right.$$

$$\left.\left[\sum_{\ell=0}^{\infty}\left\{\frac{\mu}{s+\lambda+\mu}\right\}^{\delta_{\ell,0}}\left\{\sum_{\sum_{t=1}^{u} r_t = \ell}^{1}\prod_{t=1}^{u} a_{r_t}\left\{\frac{\lambda^u\mu}{(s+\lambda+\mu)^{u+1}}\right\}\right\}^{1-\delta_{\ell,0}}\right]^{(1-\delta_{i,j})}\overline{P}_{i,j-1}(s)\right]$$ and

$$P_{.,j}(t) = \sum_{i=j}^{\infty} P_{i,j}(t) = \sum_{i=j}^{\infty}\left[\left[\sum_{\ell=0}^{\infty}\left\{\mu e^{-\lambda t}\right\}^{\delta_{\ell,0}}\left\{\sum_{\sum_{t=1}^{u} r_t = \ell}^{1}\prod_{t=1}^{u} a_{r_t}\left\{(\lambda^u\mu)B_{1,u}^{\lambda,(\lambda+\mu)}(t)\right\}\right\}^{1-\delta_{\ell,0}}\right]^{\delta_{i,j}}\right.$$

$$\left.\left[\sum_{\ell=0}^{\infty}\left\{\frac{\mu e^{-(\lambda+\mu)t}}{s+\lambda+\mu}\right\}^{\delta_{\ell,0}}\left\{\sum_{\sum_{t=1}^{u} r_t = \ell}^{1}\prod_{t=1}^{u} a_{r_t}\left\{\lambda^u\mu\left(\frac{e^{-(\lambda+\mu)t}t^u}{u!}\right)\right\}\right\}^{1-\delta_{\ell,0}}\right]^{(1-\delta_{i,j})} * P_{i,j-1}(t)\right]$$

4. The Laplace transform $\overline{P}_n(s)$ of the probability $P_n(t)$ that exactly n customers in the system at time t, can be expressed in terms of $\overline{P}_n(s)$ as

$$\overline{P}_n(s)=\sum_{j=0}^{\infty}\overline{P}_{j+n,j}(s)$$

For n=0

$$\overline{P}_0(s)=\left(\frac{\mu}{s+\lambda}\right)\left[1+\sum_{j=0}^{\infty}\overline{P}_{j,j\text{-}1}(s)\right] \quad \text{and} \quad P_0(t)=\mu\left[e^{-\lambda t}+\sum_{j=0}^{\infty}\left(e^{-\lambda t}\right)*P_{j,j\text{-}1}(t)\right]$$

For n>0

$$\overline{P}_n(s)=\sum_{j=0}^{\infty}\sum_{r=1}^{n}\left(\frac{\lambda a_{n+1-r}}{s+\lambda+\mu}\right)\overline{P}_{j+n,j}(s)+\sum_{j=0}^{\infty}\left(\frac{\mu}{s+\lambda+\mu}\right)\overline{P}_{j+n,j\text{-}1}(s)$$

and

$$P_n(t)=\sum_{j=0}^{\infty}\sum_{r=1}^{n}\left(\lambda\, a_{n+1-r}\; e^{-(\lambda+\mu)t}\right)*P_{j+n,j}(t)+\sum_{j=0}^{\infty}\left(\mu\, e^{-(\lambda+\mu)t}\right)*P_{j+n,j\text{-}1}(t)$$

5. The waiting time distribution for a customer can be derived as P(W>t1/t), the probability that a customer waits more than t1 time units in the system, given that the customer arrives at time t.

$$\begin{aligned}P(W>t_1/t)&=\sum_{n=0}^{\infty}P(W>t_1/\ n\ \text{ customers in the system at time t})P_n(t)\\&=\sum_{n=0}^{\infty}P(\text{number of service by time } t_1<n+1\,)\,P_n(t)\\&=\sum_{n=0}^{\infty}\sum_{g=0}^{n}\left(\frac{e^{-\mu t_1}\left(\mu t_1\right)^g}{g!}\right)P_n(t)\end{aligned}$$

Therefore the cumulative distribution for the sojourn time in the system is

$$P(W\le t_1/t)=\sum_{n=0}^{\infty}\sum_{g=0}^{n}\left(\frac{e^{-\mu t_1}\left(\mu t_1\right)^g}{g!}\right)P_n(t)$$

The density function of sojourn time for a customer arriving at time t is obtained by differentiating this expression with respect to t1.

6. The system utilization, i.e., the fraction of time the server is busy until time t can also be obtained in terms of

Pi,j(t). The probability that the system is empty at some time t1 is $\sum_{j=0}^{\infty}P_{j,j}(t_1)$ Thus the fraction of the time that the system is empty and consequently the server is idle is

$$I(t)=\left(\frac{1}{t}\right)\int_0^t\sum_{j=0}^{\infty}P_{j,j}(t_1)\,dt_1$$

and the fraction of time that the system is non-empty and, hence, the server utilized is

$$U(t)=1-\left(\frac{1}{t}\right)\int_0^t\sum_{j=0}^{\infty}P_{j,j}(t_1)\,dt_1$$

**3.2 PARTICULAR CASE**

When arrivals are occurring one by one, i.e. by substituting a1=1 and a2, a3, a4…=0, in the equations (9) to (12), we have

$$P_{0,0}(t)=e^{-\lambda t} \tag{17}$$

$$P_{i,0}(t)=\left(\lambda^i\right)\left\{B_{1,i}^{\lambda,(\lambda+\mu)}(t)\right\};\ i>0 \tag{18}$$

Equations (17) to (19) coincide with equation (5) of Pegden and Rosenshine [17].

## 4. CONCLUSION

In this paper a batch arrival two-state queuing model is studied. I obtain, Pi,j(t), the transient probabilities of exact number of arrivals and departures by time t. Also, I obtained (i) the probability Pi,.(t) that there are exactly i units arrive by time t and mean number of arrivals by time t, (ii) the probability P.,j(t) that exactly j customers served by time t, (iii) the probability Pn(t) that exactly n customers in the system by time t, (iv) the cumulative distribution for the sojourn time in the system, and (v) server's idle time and utilization times. All these results provide better insight into the behavior of queueing systems with batch arrivals

## ACKNOWLEDGMENTS

Author is thankful to the authorities of the Sharda University for providing necessary facilities and encouragement for carrying out this work.

## REFERENCES

[1] Brockemeyer, E., H.L. Halstrom, and A. Jensen, The life and works of A.K. Erlang, The Copenhagen telephone company, 1948,Copenhagen, Denmark.

[2] Gaver, D.P., Imbedded Markov Chain analysis of a waiting time in continuous time, Ann. Math. Stat. 30, 1959, P. 698-720.

[3] Sharda, A queueing problem with batch arrivals and correlated departures, Metrika, Vol. 20, 1973, p. 81-92.

[4] Yao, D. D. , Some results for the queues MX/M/c and GIX/G/C, Operations Research Letters, 4, 1985, P. 79–83.

[5] Chaudhry, M.L. and Templeton, J.G.C. , A first course in bulk queues, John Wiley, 1983, New York.

[6] Madan, K.C., Al- Naseer, A.D., and Al-Masri, On $M^{[X]}/\left(\begin{smallmatrix}G_1\\G_2\end{smallmatrix}\right)1$ queue with optional re-service, Applied Mathematics and Computation, Vol. 152, A.Q., 2004, p. 71-88.

[7] Indra and Sharda, A Batch Arrival Two-State M/M/1 Queueing System with Latest Arrival Run (LAR) Having Maximum Effective Length One, International journal of Management Science and Systems,15(2), 2004, p.71-80.

[8] Kim J. and Kim B., The processor-sharing queue with bulk arrivals and phase-type services, Performance Evaluation, Volume 64 , Issue 4, 2007, P. 277-297.

[9] Schleyer, M. and Furmans, K., An analytical method for the calculation of the waiting time distribution of a discrete time G/G/1-queueing systems with batch arrivals, OR Spectrum, Vol. 29, no. 4, 2007, p. 745-763.

[10] Ahmed, M.M.S., Multi-channel bi-level heterogeneous servers bulk arrivals queueing system with Erlangian service time, Mathematical and Computational Applications, Vol. 12, No. 2, 2007, p. 97-105.

[11] M.S. El-Paoumy, The Non-Truncated Bulk Arrival Queue MX/M/1 with Reneging, Balking, State-Dependent and an Additional Server for Longer Queues, Applied Mathematical Sciences, Vol. 2, no. 15, 2008, p. 747 – 752.

[12] F. A. Maraghi, K. C. Madan, and K. Darby-Dowman, (2009), Batch arrival queueing system with random breakdowns and Bernoulli schedule server vacations having general vacation time distribution, International Journal of Information and Management Sciences, vol. 20, no. 1, 2009, p. 55–70.

[13] Wei Li, Fretwell R.J., Kouvatsos D.D. , General Solution of Queueing Model with Batch Renewal Arrival by Two Approaches, IEEE, 2010, p. 73-76.

[14] Rehab F. Khalaf, K.C. Madan, and C.A. Lukas, On a Batch Arrival Queueing System Equipped with a Stand-by Server during vacation Periods or the Repair Times of the Main Server, Journal of Probability and Statistics, Vol. 2011, Article ID 812726, 11 pages, doi:10.1155/2011/812726.

[15] Charan Jeet Singh, Madhu Jain, Binay Kumar , Queueing model with state-dependent bulk arrival and second optional service, International Journal of Mathematics in Operational Research 2011 - Vol. 3, no.3, 2011, p. 322 - 340.

[16] Vijay Kumar, Bulk Queueing Models, GYANPRATHA (Accman Journal of Management Science), Vol. 2, Issue No. 2, 2010.

[17] Pegden C.D. and Rosenshine, M., Some new results for the M/M/1 queue, Mgt Sci 28, 1982, p. 821-828.

# APPENDIX

$$\overline{P}_{0,0}(s)=\left(\frac{1}{s+\lambda}\right)$$

$$\overline{P}_{1,0}(s)=\left(\frac{1}{s+\lambda}\right)\left(\frac{\lambda a_1}{s+\lambda+\mu}\right)$$

$$\overline{P}_{2,0}(s)=\left(\frac{1}{s+\lambda}\right)\left(\frac{\lambda^2 a_1^{\,2}}{(s+\lambda+\mu)^2}+\frac{\lambda a_2}{s+\lambda+\mu}\right)$$

$$\overline{P}_{3,0}(s)=\left(\frac{1}{s+\lambda}\right)\left(\frac{\lambda^3 a_1^{\,3}}{(s+\lambda+\mu)^3}+\frac{2\lambda^2 a_1a_2}{(s+\lambda+\mu)^2}+\frac{\lambda a_3}{s+\lambda+\mu}\right)$$

or

$$\overline{P}_{3,0}(s)=\left(\frac{1}{s+\lambda}\right)\left\{\sum_{\sum_{t=1}^{u} r_t=3}^{1}\prod_{t=1}^{u} a_{r_t}\left\{\frac{\lambda}{s+\lambda+\mu}\right\}^u\right\}=\left(\frac{1}{s+\lambda}\right)\left(\frac{\lambda^3 a_1^{\,3}}{(s+\lambda+\mu)^3}+\frac{2\lambda^2 a_1a_2}{(s+\lambda+\mu)^2}+\frac{\lambda a_3}{s+\lambda+\mu}\right)$$

or

$$\overline{P}_{3,0}(s)=\left\{\sum_{\sum_{t=1}^{u} r_t=3}^{1}\prod_{t=1}^{u} a_{r_t}\left\{\frac{\lambda^u}{(s+\lambda)(s+\lambda+\mu)^u}\right\}\right\}==\left(\frac{\lambda^3 a_1^{\,3}}{(s+\lambda)\,(s+\lambda+\mu)^3}+\frac{2\lambda^2 a_1a_2}{(s+\lambda)(s+\lambda+\mu)^2}+\frac{\lambda a_3}{(s+\lambda)(s+\lambda+\mu)}\right)$$

or

$$\overline{P}_{3,0}(s)=\left\{\sum_{\sum_{t=1}^{u} r_t=3}^{1}\prod_{t=1}^{u} a_{r_t}\left\{\left(\lambda^u\right)\overline{B}_{1,u}^{\lambda,(\lambda+\mu)}(s)\right\}\right\}==\left(\frac{\lambda^3 a_1^{\,3}}{(s+\lambda)\,(s+\lambda+\mu)^3}+\frac{2\lambda^2 a_1a_2}{(s+\lambda)(s+\lambda+\mu)^2}+\frac{\lambda a_3}{(s+\lambda)(s+\lambda+\mu)}\right)$$

Where, $\sum_{\sum_{t=1}^{u} r_t=n}^{1}$ The summation over all those permutations of n objects taken u

(=1, 2…n) at a time, such that $\sum_{t=1}^{u} r_t = n \quad , r_t > 0$

For example, when n=3

$\sum_{\sum_{t=1}^{u} r_t=3}^{1}$ , The summation over all those permutations of 3 is the sum of

permutation of 3 taken one (u=1) at a time i.e., $r_1 = 3$ permutations of

3 taken two (u=2) at a time i.e., $r_1 + r_2 = 3$ and permutations of 3 taken

(u=3) at a time i.e., $r_1 + r_2 + r_3 = 3$

Similarly,

$$\bar{P}_{4,0}(s) = \left(\frac{1}{s+\lambda}\right)\left\{\sum_{\sum_{t=1}^{u} r_t = 4}{}^{1}\prod_{t=1}^{u} a_{r_t}\left\{\frac{\lambda}{s+\lambda+\mu}\right\}^{u}\right\}$$

$$\frac{1}{s+\lambda}\Bigg)\left\{\sum_{\sum_{t=1}^{u} r_t = 4}{}^{1}\prod_{t=1}^{u} a_{r_t}\left\{\frac{\lambda}{s+\lambda+\mu}\right\}^{u}\right\} = \left(\frac{1}{s+\lambda}\right)\left(\frac{\lambda^4 a_1{}^4}{(s+\lambda+\mu)^4} + \frac{3\lambda^3 a_1{}^2 a_2}{(s+\lambda+\mu)^3} + \frac{2\lambda^2 a_1 a_2}{(s+\lambda+\mu)^2} + \frac{\lambda^2 a_2{}^2}{(s+\lambda+\mu)^2} + \frac{\lambda a_4}{s+\lambda+\mu}\right) \text{or}$$

$$\bar{P}_{4,0}(s) = \left\{\sum_{\sum_{t=1}^{u} r_t = 4}{}^{1}\prod_{t=1}^{u} a_{r_t}\left\{\frac{\lambda^u}{(s+\lambda)(s+\lambda+\mu)^u}\right\}\right\} = \left\{\sum_{\sum_{t=1}^{u} r_t = 4}{}^{1}\prod_{t=1}^{u} a_{r_t}\left\{\left(\lambda^u\right)\bar{B}_{1,u}^{\lambda,(\lambda+\mu)}(s)\right\}\right\}$$

and so on
$\therefore$ In general

$$\bar{P}_{i,0}(s) = \left(\frac{1}{s+\lambda}\right)\left(\sum_{\sum_{t=1}^{u} r_t = i}{}^{1}\prod_{t=1}^{u} a_{r_t}\left(\frac{\lambda}{s+\lambda+\mu}\right)^{u}\right) = \left\{\sum_{\sum_{t=1}^{u} r_t = i}{}^{1}\prod_{t=1}^{u} a_{r_t}\left\{\frac{\lambda^u}{(s+\lambda)(s+\lambda+\mu)^u}\right\}\right\}$$

$$= \left\{\sum_{\sum_{t=1}^{u} r_t = i}{}^{1}\prod_{t=1}^{u} a_{r_t}\left\{\left(\lambda^u\right)\bar{B}_{1,u}^{\lambda,(\lambda+\mu)}(s)\right\}\right\};\ i > 0$$

Like this we have obtained all other equations.

# IFRS CONVERGENCE - BENEFITS, PROBLEMS AND DEVIATIONS WITH SPECIAL REFERENCE TO WIPRO LIMITED

Rakesh Anand
Director, Faulty of Management Studies
Jeev Sewaa Sansthan Group of Institutions for Women, Habbiganj, Bhopal (M.P.)
Email: ranand18@gmail.com, Mobile No 09424400975

***Key words:*** IFRS, convergence, accounting standards, financial reporting

## ABSTRACT

The increasing complexity of business transactions and capital markets makes it necessary to have single set of accounting standards. International Financial Reporting Standards (IFRS) is a set of high standard, understandable and enforceable international financial reporting system. There is a framework for the preparation and presentation of financial statements which describes the principles underlying the IFRS.As the investments are now made in different parts of the world by the investors and therefore a non-IFRS compliant country is considered one with an additional risk factor. This research article highlights the benefits, problems and deviations due to the convergence with IFRS in India, with special reference to WIPRO LIMITED as case study. There are many advantages of adopting it like saving in cost of raising capital abroad, one set of financial statements, brand building of Indian industry and massive opportunities for Indian accounting professionals abroad. More inputs and training will be required and similarly some modifications will be required in the Income-tax Act, as well as the Companies Act to complement the changes arising from the new standards. The legal and regulatory requirements in India are different from the IFRSs and therefore in such cases the Indian Accounting Standards diverge from IFRSs.

***Keywords :*** IFRS, Wipro, uniform accounting standards..

## 1. INTRODUCTION

International Financial Reporting Standards (IFRS) is a set of high standard, understandable and enforceable international financial reporting system. There is a framework for the preparation and presentation of financial statements which describes the principles underlying the IFRS.

The world is a small place now. The connectivity and trade has become global. Multi-national companies are establishing their businesses in various countries. The companies are getting their securities listed on the stock exchanges outside their country. The increasing complexity of business transactions and capital markets makes it necessary to have single set of accounting standards. As the investments are now made in different parts of the world by the investors and therefore a non-IFRS compliant country is considered one with an additional risk factor.

## 2. IFRS and WIPRO

Before starting a study of the benefits, problems, deviations and opportunities due to the convergence with IFRS in India, a feel of the environment needs to be created and hence the statements, notes and compliances of IFRS by WIPRO LIMITED are reproduced here for the good understanding of the new developments

**2.1 STATEMENT OF COMPLIANCE** The condensed consolidated interim financial statements of WIPRO LIMITED had been prepared in accordance with (IFRS) and its interpretations, as issued by the International Accounting Standards Board (IASB).

**2.2 BASIS OF PREPARATION** The condensed consolidated interim financial statements were prepared in accordance with

International Accounting Standard (IAS) 34, “Interim Financial Reporting”. The condensed consolidated interim financial statements corresponds to the classification provisions contained in IAS 1(revised), “Presentation of Financial Statements”. For clarity, various items were aggregated in the statements of income and statements of financial position. These items were disaggregated separately in the Notes, where applicable. All amounts included in the condensed consolidated interim financial statements were reported in millions of Indian rupees (Rupees in millions) except share and per share data, unless otherwise stated.

**2.3BASIS OF MEASUREMENT** The condensed consolidated interim financial statements had been prepared on a historical cost convention and on an accrual basis, except for the following material items that had been measured at fair value as required by relevant IFRS:

a. Derivative financial instruments;
b. Available-for-sale financial assets; and
c. Share based payment transactions

**2.4 CONVENIENCE TRANSLATION (UNAUDITED)** The condensed consolidated interim financial statements had been prepared and reported in Indian rupees, the national currency of India. Solely for the convenience of the readers, the condensed consolidated interim financial statements as of and for the three months ended June 30, 2010, had been translated into United States dollars at the certified foreign exchange rate of $ 1 = 46.41, as published by Federal Reserve Board of New York on June 30, 2010.

**2.5 USE OF ESTIMATES AND JUDGMENT** The preparation of the condensed consolidated interim financial statements in conformity with IFRSs requires management to make judgments, estimates and assumptions that affect the application of accounting policies and the reported amounts of assets, liabilities, income and expenses. Actual results may differ from those estimates. Estimates and underlying assumptions were reviewed on a periodic basis. Revisions to accounting estimates were recognized in the period in which the estimates were revised and in any future periods affected. In particular, information about significant areas of estimation, uncertainty and critical judgments in applying accounting policies that have the most significant effect on the amounts recognized in the condensed consolidated interim financial statements was included in the following notes:

**2.6NEW ACCOUNTING STANDARDS ADOPTED BY THE COMPANY:** The Company adopted IFRS 3, “Business Combinations” (“IFRS 3,( 2008)”) and IAS 27, “Consolidated and Separate Financial Statements” (“IAS 27, (2008)”) effective April 1, 2010. The revisions result in several changes in the accounting for business combinations. Major changes relate to the measurement of non -controlling interests, the accounting for business combinations achieved in stages as well as the treatment of contingent consideration and acquisition-related costs. Based on the new standard, non - controlling interests may be measured at their fair value (full - goodwill-methodology) or at the proportional fair value of assets acquired and liabilities assumed. In respect of business combinations achieved in stages, any previously held equity interest in the acquiree is re measured to its acquisition date fair value. Any changes to contingent consideration classified as a liability at the acquisition date are recognized in the statement of income. Acquisition related costs are expensed in the period incurred. Adoption of IFRS 3 (2008) and IAS 27, (2008), did not have a material effect on these condensed consolidated interim financial statements. The Company adopted an amendment to IAS 39, “Financial Instruments: Recognition and Measurement: Eligible Hedged Items” (“amendment to IAS 39”) effective April 1, 2010. The amendment addresses the designation of a one-sided risk in a hedged item in particular situations. The amendment applies to hedging relationships in the scope of IAS 39. Adoption of this amendment did not have a material effect on these condensed consolidated interim financial statements.

**2.7 NEW ACCOUNTING STANDARDS NOT YET ADOPTED BY THE COMPANY:** In November 2009, the IASB issued an amendment to IAS 24 (revised 2009) “Related Party Disclosures” (“IAS 24”). The purpose of the revision is to simplify the definition of a related party, clarifying its intended meaning and eliminating inconsistencies from the definition. The revision is effective for fiscal years beginning on or after January 1, 2011. Earlier application is permitted. The Company is evaluating the impact of these amendments on the Company's financial statements. In November 2009, the IASB issued IFRS 9 “Financial Instruments on the classification and measurement of financial assets”. The new standard represents the first part of a three -part project to replace IAS 39 Financial Instruments: Recognition and Measurement (IAS 39) with IFRS 9 Financial Instruments (I FRS 9). IFRS 9 uses a single approach to determine whether a financial asset is measured at amortized cost or fair value, replacing the many different rules in IAS 39. The approach in IFRS 9 is based on how an entity manages its financial instruments (its business model) and the contractual cash flow characteristics of the financial assets. IFRS 9 is effective for fiscal years beginning on or after January 1, 2013.

## 3.BENEFITS OF THE CONVERGENCE

**3.1 SAVES MANAGEMENT FROM PREPARING DIFFERENT FINANCIAL STATEMENTS** It can create confidence in the minds of foreign investors that their financial statements comply with globally accepted accounting standards. The industries are not required to prepare different set of financial statements for different countries and global investors.

Stimulate international business the convergence will allow Indian companies to grow their international business. The companies can go to foreign markets for their capital issued and therefore will have more capital at low cost.

**3.2 RELEVANT AND RELIABLE FINANCIAL STATEMENTS** Investors will be benefited by having one internationally accepted accounting standards which will build confidence in the financial state ments and comparability will enhance prudence decision making. The work of converting financial statement from one countries standard to another was a cumbersome work

**3.3 GROWTH OF SERVICE INDUSTRY** BPO and KPO industries will see a massive growth in it due to increased requirement of such professionals. Convergence with IFRSs also benefits the accounting professionals for they can render services in any part of the world

## 4. PROBLEMS

More inputs and training will be required and similarly some modifications will be required in the Income-tax Act, as well as the Companies Act to complement the changes arising from the new standards

**4.1 IFRS REPORTING TIMELINES** Reporting under IFRS, as proposed by ICAI, would be applicable for accounting periods beginning on or after April 1, 2011. As a result, the financial results of public entities for the quarter ended June 2011 would be reported under IFRS. Accepting the change The adoption of IFRS will require massive preparations and obviously the implications will be multi facets. It will require harmonization of internal and external reporting. The business plans, earnings estimates and management plans to undergo a change due to this convergence.

**4.2 MANAGING INVESTORS** Managing the investors and market expectations will be very different and will require attitudinal change.

**4.3 PREPARATION OF THE BALANCE SHEET** The variations in the Indian Company law and the IFRS will raise confusions for the accountants. The familiar Schedule VI will be a history in a few days because the format of presentation of the balance sheet under IFRS would be in according to a different prescription. But the Companies Act will need to be amended to make way for a smarter presentation of financial statements than Schedule VI.

## 5. DEVIATIONS

The legal and regulatory requirements in India are different from the IFRSs and therefore in such cases the Indian Accounting Standards diverge from IFRSs. Few examples of the variations in the two are given here.

**5.1 AS 21 AND IAS 27** Consolidated Financial Statements, defines 'control' as ownership of more than one-half of the voting power of an enterprise. This definition of 'control' is based on the definitions of 'holding company' and 'subsidiary company' as per the Companies Act, 1956. But according to IAS 27, control is “the power to govern the financial and operating policies of an enterprise so as to obtain benefits from its activities”

**5.2 AS 13 AND IAS 39** AS 13 require current investments to be valued at the lower of cost and 15 fair value whereas the corresponding IAS 39 requires measurement of similar investments at fair value.

**5.4 AS 29 AND IAS 37** AS 29, does not specifically deal with constructive obligation. It requires a provision to be created in respect of obligations arising from normal business practice, custom and a desire to maintain good business relations or act in an equitable manner but IAS 37 specifically deals with constructive obligation in the context of creation of a provision.

## 6. CONCLUSION

The difference between convergence and adoption need to be understood. India has not adopted the IFRS in full but it is revising its Accounting Standards to get them in line with the international reporting standards. The Indian Ministry of Corporate Affairs has issued 35 Indian Accounting Standards that are converged with IFRS, but has not given a date for implementation. The listed companies will do the convergence first as this would help their business and give them more credibility in the foreign markets. Inspite of the fact that there will be saving in cost of raising capital abroad, brand building of Indian industry and massive opportunities for Indian accounting professionals abroad, the convergence will require more inputs and training. The legal and regulatory requirements in India are different from the IFRSs and therefore in such cases the Indian Accounting Standards diverge from IFRSs. Some modifications will be required in the Income-tax Act, as well as the Companies Act to complement the changes arising from the new standards.

# REFERENCES


1. A.L. Saini: IFRS For India, published by Snow White Publications Pvt. Ltd
2. Barry J. Epstein And Eva K. Jermakowicz , Interpretation And Application Of International Financial Reporting Standards For Indian Companies, published by Wiley India
3. Barry J. Epstein, Eva K. Jermakowicz, Deloitt,Wiley IFRS 2009-10: For Indian Companies, Deloitte , published by Wiley India
4. Ernst and Young: International GAAP® 2009, published by Wiley India.
5. Deloitte, Financial Reporting Standards In India Including A Comparison With IFRS (2 Volumes), Wolters Kluwer India Pvt Ltd.
6. Kamal Garg, Accounting Standards & IFRS, Bharat Law House Pvt. Ltd.
7. Kamal Garg, IFRS Concepts & Application , Bharat Law House Pvt. Ltd
8. International Financial Reporting Standards (IFRSs) - published by Taxmann Publications P Ltd.
9. International Financial Reporting Standards July 2008-published by IASB
10. T.P.Ghosh,CA.Srinavasan Anand: Indian Accounting Standards (IND AS) And IFRSs for Non-Finance Executive, published by Taxmann Allied Services Pvt. Ltd.
11. Eva K. Jermakowicz: Interpretation and application of International Accounting and Financial Reporting Standards 2008, published by Wiley IFRS 2008
12. UK Accounting Consulting Services team of PricewaterhouseCoopers LLP: The IFRS Manual of Accounting, published by CCH
13. Robert Kirk: IFRS, A Quick Reference Guide
14. Abbas Ali Mirza, Graham J Holt and Magnus Orrell: Practical Implementation Guide and Workbook, published by Wiley IFRS


# WEBSITES

**www.icai.org**
**www.wipro.com**
**www.in.kpmg.com**
**www.moneycontrol.com**
**www.taxguru.com**
**www.caclubindia.com**

# APPENDIX

**List of IFRS**
**IFRS is a combination of IFRS and IAS standards and is very exhaustive. The below list provides what each one is and what they cover:**
**IFRS 1 – First time adoption of IFRS**
**IFRS 2 – Share based payment**
**IFRS 3 – Business Combination**
**IFRS 4 – Insurance contracts**
**IFRS 5 – Non current assets held for sale and discontinued operations**
**IFRS 6 – Exploration for and evaluation of mineral assets**
**IFRS 7 – Financial Instruments: disclosures**
**IFRS 8 – Operating segments**

**IFRS also includes the International Accounting Standards that specify accounting guidelines to be followed in different areas. There are about 41 International Accounting Standards**
**IAS 1 – Presentation of Financial Statements**
**IAS 2 – Inventories**
**IAS 7 – Cash Flow Statements**
**IAS 8 – Accounting Policies, Changes in Accounting Estimates and Errors**
**IAS 10 – Events after balance sheet date**
**IAS 11 – Construction contracts**
**IAS 12 – Income Taxes**
**IAS 14 – Segment Reporting**
**IAS 16 – Property, Plant and Equipment**

**IAS 17 – Leases**
**IAS 18 – Revenue**
**IAS 19 – Employee Benefits**
**IAS 20 – Accounting for Government Grants and Disclosure of Government Assistance**
**IAS 21 – Effects of Changes in Foreign Exchange Rates**
**IAS 23 – Borrowing Costs**
**IAS 24 – Related Party Disclosures**
**IAS 26 – Accounting and Reporting by Retirement Benefit Plans**
**IAS 27 – Consolidated and Separate Financial Statements**
**IAS 28 – Investments in Associates**
**IAS 29 – Financial Reporting in Hyperinflationary Economies**
**IAS 31 – Interests in Joint Ventures**
**IAS 33 – Earnings Per Share**
**IAS 34 – Interim Financial Reporting**
**IAS 36 – Impairment of Assets**
**IAS 37 – Provisions, Contingent Liabilities and Contingent Assets**
**IAS 38 – Intangible Assets**
**IAS 39 – Financial Instruments: Recognition and Movement**
**IAS 40 – Investment Property**
**IAS 41 – Agriculture**

# INTERNATIONAL JOURNAL OF ENGINEERING SCIENCES AND MANAGEMENT (ISSN: 2231-3273)

*International Journal of Engineering Sciences and Management* is a bi-annual journal of Dronacharya Group of Institutions, Greater Noida, UP, India.

## SCOPE OF THE JOURNAL

To publish full-length research papers in any one or more of the following disciplines:
**Computer Science & Engineering, Information Technology, Electrical, Electronics & Communication Engineering, Mechanical Engineering, Civil Engineering, Physics, Mathematics, Economics, and Management.**

## PURPOSE OF THE JOURNAL

To keep the academic community abreast of the research and technical scenario in the stated disciplines in the world.

## CHERISHED AIM OF THE JOURNAL

To excite and ignite the young minds and to motivate them for involving themselves in research and development activities. This will empower our manpower in the context of fast changing technologies across the globe.

## GUIDELINES FOR AUTHORS

**SUBMISSION OF MANUSCRIPTS**:
Soft copy of the manuscript for consideration of publication should be sent (as MS Word Windows 2007 attachment) by Email to the Executive Editor at advisor.r&d@gnoida.dronacharya.info. There are "no page charges" for the publication of papers in IJESM.

All papers, received for publication and complying with the below-mentioned format will be sent for review to at least two referees. In accepting the paper for publication, the Editors and reviewers will give special weight to readability and interest value for a wide readership besides the originality and the high-standard of its content.

The Executive Editor's decision is final in case of non-unanimity of opinion of referees. Under normal circumstances, the contributors of papers will be informed about the status of their papers by the Executive Editor within eight weeks of their submission.

# PREPARATION OF MANUSCRIPTS

- **Manuscript:** Manuscript should be in English, the preferred spelling being that of the Concise Oxford Dictionary. It should be in 'Times New Roman', single-spaced, and typed on 8.5" x 11" or A4-size paper with margins of 1" (25 mm) on each side. Manuscript should be typed in single column only (and not in double or triple columns).
- **Title of Paper:** Font size 16, ALL CAPITALS, bold, centered, and not underlined. The title must be 12.5 mm below the top of the page (in addition to the standard 25 mm margin). The Title should adequately describe the contents of the paper
- **Full names of all Authors**, with * as superscript with corresponding author's name and his/her Email ID (Font size 12, centered) and also the contact number. A blank line should be left between the title and the author's name(s).
- **Full postal address** along with affiliations (Font size 10, centered).
- **Abstract** (Font size 10, capitals, bold, centered) All papers must have a non-mathematical abstract of not more than 200 words. The abstract should indicate the general scope of the paper, the important findings and the conclusions drawn. The abstract should include only text. It should be specific about the methodologies used and the conclusion drawn of the work reported. Please avoid the use of abbreviations and references. (Text of the Abstract: Font size 9, single-space, justified).
- **Keywords:** Include up to six keywords that describe your paper for indexing and for web searches. The more discriminating your keywords are, the greater is the likelihood that your article will be found and cited. (Font size 9, italics, left-justified).
- **Text:** (Font size 10, Justified). The paper must be divided into sections starting preferably with "Introduction" and ending with "Conclusion". The main sections should be numbered 1, 2, 3 etc and subsections as 2.1, 2.2 etc. Main headings should be typed in capitals, subheadings in lower case. Both types of heading should be bold and left-justified. Footnotes should be avoided. Equations should be typewritten and with the equation number placed in parentheses at the right margin. Reference to the equation should use the form 'Eq. (3)'. Use extra line spacing between equations, illustrations, figures and tables. The use of SI units is strongly recommended
- **Tables and Figures:** Tables and Figures should be integrated with the text (and not sent separately at the end of the manuscript) and numbered consecutively in the order in which reference is made to them in the text of the paper. All captions must be centrally located above a Table and below a Figure (Font size 10, bold). All tables and figures must be numbered consecutively in Arabic numerals (not Roman) (e.g., Table 3 or Fig. 3) in the order of appearance in the text. Tables & Figures should be reproduced in the exact format and at the exact place as desired to appear in the journal.
- **Conclusion:** A conclusion section must be included and should indicate clearly the advantages, limitations and possible applications of the paper. Authors may also discuss about the scope of future work
- **Acknowledgements:** An acknowledgement section may be included after the 'Conclusion'.
  **References:** References should be placed at the end of the text, should be numbered consecutively in order of their citation in the text and be indicated by superscripts in the text of the manuscript. Examples of different citations as References are given below:

**(i) In case of referring to an Article in a Journal**
Kuebel, D.; Lahiri, M. & Wolf, E. An Inverse Problem in the Theory of Stochastic Electromagnetic Beams, Opt. Commn., 282, 2009, p.141.

**(ii) In case of referring to a Book/Monograph**
Rao, C.N.R. & Raveau, B. (Eds.). Transition Metal Oxides, Wiley-VCH, 2nd Edition, 1998, Ch. 2.

**(iii) In case of referring to a Conference Paper**
Ctvrtnickova, T.; Mateo, M; Yanez, A. & Nicolas, G. Characterization of Coal Fly Ash Components by Laser-Induced Breakdown Spectroscopy. Presented at the Fifth International Conf. on Laser-Induced Breakdown Spectroscopy, Berlin, Adlershof, Germany. Sep 22-26, 2008, CP-15, p. 67-68.

**(iv) In case of referring to a Report**
Marine, R.E. & Iliff, K.W. Application of Parameter Estimation to Aircraft Stability and Control. NASA, USA, 1986, Report No. NASA-RP-1168.
Papers quoting the LATEST references from the referred journals will be preferred for publication unless the original contribution from the author/s is of a very high standard.

- **UNDERTAKING**

  Authors must include, in the covering Email that their paper has not been published//accepted/submitted for publication/presentation to any other journal/ book/conference in any form and the work submitted by them is their own and original. The same 'Undertaking' should also be attached, on a separate page, along with the manuscript. This ethical policy of the Journal will be strictly adhered to.

***Note: Manuscripts not in conformity with these 'Guidelines' will not be forwarded to the experts for review.***

# A GURUKUL COMBINING TRADITION AND MODERNITY

DGI, A flagship Institution reputed for its disciplined environment
Where faculty development, career-consciousness & merits are a tradition
Where academia, placement and industry face are in sync.
Where infra-structural growth is an offshoot of the institution growth
Where aspirants can dare to dream to ascend to the highest attitude of success

**DRONACHARYA GROUP OF INSTITUTIONS, GREATER NOIDA, U.P.**

Approved by
All India Council for Technical Education, New Delhi

Affiliated To:
Mahamaya Technical University, Noida

***Corporate Office:***
76P, Part-III, Sector-5, Gurgaon, 122001, Haryana (India)
Phone: 0124-2251602, 2253144, Email: info@dronacharya.info

www.dronacharya.info